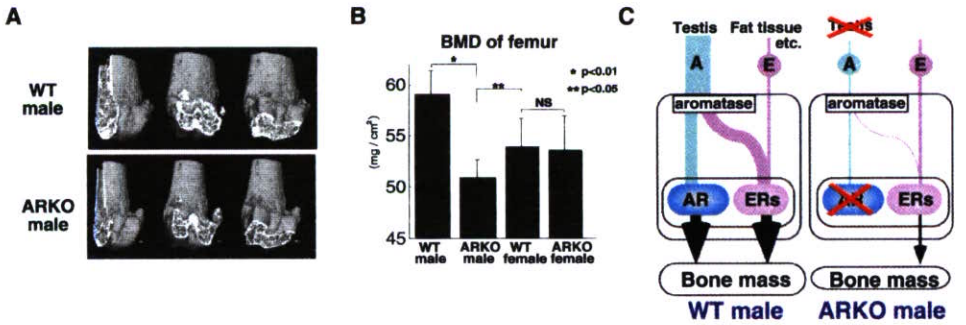

Fig. 3. **Osteopenia in male ARKO mice.** (A) Three-dimensional computed tomography images of distal femora from representative 8-week-old male ARKO mice. (B) Bone loss in femur of 8-week-old male ARKO mice by BMD analysis. (C) Schema of skeletal sex hormone action.

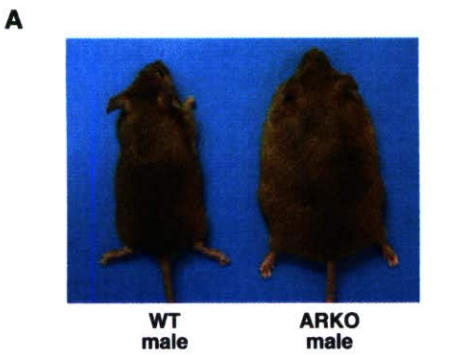

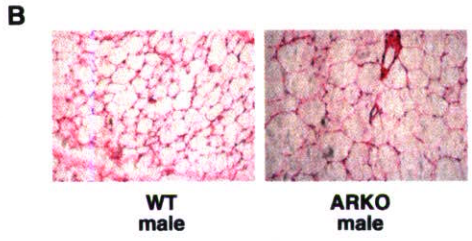

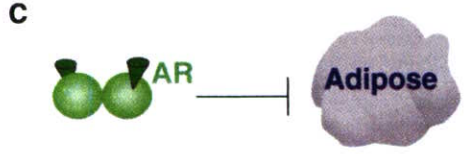

organs. The AR gene is located on the X chromosome, and therefore exists as a single copy in males. As male animals lacking a functional AR gene would be expected to show Tfm abnormalities with complete infertility, successful targeted disruption of the AR gene, essential for reproduction, necessarily prohibits its transmission to the next generation. Therefore, to define AR function, an AR-null mutant mouse line was generated by means of the Cre-loxP system (*19*), which was used to circumvent the problem of male infertility. We first generated floxed AR mice, in which the AR gene locus was flanked by loxP sites. Floxed AR mice were fully fertile and showed normal expression of AR protein. We then crossed these mice with mice that expressed the Cre recombinase ubiquitously under the control of a CMV promoter, and obtained male and female ARKO mice at theoretical Mendellian frequencies. No AR transcript or protein was detected, which indicates that they were complete null mutant mice for the AR gene.

Tfm abnormalities in male ARKO mice

As expected, the AR-null mutation in males resulted in the ablation of masculinization of reproductive organs (*11*). ARKO mice exhibited female-typical external appearance, including a vagina with a blind end and a clitoris-like phallus, instead of a penis and scrotum (Fig. 1). Male reproductive organs, such as seminal vesicles, vas deferens, epididymis and prostate were absent in ARKO males. However, no ovaries or uteri were observed, although small inguinal testes were present. Histological examination of the testes showed that spermatogenesis was severely arrested. These observations in ARKO males are similar to a human hereditary disorder, AIS or Tfm, in which mutations in the AR gene have been identified in several families. Testicular androgen levels were very low, whereas serum estrogen levels appeared normal in ARKO males.

Fig. 4. **Late onset of obesity in male ARKO mice.** (A) External appearance of 30-week-old male ARKO mice. (B) Subcutaneous white adipose tissues from 30-week-old male ARKO mice. (C) Schema of AR function in adipogenesis.

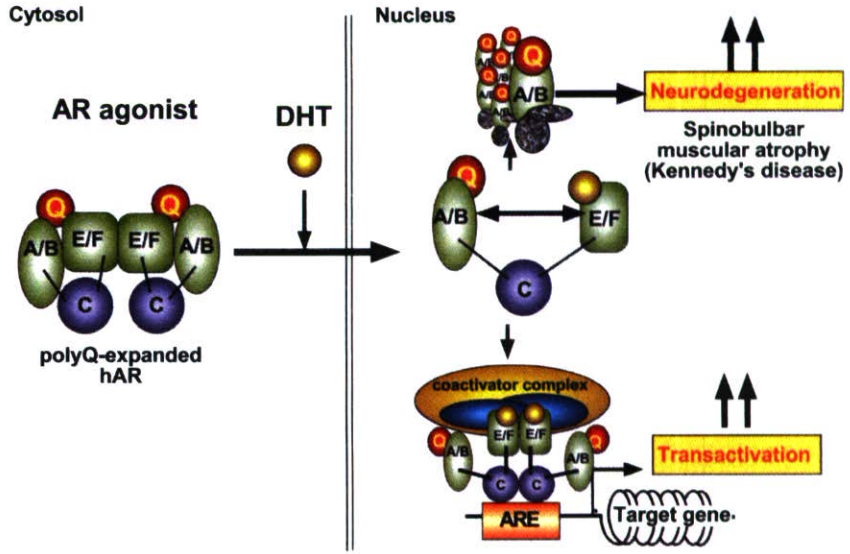

Fig. 5. **Androgen-dependent structural alteration by the polyQ-expanded human AR.** It is considered that the polyQ-expanded AR is inactive in the transactivation without the agonists (androgens); but in the presence of the agonists, it alters the molecular structure and also recruits the co-activators, while the polyQ repeat induces apoptosis by their aggregation.

Brain masculinization requires AR function

Next, we investigated the AR function in perinatal brain masculinization (*11*). Intact ARKO males showed no male sexual behaviors and impaired male aggressive behaviors (Fig. 2A). Treatment with the non-aromatizable androgen 5α-dihydrotestosterone (DHT) partially rescued impaired male aggressive behaviors in ARKO males, suggesting that DHT activity in male aggressive behaviors is mediated via both AR-independent and -dependent pathways in the adult. In contrast, no female sexual behavior was induced in ARKO males even when estrogen alone or both estrogen and progesterone was administered (Fig. 2B), suggesting that the brains of ARKO males were defeminized (Fig. 2C). The AR function in brain masculinization at a limited perinatal stage was further studied in ARKO females. While DHT-induced masculinization of female brain at the perinatal stage led to adult female mice sensitive to both E2 and DHT with the expression of male-typical behaviors, such responses were completely abolished in ARKO females. These data provide genetic evidence that once the brain is perinatally masculinized through liganded-AR, the sexually developed brain becomes sensitive to both androgen and estrogen with regard to the expression of male-typical behaviors in adulthood (Fig. 2C).

High turnover osteopenia in male ARKO mice

Beyond the reproductive physiology, sex steroid hormones are implicated in involvement of homeostatic processes, such as bone metabolism. Sex hormone status is reflected in bone mass, and hormonal deficiency is well known to lead to progressive bone loss. The most striking example, osteoporosis in postmenopausal women, is a state of estrogen deficiency coupled with imbalanced bone remodeling. However, the physiological role of the AR-mediated androgen signaling in the skeletal tissues has not yet been established. We performed in vivo analyses of the bone of 8-week-old ARKO males and found that the trabecular and cortical bone volumes were remarkably reduced (Fig. 3, A–B) (*12*). Bone loss in ARKO mice was only partially prevented by treatment with aromatizable testosterone (Fig. 3C). Histomorphometric analysis further showed that both bone formation and resorption were enhanced in ARKO males, but the increase in bone resorption exceeded that in formation. In view of these findings, we concluded that bone loss found in ARKO males was based on the high bone turnover osteopenia.

Late onset of obesity in male ARKO mice

Another hallmark of ARKO males was late-onset obesity (Fig. 4A) (*10*). From birth, ARKO male mice were externally indistinguishable from normal female WT littermates in terms of ano-genital distance and growth curve up to 10 weeks. However, thereafter, the growth of ARKO males rapidly increased, and at 12 weeks of age, male ARKO mouse body weights exceeded that of WT male littermates. This late onset of drastically increased ARKO male growth curve led to the clear development of obesity, with 30-week old ARKO males showing significantly increased wet tissue weights in white adipose tissues (Fig. 4B). Such clear increases were not detected in

white adipose tissues of 8-week-old ARKO males. As no significant alterations in food intake were observed, our results suggested that AR may serve as a negative regulator of adipocyte development in adult males (Fig. 4C).

Drosophila model to dissect human AR mutants with expanded polyQ stretches in neurodegeneration

Another characteristic clinical disorder with an AR mutation is spinal and bulbar muscular atrophy (SBMA), also known as Kennedy's disease (*5*, *7*). SBMA is a rare degenerative disease of the motor neurons characterized by progressive muscle atrophy and weakness in male patients, usually beginning at 30 to 50 years of age. Previous analyses of SBMA revealed expansions in the number of trinucleotide CAG repeats in the first exon of the AR gene, which generated expanded polyQ stretches in the A/B domain of the AR protein (*5*, *7*, *20*). It was found that disease onset occurred when these repeat stretches encoded more than 40 glutamine residues, compared to a range of 15 to 35 polyQ residues in normal individuals.

To dissect the molecular mechanism of human AR (hAR) mutants with expanded polyQ stretches in neurodegeneration, we established a *Drosophila* model that ectopically overexpressed a mutated AR in photoreceptor neurons (*13*). We first expressed WT and mutated hAR in photoreceptor neurons in developing eye discs under the glass multimer reporter (*GMR*) gene promoter (*21*) using the *Drosophila melanogaster* GAL4-UAS system (*22*). To monitor the ligand-induced transactivation function of hAR, hAR-expressing flies were further crossed to flies carrying a *GFP* reporter gene, with the result that GFP expression was induced by the binding of ligand-bound AR to the consensus *ARE* in the GFP promoter (*23*). Expressed hAR proteins were then detected as red fluorescence *in situ* using an immunofluorescent antibody.

Although eyes that expressed a mutant hAR containing an expanded 52-stretch polyQ (Q52) appeared normal, dietary ingestion of dihydrotestosterone (DHT) or androgen antagonists induced marked degeneration and apoptosis of the photoreceptor neurons, despite the mutant hAR retaining only reduced transactivation function. Ligand-independent toxicity was detected in fly eyes expressing truncated polyQ-expanded A/B domains alone, but this was abrogated by the co-expression of unliganded LBD domains. Thus, our results suggested that hormone binding and subsequent structural alteration of hAR mutants with nuclear localization appeared to be critical for SBMA onset (Fig. 5), and that the fly-eye model may be useful for the development of novel therapeutic approaches to SBMA.

We thank members of the laboratory of Nuclear Signaling, IMCB for support and H. Higuchi for manuscript preparation. This work was supported in part by a grant-in-aid for priority areas from the Ministry of Education, Science, Sports and Culture of Japan (K.-i.T. and S.K.).

REFERENCES

1. Mooradian, A.D., Morley, J.E., and Korenman, S.G. (1987) Biological actions of androgens. *Endocr. Rev.* **8**, 1–28
2. Wilson, J.D. (1999) The role of androgens in male gender role behavior. *Endocr. Rev.* **20**, 726–737
3. Glass, C.K. and Rosenfeld, M.G. (2000) The coregulator exchange in transcriptional functions of nuclear receptors. *Genes Dev.* **14**, 121–141
4. Mangelsdorf, D.J., Thummel, C., Beato, M., Herrlich, P., Schutz, G., Umesono, K., Blumberg, B., Kastner, P., Mark, M., Chambon, P., and *et al.* (1995) The nuclear receptor superfamily: the second decade. *Cell* **83**, 835–839
5. Choong, C.S. and Wilson, E.M. (1998) Trinucleotide repeats in the human androgen receptor: a molecular basis for disease. *J. Mol. Endocrinol.* **21**, 235–257
6. Griffin, J.E. (1992) Androgen resistance–the clinical and molecular spectrum. *N. Engl. J. Med.* **326**, 611–618
7. La Spada, A.R., Wilson, E.M., Lubahn, D.B., Harding, A.E., and Fischbeck, K.H. (1991) Androgen receptor gene mutations in X-linked spinal and bulbar muscular atrophy. *Nature* **352**, 77–79
8. McPhaul, M.J. (1999) Molecular defects of the androgen receptor. *J. Steroid Biochem. Mol. Biol.* **69**, 315–322
9. Quigley, C.A., De Bellis, A., Marschke, K.B., el-Awady, M.K., Wilson, E.M., and French, F.S. (1995) Androgen receptor defects: historical, clinical, and molecular perspectives. *Endocr. Rev.* **16**, 271–321
10. Sato, T., Matsumoto, T., Yamada, T., Watanabe, T., Kawano, H., and Kato, S. (2003) Late onset of obesity in male androgen receptor-deficient (AR KO) mice. *Biochem. Biophys. Res. Commun.* **300**, 167–171
11. Sato, T., Matsumoto, T., Kawano, H., Watanabe, T., Uematsu, Y., Sekine, K., Fukuda, T., Aihara, K., Krust, A., Yamada, T., Nakamichi, Y., Yamamoto, Y., Nakamura, T., Yoshimura, K., Yoshizawa, T., Metzger, D., Chambon, P., and Kato, S. (2004) Brain masculinization requires androgen receptor function. *Proc. Natl Acad. Sci. USA* **101**, 1673–1678
12. Kawano, H., Sato, T., Yamada, T., Matsumoto, T., Sekine, K., Watanabe, T., Nakamura, T., Fukuda, T., Yoshimura, K., Yoshizawa, T., Aihara, K., Yamamoto, Y., Nakamichi, Y., Metzger, D., Chambon, P., Nakamura, K., Kawaguchi, H., and Kato, S. (2003) Suppressive function of androgen receptor in bone resorption. *Proc. Natl Acad. Sci. USA* **100**, 9416–9421
13. Takeyama, K., Ito, S., Yamamoto, A., Tanimoto, H., Furutani, T., Kanuka, H., Miura, M., Tabata, T., and Kato, S. (2002) Androgen-dependent neurodegeneration by polyglutamine-expanded human androgen receptor in Drosophila. *Neuron* **35**, 855–864
14. Lubahn, D.B., Joseph, D.R., Sullivan, P.M., Willard, H.F., French, F.S., and Wilson, E.M. (1988) Cloning of human androgen receptor complementary DNA and localization to the X chromosome. *Science* **240**, 327–330
15. Poujol, N., Wurtz, J.M., Tahiri, B., Lumbroso, S., Nicolas, J.C., Moras, D., and Sultan, C. (2000) Specific recognition of androgens by their nuclear receptor. A structure-function study. *J. Biol. Chem.* **275**, 24022–24031
16. Shiau, A.K., Barstad, D., Loria, P.M., Cheng, L., Kushner, P.J., Agard, D.A., and Greene, G.L. (1998) The structural basis of estrogen receptor/coactivator recognition and the antagonism of this interaction by tamoxifen. *Cell* **95**, 927–937
17. Yanagisawa, J., Kitagawa, H., Yanagida, M., Wada, O., Ogawa, S., Nakagomi, M., Oishi, H., Yamamoto, Y., Nagasawa, H., McMahon, S.B., Cole, M.D., Tora, L., Takahashi, N., and Kato, S. (2002) Nuclear receptor function requires a TFTC-type histone acetyl transferase complex. *Mol. Cell* **9**, 553–562
18. Kato, S., Endoh, H., Masuhiro, Y., Kitamoto, T., Uchiyama, S., Sasaki, H., Masushige, S., Gotoh, Y., Nishida, E., Kawashima, H., and *et al.* (1995) Activation of the estrogen receptor through phosphorylation by mitogen-activated protein kinase. *Science* **270**, 1491–1494
19. Li, M., Indra, A.K., Warot, X., Brocard, J., Messaddeq, N., Kato, S., Metzger, D., and Chambon, P. (2000) Skin abnormalities generated by temporally controlled RXRalpha mutations in mouse epidermis. *Nature* **407**, 633–636

20. Merry, D.E., Kobayashi, Y., Bailey, C.K., Taye, A.A., and Fischbeck, K.H. (1998) Cleavage, aggregation and toxicity of the expanded androgen receptor in spinal and bulbar muscular atrophy. *Hum. Mol. Genet.* **7**, 693–701
21. Moses, K. and Rubin, G.M. (1991) Glass encodes a site-specific DNA-binding protein that is regulated in response to positional signals in the developing Drosophila eye. *Genes Dev.* **5**, 583–593
22. Brand, A.H. and Perrimon, N. (1993) Targeted gene expression as a means of altering cell fates and generating dominant phenotypes. *Development* **118**, 401–415
23. Yamamoto, A., Hashimoto, Y., Kohri, K., Ogata, E., Kato, S., Ikeda, K., and Nakanishi, M. (2000) Cyclin E as a coactivator of the androgen receptor. *J. Cell Biol.* **150**, 873–880.

Premature ovarian failure in androgen receptor-deficient mice

Hiroko Shiina*†‡, Takahiro Matsumoto*‡§, Takashi Sato*, Katsuhide Igarashi¶, Junko Miyamoto*, Sayuri Takemasa*, Matomo Sakari*§, Ichiro Takada*, Takashi Nakamura*§, Daniel Metzger‖, Pierre Chambon‖, Jun Kanno¶, Hiroyuki Yoshikawa†, and Shigeaki Kato*§**

*Institute of Molecular and Cellular Biosciences, University of Tokyo, 1-1-1 Yayoi, Bunkyo-ku, Tokyo 113-0032, Japan; §Exploratory Research for Advanced Technology, Japan Science and Technology, 4-1-8 Honcho, Kawaguchi, Saitama 332-0012, Japan; †Department of Obstetrics and Gynecology, Institute of Clinical Medicine, University of Tsukuba, 1-1-1 Tennoudai, Tsukuba, Ibaraki 305-8575, Japan; ¶Division of Cellular and Molecular Toxicology, National Institute of Health Sciences, 1-18-1 Kamiyoga, Setagaya-ku, Tokyo 158-8501, Japan; and ‖Institut de Genetique et de Biologie Moleculaire et Cellulaire, Centre National de la Recherche Scientifique, Institut National de la Santé et de la Recherche Médicale, Universite Louis Pasteur, College de France, 67404 Illkirch, Strasbourg, France

Edited by Bert W. O'Malley, Baylor College of Medicine, Houston, TX, and approved November 10, 2005 (received for review August 5, 2005)

Premature ovarian failure (POF) syndrome, an early decline of ovarian function in women, is frequently associated with X chromosome abnormalities ranging from various Xq deletions to complete loss of one of the X chromosomes. However, the genetic locus responsible for the POF remains unknown, and no candidate gene has been identified. Using the Cre/LoxP system, we have disrupted the mouse X chromosome androgen receptor (*Ar*) gene. Female $AR^{-/-}$ mice appeared normal but developed the POF phenotype with aberrant ovarian gene expression. Eight-week-old female $AR^{-/-}$ mice are fertile, but they have lower follicle numbers and impaired mammary development, and they produce only half of the normal number of pups per litter. Forty-week-old $AR^{-/-}$ mice are infertile because of complete loss of follicles. Genome-wide microarray analysis of mRNA from $AR^{-/-}$ ovaries revealed that a number of major regulators of folliculogenesis were under transcriptional control by AR. Our findings suggest that AR function is required for normal female reproduction, particularly folliculogenesis, and that AR is a potential therapeutic target in POF syndrome.

male hormone | nuclear receptor | female physiology | folliculogenesis | kit ligand

Premature ovarian failure (POF) is defined as an early decline of ovarian function after seemingly normal folliculogenesis (1). Genetic causes of POF have been frequently associated with X chromosome abnormalities (1, 2). Complete loss of one of the X chromosomes, as in Turner syndrome, and various Xq deletions are commonly identified as a cause of POF. However, responsible X-linked genes and their downstream targets have not been identified so far.

The androgen receptor (*Ar*) gene, which is the only sex hormone receptor gene on the X chromosome, is well known to be essential not only for the male reproductive system, but also for male physiology. In contrast, androgens are considered as male hormones; therefore, little is known about androgens' actions in female physiology, although AR expression in growing follicles has been described (3). However, because excessive androgen production in polycystic ovary syndrome causes infertility with abnormal menstrual cycles (4, 5), it is possible that AR-mediated androgen signaling also plays an important physiological role in the female reproductive system. Recently, using Cre/LoxP system, we generated an AR-null mutant mouse line (6) and demonstrated that inactivation of AR resulted in arrest of testicular development and spermatogenesis, impaired brain masculinization, high-turnover osteopenia, and late onset of obesity in males (7–9). At the same time, no overt physical or growth abnormalities were observed in female $AR^{-/-}$ mice. Therefore, to further examine potential role of AR in female physiology, we characterized female reproductive system in $AR^{-/-}$ females. Herein we show that female $AR^{-/-}$ mice develop the POF phenotype. At 3 weeks of age, $AR^{-/-}$ females had apparently normal ovaries with numbers of follicles similar to those in the wild-type females. However, thereafter the number of healthy follicles in the $AR^{-/-}$ ovary gradually declined, with a marked increase of atretic follicles, and by 40 weeks $AR^{-/-}$ mice became infertile, with no follicle detectable in the ovary. Reflecting this age-dependent progression in ovarian abnormality, several genes known to be involved in the oocyte–granulosa cell regulatory loop were identified by microarray analysis as AR downstream target genes. These findings clearly demonstrate that AR-mediated androgen signaling is indispensable for the maintenance of folliculogenesis and implicate impaired androgen signaling as a potential cause of the POF syndrome.

Materials and Methods

Generation of AR Knockout Mice. *AR* genomic clones were isolated from a TT2 embryonic stem cell genomic library by using human *AR* A/B domain cDNA as a probe (6). The targeting vector consisted of a 7.6-kb 5′ region containing exon 1, a 1.3-kb 3′ homologous region, a single loxP site, and a neo cassette with two loxP sites (10). Targeted clones (FB-18 and FC-61) were aggregated with single eight-cell embryos from CD-1 mice (11, 12). Floxed *AR* mice (C57BL/6) were then crossed with CMV-Cre transgenic mice (6). The two lines exhibited the same phenotypic abnormalities. The chromosomal sex of each pup was determined by genomic PCR amplification of the Y chromosome *Sry* gene (13).

Western Blot Analysis. To detect AR protein expression, ovarian cell lysates were separated by SDS/PAGE and transferred onto nitrocellulose membranes (14). Membranes were probed with polyclonal AR antibodies (N-20; Santa Cruz Biotechnology), and blots were visualized by using peroxidase-conjugated second antibody and an ECL detection kit (Amersham Pharmacia Biosciences).

Morphologic Classification of Growing Follicles. Sections were taken at intervals of 30 μm, and 6-μm paraffin-embedded sections were mounted on slides. Routine hematoxylin and eosin staining was performed for histologic examination by light microscopy. Follicle numbers in 12 sections per ovary were evaluated as primary follicles (oocyte surrounded by a single layer of cuboidal granulosa cells), preantral follicles (oocyte surrounded by two or more layers of granulosa cells with no antrum), or antral follicles (antrum within the granulosa cell layers enclosing the oocyte). Follicles were determined to be atretic if they displayed two or more of the following criteria within a single cross section: more than two pyknotic nuclei, granulosa cells within the antral cavity, granulosa cells pulling away from the basement membrane, or uneven granulosa cell layers (15).

Conflict of interest statement: No conflicts declared.

This paper was submitted directly (Track II) to the PNAS office.

Abbreviations: AR, androgen receptor; DHT, 5α-dihydrotestosterone; POF, premature ovarian failure.

‡H.S. and T.M. contributed equally to this work.

**To whom correspondence should be addressed. E-mail: uskato@mail.ecc.u-tokyo.ac.jp.

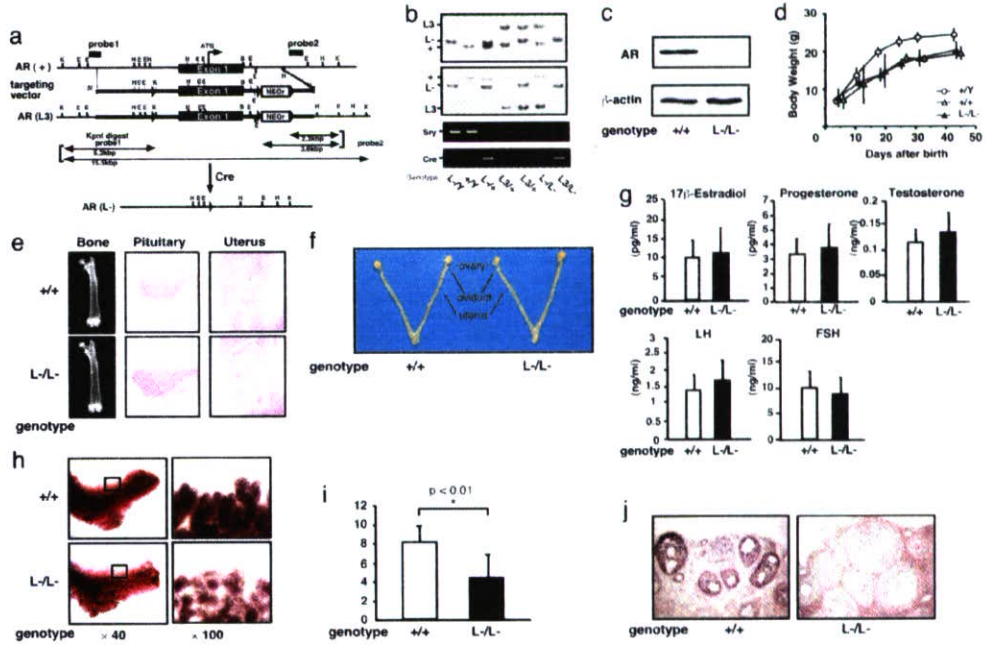

Fig. 1. Phenotypic characterization of AR knockout female mice. (*a*) Diagram of the wild-type *Ar* genomic locus (+), floxed *AR* L3 allele (L3), and *AR* allele (L-) obtained after Cre-mediated excision of exon 1. K, KpnI; E, EcoRI; H, HindIII; B, BamHI. LoxP sites are indicated by arrowheads. The targeting vector consisted of a 7.6-kb 5′ homologous region containing exon 1, a 1.3-kb 3′ homologous region, a single loxP site, and the neo cassette with two loxP sites. (*b*) Detection of the Y chromosome-specific *Sry* gene in $AR^{-/Y}$ mice by PCR. (*c*) Absence of AR protein in $AR^{-/-}$ mice ovaries by Western blot analysis using a specific C-terminal antibody. (*d*) Normal weight gain in $AR^{-/-}$ females. (*e*) Histology of pituitary, uterus, and bone tissues in $AR^{+/+}$ and $AR^{-/-}$ females at 8 weeks of age. (*f*) Female reproductive organs were macroscopically normal in $AR^{-/-}$ mice. (*g*) Serum hormone levels at the proestrus stage in $AR^{-/-}$ mice were not significantly altered. Serum 17β-estradiol, progesterone, testosterone, luteinizing hormone (LH), and follicle-stimulating hormone (FSH) levels in $AR^{+/+}$ ($n = 13$) and $AR^{-/-}$ ($n = 10$) females at 8–10 weeks of age are shown. (*h*) Lobuloalveolar development is impaired in $AR^{-/-}$ mammary glands. Whole mount of inguinal mammary glands (*Left*) and its higher magnification (*Right*) were prepared on day 3 of lactation. (*i*) Average number of pups per litter is markedly reduced in $AR^{-/-}$ mice at 8 weeks of age. Data are shown as mean ± SEM and analyzed by using Student's *t* test. (*j*) AR immunocytochemistry in $AR^{+/+}$ and $AR^{-/-}$ ovaries. Sections were counterstained with eosin.

Immunohistochemistry. Sections were subjected to a microwave antigen retrieval technique by boiling in 10 mM citrate buffer (pH 6.0) in a microwave oven for 30 min (16). The cooled sections were incubated in 1% H_2O_2 for 30 min to quench endogenous peroxidase and then incubated with 1% Triton X-100 in PBS for 10 min. To block nonspecific antibody binding, sections were incubated in normal goat serum for 1 h at 4°C. Sections were then incubated with anti-AR (1:100) or anti-cleaved caspase-3 (1:100) in 3% BSA overnight at 4°C. Negative controls were incubated in 3% BSA without primary antibody. The ABC method was used to visualize signals according to the manufacturer's instructions. Sections were incubated in biotinylated goat anti-rabbit IgG (1:200 dilution) for 2 h at room temperature, washed with PBS, and incubated in avidin–biotin–horseradish peroxidase for 1 h. After thorough washing in PBS, sections were developed with 3,3′-diaminobendizine tetrahydrochloride substrate, slightly counterstained with eosin, dehydrated through an ethanol series and xylene, and mounted.

Estrus Cycles and Fertility Test. To determine the stage of the estrus cycle (proestrus, estrus, and diestrus), vaginal smears were taken every morning and stained with Giemsa solution. For evaluation of female fertility for 15 weeks, an 8- or 24-week-old wild-type or $AR^{-/-}$ female was mated with a wild-type fertile male, replaced every 2 weeks with the other fertile male. Cages were monitored daily and for an additional 23 days, and the presence of seminal plugs and number of litters were recorded.

RNA Extraction and Quantitative Competitive RT-PCR. Total ovarian RNA was extracted by using TRIzol (Invitrogen) (16). Oligo-dT-primed cDNA was synthesized from 1 μg of ovarian RNA by using SuperScript reverse transcriptase (Gibco BRL, Gaithersburg, MD) in a 20-μl reaction volume, 1 μl of which was then diluted serially (2- to 128-fold) and used to PCR-amplify an internal control gene, *cycA*, to allow concentration estimation.

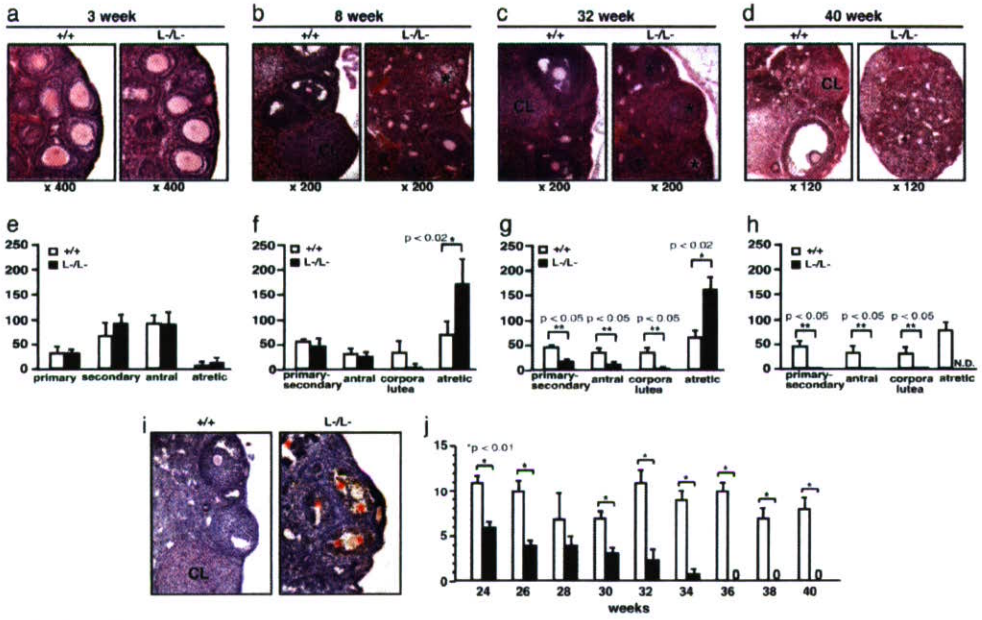

Fig. 2. POF in $AR^{-/-}$ female mice. (*a–d*) Histology of $AR^{+/+}$ and $AR^{-/-}$ ovaries at 3 weeks, 8 weeks, 32 weeks, and 40 weeks of age. All sections were stained with hematoxylin and eosin. An asterisk marks the atretic follicle. CL, corpus luteum. (*e–h*) Relative follicle counts at 3 weeks (*e*), 8 weeks (*f*), 32 weeks (*g*), and 40 weeks (*h*) of age. Numbers represent total counts of every fifth section from serially sectioned ovaries ($n = 4$ animals per genotype). (*i*) Immunohistochemical study for activated, cleaved caspase-3 revealed increased positive cells (apoptotic cells) in $AR^{-/-}$ ovaries. Sections were counterstained with hematoxylin. An asterisk marks the caspase-3-positive cell. CL, corpus luteum. (*j*) Age-dependent reduction in the number of pups per litter in $AR^{-/-}$ female mice. A continuous breeding assay was started at 24 weeks of age ($n = 6$–10 animals per genotype). For all panels, data are shown as mean ± SEM and were analyzed by using Student's *t* test.

Primers were designed from cDNA sequences of *Kitl* (M57647; nucleotides 1099–1751), Gdf9 (NM008110; nucleotides 720-1532), *Bmp15* (NM009757; nucleotides 146–973), *Ers2* (NM010157; nucleotides 1139–1921), *Pgr* (NM008829; nucleotides 1587–2425), *Cyp11a1* (NM019779; nucleotides 761-1697), *Cyp17al* (M64863; nucleotides 522–932), *Cyp19* (D00659; nucleotides 699-1049), *Fshr* (AF095642; nucleotides 625-1427), *Lhr* (M81310; nucleotides 592-1331), *Ptgs2* (AF338730; nucleotides 3–605), and *Ccnd2* (NM009829; nucleotides 150-1065) and chosen from different exons to avoid amplification from genomic DNA.

GeneChip Analysis. Ovaries were isolated and stabilized in RNA-*later* RNA Stabilization Reagent (Ambion, Austin, TX) before RNA purification (17). Total RNA was purified by using an RNeasy mini kit (Qiagen, Valencia, CA) according to the manufacturer's instructions. First-strand cDNA was synthesized from 5 μg of RNA by using 200 units of SuperScript II reverse transcriptase (Invitrogen, Carlsbad, CA), 100 pmol T7-$(dT)_{24}$ primer [5′-GGCCAGTGAATTGTAATACGACTCAC-TATAGGGAGGCGG-$(dT)_{24}$-3′], 1× first-strand buffer, and 0.5 mM dNTPs at 42°C for 1 h. Second-strand synthesis was performed by incubating first-strand cDNA with 10 units of *Escherichia coli* ligase (Invitrogen), 40 units of DNA polymerase I (Invitrogen), 2 units of RNase H (Invitrogen), 1× reaction buffer, and 0.2 mM dNTPs at 16°C for 2 h, followed by 10 units of T4 DNA polymerase (Invitrogen) and incubation for another 5 min at 16°C. Double-stranded cDNA was purified by using GeneChip Sample Cleanup Module (Affymetrix, Santa Clara, CA) according to the manufacturer's instructions and labeled by *in vitro* transcription by using a BioArray HighYield RNA transcript labeling kit (Enzo Diagnostics, Farmingdale, NY). Briefly, dsDNA was mixed with 1× HY reaction buffer, 1× biotin-labeled ribonucleotides (NTPs with Bio-UTP and Bio-CTP), 1× DTT, 1× RNase inhibitor mix, and 1× T7 RNA polymerase and incubated at 37°C for 4 h. Labeled cRNA was then purified by using GeneChip Sample Cleanup Module and fragmented in 1× fragmentation buffer at 94°C for 35 min. For hybridization to the GeneChip Mouse Expression Array 430A or 430B or Mouse Genome 430 2.0 Array (Affymetrix), 15 μg of fragmented cRNA probe was incubated with 50 pM control oligonucleotide B2, 1× eukaryotic hybridization control, 0.1 mg/ml herring sperm DNA, 0.5 mg/ml acetylated BSA, and 1× hybridization buffer in a 45°C rotisserie oven for 16 h. Washing and staining were performed by using a GeneChip Fluidic Station (Affymetrix) according to the manufacturer's protocol. Phycoerythrin-stained arrays were scanned as digital image files and analyzed with GENECHIP OPERATING SOFTWARE (Affymetrix) (17).

Luciferase Assay. The *Kitl* promoter region (−2866 to −1 bp) was inserted into the pGL3-basic vector (Promega) for assay using the Luciferase Assay System (Promega) (14, 16). Cells at 40–50% confluence were transfected with a reference pRL-CMV plasmid (Promega) using Lipofectamine reagent (GIBCO/BRL, Grand Island, NY) to normalize transfection. Results shown are representative of five independent experiments.

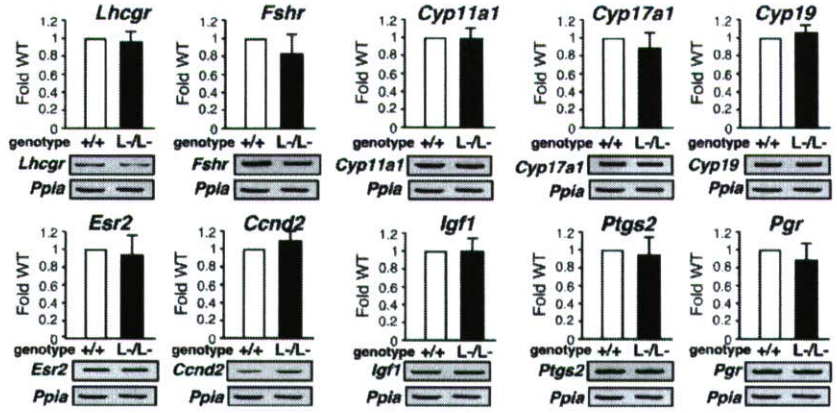

Fig. 3. No significant alterations in mRNA levels of several major regulators in folliculogenesis. Shown is semiquantitative RT-PCR of LH receptor (*Lhr*), FSH receptor (*Fshr*), p450 side chain cleavage enzyme (*Cyp11a1*), 17-α-hydroxylase (*Cyp17a1*), Aromatase (*Cyp19*), estrogen receptor-β (*Esr2*), cyclin D2 (*Ccnd2*), insulin-like growth factor 1 (*Igf1*), cyclooxygenase 2 (*Ptgs2*), or progesterone receptor (*Pgr*) gene expression in $AR^{+/+}$ and $AR^{-/-}$ ovaries. Results shown were representative (using one ovary per genotype in each experiment) of five independent experiments.

Results and Discussion

Subfertility of $AR^{-/-}$ Female Mice at 8 Weeks of Age. The *Ar* gene located on the X chromosome was disrupted in mice by using the Cre/Lox P system (6) (Fig. 1 *a–c*). Female $AR^{-/-}$ mice showed normal growth compared with the wild-type littermates (Fig. 1*d*), with no detectable bone loss (Fig. 1*e*) or obesity common for male $AR^{-/Y}$ mice (8, 9). Young (8-week-old) $AR^{-/-}$ females appeared indistinguishable from the wild-type littermates, displayed normal sexual behavior (7), and produced the first offspring of normal body size at the expected age. Macroscopic appearance of their reproductive organs, including uteri, oviducts, and ovaries, also appeared normal (Fig. 1*f*). Histological analysis showed no significant abnormality in the uterus or pituitary (Fig. 1*e*), whereas mammary ductal branching and elongation were substantially reduced, as revealed by whole-mount analysis (Fig. 1*h*). Serum levels of 17β-estradiol, progesterone, testosterone, luteinizing hormone, and follicle-stimulating hormone were also within normal range in 8-week-old mutant females at the proestrus stage (Fig. 1*g*), suggesting that the two-cell two-gonadotrophin system in female reproductive and endocrine organs (18) was intact in $AR^{-/-}$ mice at 8 weeks of age. The most obvious early sign of abnormal reproductive function in the $AR^{-/-}$ females was that their average numbers of pups per litter were only about half of those of the wild-type littermates, ($AR^{+/+}$, 8.3 ± 0.4 pups per litter; $AR^{-/-}$, 4.5 ± 0.5 pups per litter) (Fig. 1*i*).

***AR*$^{-/-}$ Female Mice Developed POF Phenotypes.** Histological analysis of 8-week-old $AR^{-/-}$ ovaries clearly showed that numbers of atretic follicles were significantly increased, with decreased numbers of corpora lutea (Fig. 2 *b* and *f*). This finding suggests that the reduced pup numbers were due to impaired folliculogenesis in AR-deficient ovaries. Indeed, AR protein expression was readily detectable in the wild-type 8-week-old ovaries (Fig. 1*j*), with AR expressed at the highest levels in growing follicle granulosa cells at all developmental stages and at relatively low levels in corpora lutea. Thus, AR appears to play a regulatory role in granulosa cells during their maturation to the luteal phase.

To investigate this possibility, we examined the ovarian phenotype of female $AR^{-/-}$ mice at different ages. At 3 weeks, ovaries contain various stages of follicles, including primary, secondary, and antral follicles in wild-type animals (Fig. 2*a*) (19). In $AR^{-/-}$ ovaries at 3 weeks of age, the folliculogenesis appeared to be unaltered, with normal numbers and localization of primary and secondary follicles (Fig. 2 *a* and *e*). However, degenerated folliculogenesis became evident with further aging. Although follicles and corpora lutea at all developmental stages were still present, corpora lutea numbers were clearly reduced in 8-week-old $AR^{-/-}$ mutants (Fig. 2 *b* and *f*), similar to that observed in another mouse line (20). Expected apoptosis was seen in atretic follicles by activated caspase-3 immunohistochemistry assays (Fig. 2*i*). But, by 32 weeks of age, defects in folliculogenesis in $AR^{-/-}$ ovaries became profound, with fewer follicles observed and increased atretic follicles (Fig. 2 *c* and *g*), and >40% (5 of 12 mice) of the $AR^{-/-}$ females were already infertile. By 40 weeks, all $AR^{-/-}$ females became infertile, with no follicles remaining (Fig. 2 *d* and *h*); at the same age, $AR^{+/+}$ females were fertile and had normal follicle numbers. Consistent with progressive deficiency in folliculogenesis, the pup number per litter steadily decreased in aging $AR^{-/-}$ females (Fig. 2*i*). These data indicate that AR plays an important physiological role at the preluteal phase of folliculogenesis.

Alteration in Gene Expressions of Several Major Regulators Involved in the Oocyte–Granulosa Cell Regulatory Loop. To explore the molecular basis underlying the impaired folliculogenesis in $AR^{-/-}$ ovaries, we analyzed expression of several major known regulators and markers of folliculogenesis (21–23). Surprisingly, no significant alterations in mRNA levels of LH receptor (*Lhr*), FSH receptor (*Fshr*), p450 side chain cleavage enzyme (*Cyp11a1*), 17-α-hydroxylase (*Cyp17a1*), aromatase (*Cyp19*), estrogen receptor-β (*Esr2*), cyclin D2 (*Ccnd2*), or insulin-like growth factor 1 (*Igf1*) of 8-week-old $AR^{-/-}$ ovaries at the proestrus stage, and further cyclooxygenase 2 (*Ptgs2*) or progesterone receptor (*Pgr*) at the estrus stage, were detected by

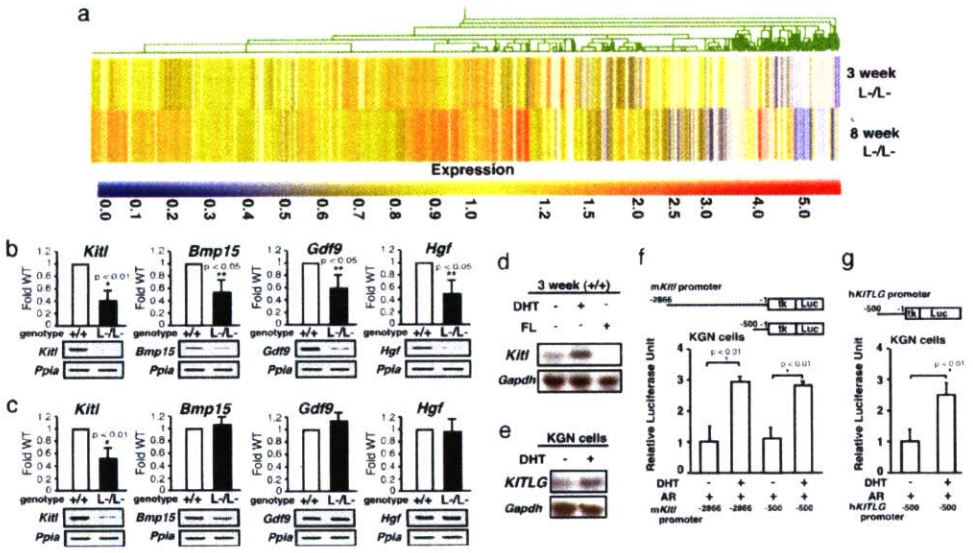

Fig. 4. Genome-wide microarray analysis and semiquantitative RT-PCR revealed that expression of the oocyte–granulosa cell regulator loop was down-regulated in $AR^{-/-}$ ovaries. (*a*) Microarray analysis of $AR^{-/-}$ compared with $AR^{+/+}$ ovaries at 3 and 8 weeks of age. Data obtained from microarray analysis as described in *Materials and Methods* were used to generate a cluster analysis. Each vertical line represents a single gene. The ratios of gene expression levels in $AR^{-/-}$ ovaries compared with wild type are presented. (*b* and *c*) Semiquantitative RT-PCR analysis of AR-regulated genes identified from the microarray study. Results shown are representative (using one ovary per genotype in each experiment) of five independent experiments. Data are shown as mean ± SEM and were analyzed by using Student's *t* test. (*d*) Comparison of *Kitl* gene expression by Northern blot analysis among placebo-, DHT-, and flutamide (FL)-treated $AR^{+/+}$ mouse ovaries. (*e*) Induction of *KITLG* gene expression by DHT treatment in KGN cells. (*f* and *g*) Androgen responsiveness in the mouse and human *kit ligand* promoters by a luciferase assay performed by using KGN cells. Data are shown as mean ± SEM and were analyzed by using Student's *t* test.

semiquantitative RT-PCR analysis (Fig. 3). Genome-wide microarray analysis (17) of RNA from 8-week-old $AR^{-/-}$ ovaries at the proestrus stage has been undertaken to identify AR-regulated genes. In comparison with $AR^{+/+}$ ovaries, expressions of 772 genes were down-regulated, whereas 351 genes were up-regulated in $AR^{-/-}$ ovaries (Fig. 4*a*; see also Tables 1 and 2, which are published as supporting information on the PNAS web site). Several genes known to be involved in the oocyte–granulosa cell regulatory loop (24) were identified as candidate AR target genes, including KIT ligand (*Kitl*) (25), morphogenetic protein 15 (*Bmp15*) (26), growth differentiation factor-9 (*Gdf9*) (27), and hepatocyte growth factor (*Hgf*) (28). Impaired folliculogenesis had been reported in mice deficient in each of these three regulators (26, 27, 29). To validate the microarray data, we performed semiquantitative RT-PCR analysis of 8-week-old $AR^{-/-}$ ovary RNA and confirmed that expression of these factors was down-regulated (Fig. 4*b*). To identify a regulator downstream of the AR signaling at an earlier stage of folliculogenesis, 3-week-old $AR^{-/-}$ ovaries that, as pointed out earlier, display no apparent phenotypic abnormality were examined. Fewer genes had altered expression levels (519 genes up-regulated; 326 genes down-regulated) (Fig. 4*a*; see also Tables 3 and 4, which are published as supporting information on the PNAS web site), and, of the four regulators tested by RT-PCR, only *Kitl* was found to be down-regulated at this age (Fig. 4*c*). Because *Kitl* is a granulosa cell-derived factor and stimulates oocyte growth and maturation (29–31), down-regulation of the *Kitl* expression in 3-week-old or even younger $AR^{-/-}$ ovaries may trigger impairment in folliculogenesis at a later age. To test for possible *Kitl* gene regulation by AR, 3-week-old wild-type females were treated with 5α-dihydrotestosterone (DHT). At 4 h after hormone injection, a clear induction of *Kitl* expression was observed in the ovaries, whereas a known antiandrogen flutamide attenuated the induction by DHT (Fig. 4*d*). The induction of endogenous human *kit ligand* (*KITLG*) gene by DHT was also observed in human granulosa-like tumor cells (KGN) in culture (Fig. 4*e*). Furthermore, androgen-induced transactivation of mouse and human *kit ligand* promoters (32) was observed by a luciferase reporter assay (33) in KGN (Fig. 4 *f* and *g*), 293T, and HeLa (data not shown) cells. However, no response to DHT was detected in the similar assay using promoters of the *Bmp15*, *Gdf9*, and *Hgf* genes (data not shown). Thus, we have shown that, in a regulatory cascade controlling folliculogenesis, *Kitl* represents a direct downstream target of androgen signaling.

As an upstream regulator, AR may also be indirectly involved in control of expression of other genes critical for folliculogenesis, because an age-dependent down-regulation of *Bmp15*, *Gdf9*, and *Hgf* gene expression was also observed in $AR^{-/-}$ ovaries. *Bmp15* and *Gdf9* are oocyte-derived factors that promote the development of surrounding granulosa cells in growing follicles (34, 35), whereas *Hgf* is secreted by theca cells and acts as a granulosa cell growth factor (36). Down-regulation of these factors, presumably due to decreased *Kitl* expression, may lead to impaired bidirectional communication between oocyte and granulosa cells (24) and, eventually, to early termination of folliculogenesis, as in POF syndrome.

Thus, we have identified AR as a novel regulator of folliculogenesis that apparently acts in the regulatory cascade upstream of the major factors controlling ovarian function, confirming the previous findings of the AR expression in granulose cells of growing follicles (3). Although not immediately relevant to the ovarian physiology, abnormal development of the mammary glands observed in our AR-deficient mice adds further strong evidence of an essential role of the AR not only in male, but also in female, reproductive function.

With increasing age of the first childbirth by women in the modern society, POF syndrome has become an important social and medical problem. Our findings suggest that POF syndrome may be caused by an impairment in androgen signaling and that X chromosomal mutations affecting the *AR* gene function may play a key role in hereditary POF. From clinical perspective, the present study provides evidence that AR can be a beneficial therapeutic target in treatment of POF syndrome patients.

We thank T. Iwamori and H. Tojo for expert advice on mammary gland anatomy, Y. Kanai for ovarian phenotypic analysis, members of the KO project team at the laboratory of Nuclear Signaling (Institute of Molecular and Cellular Biosciences) for their support, A. P. Kouzmenko for helpful suggestions, and H. Higuchi for manuscript preparation. This work was supported in part by the Program for Promotion of Basic Research Activities for Innovative Biosciences and priority areas from the Ministry of Education, Culture, Sports, Science, and Technology (to S.K.).

1. Laml, T., Preyer, O., Umek, W., Hengstschlager, M. & Hanzal, H. (2002) *Hum. Reprod. Update* **8,** 483–491.
2. Davison, R. M., Davis, C. J. & Conway, G. S. (1999) *Clin. Endocrinol. (Oxford)* **51,** 673–679.
3. Tetsuka, M., Whitelaw, P. F., Bremner, W. J., Millar, M. R., Smyth, C. D. & Hillier, S. G. (1995) *J. Endocrinol.* **145,** 535–543.
4. Ehrmann, D. A., Barnes, R. B. & Rosenfield, R. L. (1995) *Endocr. Rev.* **16,** 322–353.
5. Norman, R. J. (2002) *Mol. Cell. Endocrinol.* **191,** 113–119.
6. Kato, S. (2002) *Clin. Pediatr. Endocrinol.* **11,** 1–7.
7. Sato, T., Matsumoto, T., Kawano, H., Watanabe, T., Uematsu, Y., Sekine, K., Fukuda, T., Aihara, K., Krust, A., Yamada, T., *et al.* (2004) *Proc. Natl. Acad. Sci. USA* **101,** 1673–1678.
8. Sato, T., Matsumoto, T., Yamada, T., Watanabe, T., Kawano, H. & Kato, S. (2003) *Biochem. Biophys. Res. Commun.* **300,** 167–171.
9. Kawano, H., Sato, T., Yamada, T., Matsumoto, T., Sekine, K., Watanabe, T., Nakamura, T., Fukuda, T., Yoshimura, K., Yoshizawa, T., *et al.* (2003) *Proc. Natl. Acad. Sci. USA* **100,** 9416–9421.
10. Li, M., Indra, A. K., Warot, X., Brocard, J., Messaddeq, N., Kato, S., Metzger, D. & Chambon, P. (2000) *Nature* **407,** 633–636.
11. Sekine, K., Ohuchi, H., Fujiwara, M., Yamasaki, M., Yoshizawa, T., Sato, T., Yagishita, N., Matsui, D., Koga, Y., Itoh, N. & Kato, S. (1999) *Nat. Genet.* **21,** 138–141.
12. Yoshizawa, T., Handa, Y., Uematsu, Y., Takeda, S., Sekine, K., Yoshihara, Y., Kawakami, T., Arioka, K., Sato, H., Uchiyama, Y., *et al.* (1997) *Nat. Genet.* **16,** 391–396.
13. Gubbay, J., Collignon, J., Koopman, P., Capel, B., Economou, A., Munsterberg, A., Vivian, N., Goodfellow, P. & Lovell-Badge, R. (1990) *Nature* **346,** 245–250.
14. Yanagisawa, J., Yanagi, Y., Masuhiro, Y., Suzawa, M., Watanabe, M., Kashiwagi, K., Toriyabe, T., Kawabata, M., Miyazono, K. & Kato, S. (1999) *Science* **283,** 1317–1321.
15. Britt, K. L., Drummond, A. E., Cox, V. A., Dyson, M., Wreford, N. G., Jones, M. E., Simpson, E. R. & Findlay, J. K. (2000) *Endocrinology* **141,** 2614–2623.
16. Ohtake, F., Takeyama, K., Matsumoto, T., Kitagawa, H., Yamamoto, Y., Nohara, K., Tohyama, C., Krust, A., Mimura, J., Chambon, P., *et al.* (2003) *Nature* **423,** 545–550.
17. Fujimoto, N., Igarashi, K., Kanno, J., Honda, H. & Inoue, T. (2004) *J. Steroid Biochem. Mol. Biol.* **91,** 121–129.
18. Couse, J. F. & Korach, K. S. (1999) *Endocr. Rev.* **20,** 358–417.
19. Elvin, J. A. & Matzuk, M. M. (1998) *Rev. Reprod.* **3,** 183–195.
20. Hu, Y. C., Wang, P. H., Yeh, S., Wang, R. S., Xie, C., Xu, Q., Zhou, X., Chao, H. T., Tsai, M. Y. & Chang, C. (2004) *Proc. Natl. Acad. Sci. USA* **101,** 11209–11214.
21. Elvin, J. A., Yan, C., Wang, P., Nishimori, K. & Matzuk, M. M. (1999) *Mol. Endocrinol.* **13,** 1018–1034.
22. Zhou, J., Kumar, T. R., Matzuk, M. M. & Bondy, C. (1997) *Mol. Endocrinol.* **11,** 1924–1933.
23. Burns, K. H., Yan, C., Kumar, T. R. & Matzuk, M. M. (2001) *Endocrinology* **142,** 2742–2751.
24. Matzuk, M. M., Burns, K. H., Viveiros, M. M. & Eppig, J. J. (2002) *Science* **296,** 2178–2180.
25. Joyce, I. M., Pendola, F. L., Wigglesworth, K. & Eppig, J. J. (1999) *Dev. Biol.* **214,** 342–353.
26. Yan, C., Wang, P., DeMayo, J., DeMayo, F. J., Elvin, J. A., Carino, C., Prasad, S. V., Skinner, S. S., Dunbar, B. S., Dube, J. L., *et al.* (2001) *Mol. Endocrinol.* **15,** 854–866.
27. Dong, J., Albertini, D. F., Nishimori, K., Kumar, T. R., Lu, N. & Matzuk, M. M. (1996) *Nature* **383,** 531–535.
28. Parrott, J. A., Vigne, J. L., Chu, B. Z. & Skinner, M. K. (1994) *Endocrinology* **135,** 569–575.
29. Driancourt, M. A., Reynaud, K., Cortvrindt, R. & Smitz, J. (2000) *Rev. Reprod.* **5,** 143–152.
30. Huang, E. J., Manova, K., Packer, A. I., Sanchez, S., Bachvarova, R. F. & Besmer, P. (1993) *Dev. Biol.* **157,** 100–109.
31. Packer, A. I., Hsu, Y. C., Besmer, P. & Bachvarova, R. F. (1994) *Dev. Biol.* **161,** 194–205.
32. Grimaldi, P., Capolunghi, F., Geremia, R. & Rossi, P. (2003) *Biol. Reprod.* **69,** 1979–1988.
33. Kitagawa, H., Fujiki, R., Yoshimura, K., Mezaki, Y., Uematsu, Y., Matsui, D., Ogawa, S., Unno, K., Okubo, M., Tokita, A., *et al.* (2003) *Cell* **113,** 905–917.
34. Otsuka, F. & Shimasaki, S. (2002) *Proc. Natl. Acad. Sci. USA* **99,** 8060–8065.
35. Joyce, I. M., Clark, A. T., Pendola, F. L. & Eppig, J. J. (2000) *Biol. Reprod.* **63,** 1669–1675.
36. Parrott, J. A. & Skinner, M. K. (1998) *Endocrinology* **139,** 2240–2245.

nature medicine

Impaired flow-dependent control of vascular tone and remodeling in P2X4-deficient mice

Kimiko Yamamoto[1,6], Takaaki Sokabe[1,6], Takahiro Matsumoto[2], Kimihiro Yoshimura[2], Masahiro Shibata[1], Norihiko Ohura[1], Toru Fukuda[2], Takashi Sato[2], Keisuke Sekine[2], Shigeaki Kato[2], Masashi Isshiki[3], Toshiro Fujita[3], Mikio Kobayashi[4], Koichi Kawamura[4], Hirotake Masuda[4], Akira Kamiya[5] & Joji Ando[1]

The structure and function of blood vessels adapt to environmental changes such as physical development and exercise[1–3]. This phenomenon is based on the ability of the endothelial cells to sense and respond to blood flow[4–6]; however, the underlying mechanisms remain unclear. Here we show that the ATP-gated P2X4 ion channel[7,8], expressed on endothelial cells and encoded by *P2rx4* in mice, has a key role in the response of endothelial cells to changes in blood flow. *P2rx4*$^{-/-}$ mice do not have normal endothelial cell responses to flow, such as influx of Ca^{2+} and subsequent production of the potent vasodilator nitric oxide (NO). Additionally, vessel dilation induced by acute increases in blood flow is markedly suppressed in *P2rx4*$^{-/-}$ mice. Furthermore, *P2rx4*$^{-/-}$ mice have higher blood pressure and excrete smaller amounts of NO products in their urine than do wild-type mice. Moreover, no adaptive vascular remodeling, that is, a decrease in vessel size in response to a chronic decrease in blood flow, was observed in *P2rx4*$^{-/-}$ mice. Thus, endothelial P2X4 channels are crucial to flow-sensitive mechanisms that regulate blood pressure and vascular remodeling.

P2X-type ATP receptors are distributed throughout the entire body and are involved in the regulation of the physiological function of many tissues and organs[7]. When ATP binds to P2X receptors on the surface of cells, extracellular Ca^{2+} enters and activates signal transduction pathways that evoke a variety of cellular responses. Thus far, seven P2X subtypes, P2X1–7, have been cloned; all of them contain two transmembrane domains and function as cation channels in the form of hetero- or homo-oligomers[8]. An immunohistochemical analysis in rats has shown that P2X4 receptors are widely distributed in the central and peripheral nervous systems, the epithelium of exocrine glands and the airway, bladder smooth muscle, the gastrointestinal tract, uterus, arteries and adipose cells[9]. Recent studies including ours have shown that P2X4 is the most abundantly expressed P2X receptor subtype in vascular endothelial cells[10–12] and is the major contributor to ATP- and flow-induced Ca^{2+} influx in endothelial cells[13].

Endothelial cells are in direct contact with blood flow and are exposed to shear stress, the frictional force exerted by flowing blood. A number of recent studies have shown that endothelial cells recognize changes in shear stress and transmit signals to the interior of the cell, which leads to cellular responses that involve changes in cell morphology, cell function and gene expression[5]. These endothelial cell responses to shear stress are thought to have important roles in blood flow–dependent phenomena, such as control of vascular tone, angiogenesis, vascular remodeling and atherogenesis. Ca^{2+} signaling has an important role in shear-stress signal transduction; it has been shown that a shear stress–dependent Ca^{2+} influx occurs in bovine and human endothelial cells when exposed to flow in the presence of extracellular ATP[10,14], and treatment of endothelial cells with antisense oligonucleotides designed to knock down expression of *P2RX4* abolishes the shear stress–dependent Ca^{2+} influx[13]. Human embryonic kidney 293 cells do not exhibit a Ca^{2+} response to flow, but when transfected with *P2RX4* cDNA, they express P2X4 receptors and exhibit shear stress–dependent Ca^{2+} influx[13]. These findings suggest that P2X4 receptors have a 'shear-transducer' property through which shear stress signals are transmitted into the cell interior through influx of Ca^{2+}. It has also been shown that endothelial cells release ATP in response to shear stress[15], but the physiological and pathological significance of this shear-sensing mechanism through ATP and its receptors is not fully understood. To gain insight into its significance, we generated *P2rx4*-deficient mice using embryonic stem cells (**Supplementary Fig. 1** online).

Northern blot analysis in *P2rx4*$^{-/-}$ mice detected no *P2rx4* mRNA in pulmonary microvessel endothelial cells, confirming inactivation of *P2rx4* (**Fig. 1a**). Comparison of levels of mRNA encoding P2X subtypes by a competitive PCR method showed that P2X4 was the most strongly expressed isoform in endothelial cells of wild-type mice, but was absent in endothelial cells of *P2rx4*$^{-/-}$ mice (**Fig. 1b**). No compensatory upregulation of any subtypes occurred in the endothelial cells of *P2rx4*$^{-/-}$ mice. The absence of the P2X4 receptor in endothelial cells of *P2rx4*$^{-/-}$ mice was also confirmed at the protein level. A P2X4-specific antibody showed high levels of immunoreactivity in

[1]Department of Biomedical Engineering, Graduate School of Medicine, University of Tokyo, Tokyo 113-0033, Japan. [2]Institute of Molecular and Cellular Biosciences, University of Tokyo, Tokyo 113-0032, Japan. [3]Department of Nephrology and Endocrinology, Graduate School of Medicine, University of Tokyo, Tokyo 113-8655, Japan. [4]Second Department of Pathology, Akita University School of Medicine, Akita 010-8543, Japan. [5]Interdisciplinary Science Center, Nihon University, Tokyo 102-0074, Japan. [6]These authors contributed equally to this work. Correspondence should be addressed to J.A. (joji@m.u-tokyo.ac.jp).

Received 3 October; accepted 3 November; published online 4 December 2005; doi:10.1038/nm1338

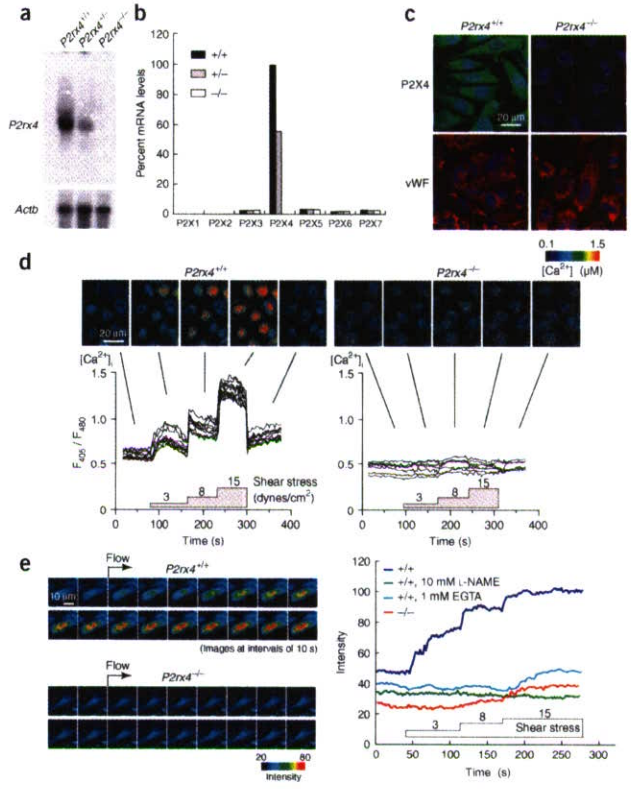

Figure 1 Impaired endothelial cell responses to flow in *P2rx4*$^{-/-}$ mice. (**a**) Northern blots of *P2rx4* mRNA from cultured pulmonary microvessel endothelial cells. The *Actb* signal was used as a loading control. (**b**) Competitive PCR analysis of the levels of mRNA encoding P2X subtypes. (**c**) Immunostaining for P2X4 receptor and an endothelial cell–specific marker, von Willebrand factor (vWF). (**d**) Flow-induced Ca^{2+} responses. Each graph represents eight $[Ca^{2+}]_i$ responses of 8–10 single cells. (**e**) Flow-induced production of NO. Left, pseudocolor images of DAF-2. Right, changes in DAF-2 intensity of 15–20 cells. Production of NO by endothelial cells of wild-type mice increased in a shear stress–dependent manner, and the increase was abolished by the NO synthase inhibitor L-NAME (10 mM) and the Ca^{2+} chelator EGTA (1 mM). Endothelial cells of *P2rx4*$^{-/-}$ mice did not show flow-induced production of NO.

wild-type mice, but no immunoreactivity in endothelial cells of *P2rx4*$^{-/-}$ mice (**Fig. 1c**). Endothelial cells of both wild-type and *P2rx4*$^{-/-}$ mice were positive for von Willebrand factor, a marker protein for endothelial cells.

The absence of P2X4 receptors impaired the response of endothelial cells to flow stimulation. When endothelial cells of wild-type mice were exposed to flow, the intracellular concentration of Ca^{2+} ($[Ca^{2+}]_i$) increased stepwise in tandem with the increases in shear stress (**Fig. 1d**), whereas no flow-induced Ca^{2+} responses occurred in endothelial cells of *P2rx4*$^{-/-}$ mice. As increases in $[Ca^{2+}]_i$ directly lead to the production of a potent vasodilator, nitric oxide (NO)[16], we examined the endothelial cells for changes in NO production with a fluorescence indicator, diaminofluorescein (DAF-2)[17]. Production of NO by endothelial cells of wild-type mice increased in response to flow, and this response was dependent on shear stress (**Fig. 1e**). Endothelial cells of *P2rx4*$^{-/-}$ mice, however, did not show flow-induced production of NO, indicating that P2X4 channels are involved in endothelial production of NO. The impaired flow-induced influx of Ca^{2+} and production of NO were rescued by *P2rx4* gene transfer using adenovirus vectors (**Fig. 2**). Adenovirus vector–mediated gene transfection was highly efficient and effective for the reintroduction of P2X4 into cultured endothelial cells. The spontaneous release of NO in healthy arteries is well known, but the exact trigger of the release remains unclear. As endothelial cells release ATP in response to shear stress, the released ATP may activate endothelial P2X4 receptors, leading to release of NO.

Increases in blood flow and administration of ATP cause vasodilation *in vivo*, and both flow- and ATP-mediated vasodilation are dependent on an intact endothelium and are mainly mediated by NO and prostaglandins[18]. We therefore examined the effects of P2X4 deficiency on the endothelium-dependent vasodilator response in mouse cremaster muscle. When acetylcholine (ACh) or ATP was administered through the jugular vein, arterioles that had been preconstricted with phenylephrine dilated in a dose-dependent manner in wild-type mice (**Fig. 3a**). In *P2rx4*$^{-/-}$ mice, however, ATP-induced vasodilation was markedly suppressed, but ACh-induced vasodilation was not suppressed at all. Occlusion of one of the branches of an arteriole with a glass micropipette increased blood flow through the other branch, and the increase in blood flow caused marked vasodilation in wild-type mice, but much less prominent vasodilation in *P2rx4*$^{-/-}$ mice (**Fig. 3b**). The blockade of NO synthesis by N^G-nitro-L-arginine methyl ester (L-NAME) markedly reduced flow-induced dilation in both types of mice. Flow-mediated vasodilator responses were also examined *ex vivo* in isolated arteries. Mesenteric arteries isolated from wild-type mice dilated in response to flow (shear stress, 20 dynes/cm^2), ATP and ACh, whereas the mesenteric arteries of *P2rx4*$^{-/-}$ mice dilated in response to ACh, but not to flow or ATP (**Fig. 3c**). The addition of EGTA or L-NAME considerably decreased flow-induced vasodilation in both types of mice, indicating that Ca^{2+} influx and NO mediate the vasodilation. The impaired flow-induced vasodilation in the *P2rx4*$^{-/-}$ mice was not the result of enhanced myogenic responses or changes in the composition or rigidity of vessel walls (**Supplementary Fig. 2** online).

No differences in external appearance, weight gain, food or water intake, or urine volume were seen between wild-type and *P2rx4*$^{-/-}$ mice during the 6-month period of the study. But we did observe a marked difference in blood pressure, as determined by intra-arterial

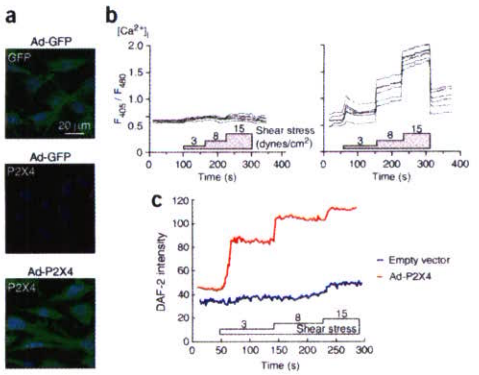

Figure 2 *P2rx4* gene transfer rescued the impaired flow-induced influx of Ca^{2+} and production of NO in cultured endothelial cells from *P2rx4*$^{-/-}$ mice. (**a**) Fluorescence photomicrographs of endothelial cells 5 d after gene transfection. Top, green fluorescent protein (GFP) expression. Ad-GFP, adenovirus vectors containing the GFP coding sequence. Center and bottom, immunostaining for the P2X4 receptor. Ad-P2X4, adenovirus vector containing mouse *P2rx4* cDNA. (**b**) Flow-induced Ca^{2+} responses. Endothelial cells transfected with Ad-P2X4 showed a shear stress–dependent increase in $[Ca^{2+}]_i$ (right), whereas endothelial cells transfected with empty vector did not (left). (**c**) Flow-induced production of NO. Production of NO by endothelial cells transfected with Ad-P2X4 increased in a shear stress–dependent manner, whereas production in endothelial cells transfected with empty vector did not. Results are representative of three experiments.

catheter measurements, with significantly higher values recorded in *P2rx4*$^{-/-}$ mice than in wild-type mice (**Fig. 4a,b**). No difference in heart rate was seen between the two groups of mice (**Fig. 4c**). But we did observe a difference in NO production. The daily amount of nitrite and nitrate (NOx) excreted in the urine was significantly less in *P2rx4*$^{-/-}$ mice than in wild-type mice (**Fig. 4d**). The decrease in NO production may be partly responsible for the increase in blood pressure in the *P2rx4*$^{-/-}$ mice.

Chronic changes in blood flow through large arteries induce structural remodeling of the vascular wall. Increases in blood flow cause enlargement of vessel diameter, whereas decreases in blood flow have the opposite effect[1,4,19]. To examine the role of the P2X4 receptor in flow-dependent vascular remodeling, we ligated the left external carotid artery of mice for 2 weeks. The ligation reduced flow in the left common carotid artery (**Supplementary Figs. 2** and **3** online), and we histologically compared the diameters of the left and the right common carotid arteries at the end of the 2-week period. Ligation of the left external carotid artery resulted in a substantial reduction in lumen diameter in the left common carotid artery in wild-type mice, but not in *P2rx4*$^{-/-}$ mice (**Fig. 4e**). The diameter of the right common carotid artery of *P2rx4*$^{-/-}$ mice was smaller than the diameter of the right common carotid artery of wild-type mice, and its walls were thicker (**Fig. 4f**), indicating that deficiency of P2X4 caused structural vascular changes under baseline conditions. The absence of flow-induced changes in diameter and the increase in medial wall thickness seen in *P2rx4*$^{-/-}$ mice resembled the structural changes that occur in eNOS-deficient mice[20], suggesting that *P2rx4* has a crucial role through endothelial production of NO in controlling vascular structural adaptation to chronic changes in blood flow.

A considerable amount of research has been devoted to the mechanotransduction of shear stress in endothelial cells. But the identity of shear stress receptors and the final signaling pathways they evoke remain unclear. Several endothelial proteins and structures,

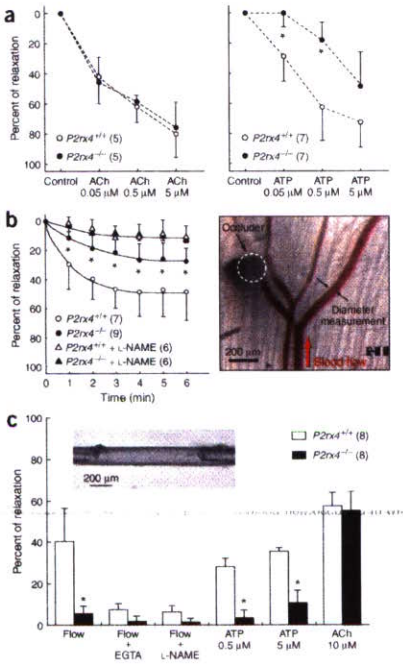

Figure 3 Impaired vasodilatory responses in *P2rx4*$^{-/-}$ mice. We examined cremaster muscle arterioles and mesenteric arteries for changes in diameter in response to various stimuli. Changes in vessel diameter are expressed as percentages: 0% represents the diameter of the vessel constricted with phenylephrine (10 μM), and 100% represents the diameter of the vessel dilated with papaverine (5 mM). (**a**) Vasodilatory response of cremaster muscle arterioles to ACh and ATP. Injection of ACh or ATP through the jugular vein induced marked vasodilation in both wild-type and *P2rx4*$^{-/-}$ mice, but vasodilation induced by ATP was significantly less in *P2rx4*$^{-/-}$ mice. (**b**) Vasodilatory response of cremaster muscle arterioles to flow. One of the branches of an arteriole was compressed with a glass micropipette (Occluder) to stop blood flow, and the other branch, in which the blood flow increased, was examined for changes in diameter. Dilation in response to increased blood flow occurred in wild-type mice, but the response was much weaker in *P2rx4*$^{-/-}$ mice. Administration of L-NAME significantly reduced the flow-induced dilation in both types of mice. (**c**) Vasodilatory response of mesenteric arteries. Data are reported as percentage relaxation 5 min after application of each stimulus, when maximum response was observed. Flow- or ATP-induced dilation was significantly weaker in *P2rx4*$^{-/-}$ mice compared with wild-type mice. Addition of EGTA or L-NAME markedly suppressed flow-induced vasodilation in both types of mice. Sample numbers are indicated in parentheses. $^*P < 0.01$.

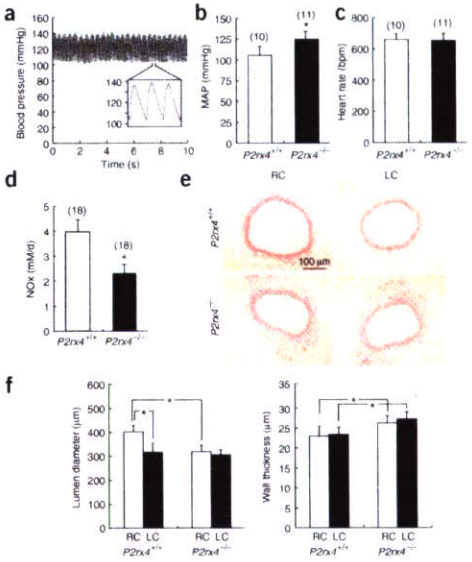

Figure 4 *P2rx4*$^{-/-}$ mice show higher blood pressure with less production of NO and impaired blood flow–induced vascular remodeling. (**a**) Representative pressure recordings of unrestrained, conscious *P2rx4*$^{-/-}$ mice 1 week after implantation of a radiotelemeter in the thoracic aorta through the left carotid artery. (**b**) Mean arterial pressure (MAP). Values are 24-h averages of the basal MAP obtained 1 week after surgery. MAP was significantly higher in *P2rx4*$^{-/-}$ mice than in wild-type mice. (**c**) Heart rate. No difference in heart rate was seen between the two types of mice. (**d**) The amount of nitrite and nitrate (NOx) in 24-h urine samples was significantly lower in *P2rx4*$^{-/-}$ mice than in wild-type mice. Sample numbers are indicated in parentheses. $^*P < 0.01$. (**e**) Hematoxylin-eosin–stained cross-sections of the right common carotid artery (RC) and left common carotid aretery (LC). In wild-type mice, the diameter of the lumen of the LC became smaller than that of the RC. By contrast, the diameter of the LC in *P2rx4*$^{-/-}$ mice did not change. Medial thickening was observed in the arteries of *P2rx4*$^{-/-}$ mice. (**f**) Quantitative analysis of changes in lumen diameter and wall thickness. After ligation the diameter of the LC decreased significantly in wild-type mice, but not in *P2rx4*$^{-/-}$ mice. The diameter of the RC of *P2rx4*$^{-/-}$ mice was significantly smaller than that of wild-type mice. The wall thickness of the RC and LC of *P2rx4*$^{-/-}$ mice was significantly greater than that of wild-type mice. Data are expressed as the mean ± s.d. $^*P < 0.01$. $n = 10$ and 12 mice for wild-type and *P2rx4*$^{-/-}$ mice, respectively.

including ion channels, tyrosine receptors, caveolae, G proteins, adhesion molecules and cytoskeletons, have been considered as potential candidates for shear stress receptors[21]. Multiple signaling pathways are activated through these receptors downstream of shear stress sensing[5]. For instance, the phosphorylation of protein kinases, such as extracellular signal–regulated kinase (ERK1/2), p130 Crk-associated substrate (Cas) and focal adhesion kinase (FAK), occurs in endothelial cells immediately after exposure to shear stress[22,23]. Flow-induced phosphorylation of ERK1/2, but not of Cas or FAK, was partially inhibited in *P2rx4*$^{-/-}$ mice (**Supplementary Fig. 4** online). Thus, P2X4-mediated signaling events do not seem to be independent, but instead are involved in cross-talk with other signaling pathways.

The gene-knockout approach has contributed to the clarification of the physiological and pathological roles of each P2X receptor subtype. For instance, mice lacking P2X1 show reduced contraction of vas deferens and male infertility[24]. Studies of *P2rx3*$^{-/-}$ mice have indicated that P2X3 is crucial for peripheral pain responses and the afferent pathway that controls urinary bladder volume reflexes[25,26]. Pharmacological blockade of P2X4 receptors has shown them to be involved in the tactile allodynia that occurs after nerve injury[27]. Here we show that P2X4 channels have a crucial role in controlling vascular tone and vascular remodeling. But the abovementioned roles may not hold in all other vascular beds, as the expression of P2X4 varies greatly among different vascular beds[12]. Deficiency of P2X4 severe enough to abolish ATP- or flow-induced Ca^{2+} influx probably reduces endothelial production of NO, which in turn increases vascular tone. In addition to its role as a vasodilator, NO negatively regulates proliferation of smooth muscle[28]; thus, a reduction in NO production may cause an increase in vascular wall thickness. These changes in vascular tone and vessel wall geometry may explain why *P2rx4*$^{-/-}$ mice are hypertensive. Vascular smooth muscle predominantly expresses P2X1; thus, it is unlikely that deficiency of P2X4 directly affects the tone of vascular smooth muscle. But the possibility remains that deficiency of P2X4 may impair nervous system function and increase vascular tone. Although further studies are needed to resolve this issue, our results provide insight that will allow better understanding of the molecular mechanisms involved in the regulation of vascular tone and vascular remodeling through ATP and its receptors. This in turn may lead to the development of new therapies for the control of blood pressure disorders.

METHODS

Northern blot analysis. We evaluated *P2rx4* mRNA levels using northern blot analysis, as previously described[10].

Competitive PCR. We performed competitive PCR as previously described[10].

Cell culture. We performed primary culture of microvessel endothelial cells from murine lung tissue as previously reported[29].

Immunohistochemistry. We performed detection of the P2X4 receptor and von Willebrand factor (NeoMarkers) using antibodies as previously described[10].

Determination of $[Ca^{2+}]_i$. We placed the coverslip on which we loaded endothelial cells with Indo-1/AM (Dojindo) in a parallel plate–type flow chamber (FCS2, Bioptechs, Inc.), and perfused Hanks balanced salt solution (HBSS) through the chamber with a peristaltic pump to stimulate cells at 37 °C. We monitored flow-induced changes in $[Ca^{2+}]_i$ with a confocal laser scanning system (MRC-1000UV, Bio-Rad) equipped with an ultraviolet argon ion laser, as previously described[10,13].

Measurement of NO production. We measured the concentration of nitrite and nitrate (NOx) in urine by fluorometric assay with a spectrofluorometer. We evaluated production of NO in cells by real-time imaging of NO with a fluorescent indicator, diaminofluorescein-2 diacetate (DAF-2 DA; 10 μM, Daiichi Pure Chemicals) as previously described[17].

Gene transfer by adenovirus vectors. We constructed adenovirus vectors containing murine *P2rx4* cDNA or cDNA encoding green fluorescent protein (GFP) using the Adeno-X Expression System (BD Biosciences) according to the manufacturer's protocol. We infected cultured endothelial cells with 50 plaque-forming units/cell of either adenovirus vector.

Mice. All protocols were approved by the Institutional Animal Care and Use Committee of the University of Tokyo.

Measurement of blood pressure. We measured blood pressure in unrestrained, conscious mice using a commercially available telemetry and computer-based data acquisition system (Data Sciences International) according to a previously described method[30]. Briefly, we anesthetized mice with halothane inhalation. We then implanted a pressure-sensing catheter in the thoracic aorta through the left carotid artery, and we placed a radio-telemetry transmitter under the skin along the right flank. After recovery from the anesthesia, we returned the mice to their home cages (placed atop telemetry receivers), where we continuously monitored their blood pressure and heart rate.

Diameter measurements in arterioles and arteries. We anesthetized mice with urethane, and we cannulated a jugular vein to facilitate the injection of chemicals. We observed microcirculation in the cremaster muscle with an intravital microscope. One of the branches of an arteriole was compressed with a glass micropipette (Occluder) to stop blood flow, and the other branch, in which the blood flow increased, was examined for changes in diameter. We filmed the microcirculation with a CCD camera, and analyzed changes in the diameter of large arterioles having a baseline diameter of 40-80 μm using images shown on a television monitor.

Mesenteric resistance-artery preparation. We isolated mesenteric artery segments that had an internal diameter of ~200 μm, cannulated them at both ends and mounted them in a video-monitored perfusion system. We bathed segments in an organ bath containing Krebs solution and perfused them at flow rates ranging from 0 to 150 μl/min at a constant pressure (60 mmHg). We monitored the pressure in both ends of the artery segment with pressure transducers.

External carotid artery ligation. We ligated the left external carotid artery of mice at its origin with 11-0 nylon sutures. After 2 weeks, we anesthetized mice with urethane and perfused them through the left ventricle with PBS at a constant pressure (100 mmHg), and then perfusion-fixed them with freshly depolymerized 4% paraformaldehyde in PBS. We excised and post-fixed both common carotid arteries overnight at 4 °C. We excised parallel segments of the left and right common carotid arteries at the midpoint of the vessels, and after embedding them in O.C.T. (Tissue-Tek), we cut cross-sections (3–5 μm thick) for hematoxylin-eosin staining and Elastica Masson staining. We morphometrically analyzed the carotid arteries by video microscopy. The image was displayed on a computer monitor, and the vessel perimeter was measured using the US National Institutes of Health image software. The perimeter of the vessel lumen was taken as the circumference of a circle (C) and lumen diameter (D) was determined from the equation $D = C/\pi$, assuming that the vessel cross-sections were circular *in vivo*. We measured medial wall thickness on images of Elastica Masson–stained vessels as the linear distance from the inner elastic lamina to the external elastic lamina at a magnification of ×200. We measured four sites 90° apart in each of two serial vessel sections, and we averaged the values.

Statistical analysis. We evaluated statistical significance by an ANOVA and a Bonferonni adjustment was applied to the results of a *t* test with SPSS software (SPSS Inc). Data are expressed as means ± s.d. $P < 0.01$ was regarded as statistically significant.

Note: Supplementary information is available on the Nature Medicine website.

ACKNOWLEDGMENTS

This study was partly supported by Grants-in-Aid for Scientific Research from the Japan Society for the Promotion of Science and by a grant from the Japan Health Sciences Foundation. The authors are grateful to U. Chung and F. Kugimiya (Divisions of Tissue Engineering and Sensory & Motor System Medicine, Faculty of Medicine, University of Tokyo) for suggestions on technical issues in establishing of adenovirus vectors. We also thank Y. Sawada for technical assistance.

COMPETING INTERESTS STATEMENT

The authors declare that they have no competing financial interests.

Published online at http://www.nature.com/naturemedicine/
Reprints and permissions information is available online at http://npg.nature.com/reprintsandpermissions/

1. Kamiya, A. & Togawa, T. Adaptive regulation of wall shear stress to flow change in the canine carotid artery. *Am. J. Physiol.* **239**, H14–H21 (1980).
2. Guyton, J.R. & Hartley, C.J. Flow restriction of one carotid artery in juvenile rats inhibits growth of arterial diameter. *Am. J. Physiol.* **248**, H540–H546 (1985).
3. Hudlicka, O., Brown, M. & Egginton, S. Angiogenesis in skeletal and cardiac muscle. *Physiol. Rev.* **72**, 369–417 (1992).
4. Langille, B.L. & O'Donnell, F. Reductions in arterial diameter produced by chronic decreases in blood flow are endothelium-dependent. *Science* **231**, 405–407 (1986).
5. Davies, P.F. Flow-mediated endothelial mechanotransduction. *Physiol. Rev.* **75**, 519–560 (1995).
6. Burnstock, G. Release of vasoactive substances from endothelial cells by shear stress and purinergic mechanosensory transduction. *J. Anat.* **194**, 335–342 (1999).
7. North, R.A. Molecular physiology of P2X receptors. *Physiol. Rev.* **82**, 1013–1067 (2002).
8. Vial, C., Roberts, J.A. & Evans, R.J. Molecular properties of ATP-gated P2X receptor ion channels. *Trends Pharmacol. Sci.* **25**, 487–493 (2004).
9. Burnstock, G. & Knight, G.E. Cellular distribution and functions of P2 receptor subtypes in different systems. *Int. Rev. Cytol.* **240**, 31–304 (2004).
10. Yamamoto, K. *et al.* P2X(4) receptors mediate ATP-induced calcium influx in human vascular endothelial cells. *Am. J. Physiol. Heart Circ. Physiol.* **279**, H285–H292 (2000).
11. Glass, R. & Burnstock, G. Immunohistochemical identification of cells expressing ATP-gated cation channels (P2X receptors) in the adult rat thyroid. *J. Anat.* **198**, 569–579 (2001).
12. Ray, F.R., Huang, W., Slater, M. & Barden, J.A. Purinergic receptor distribution in endothelial cells in blood vessels: a basis for selection of coronary artery grafts. *Atherosclerosis* **162**, 55–61 (2002).
13. Yamamoto, K., Korenaga, R., Kamiya, A. & Ando, J. Fluid shear stress activates Ca^{2+} influx into human endothelial cells via P2X4 purinoceptors. *Circ. Res.* **87**, 385–391 (2000).
14. Mo, M., Eskin, S.G. & Schilling, W.P. Flow-induced changes in Ca^{2+} signaling of vascular endothelial cells: effect of shear stress and ATP. *Am. J. Physiol.* **260**, H1698–H1707 (1991).
15. Milner, P., Bodin, P., Loesch, A. & Burnstock, G. Rapid release of endothelin and ATP from isolated aortic endothelial cells exposed to increased flow. *Biochem. Biophys. Res. Commun.* **170**, 649–656 (1990).
16. Fleming, I., Bauersachs, J. & Busse, R. Calcium-dependent and calcium-independent activation of the endothelial NO synthase. *J. Vasc. Res.* **34**, 165–174 (1997).
17. Kojima, H. *et al.* Detection and imaging of nitric oxide with novel fluorescent indicators: diaminofluoresceins. *Anal. Chem.* **70**, 2446–2453 (1998).
18. Koller, A., Sun, D., Huang, A. & Kaley, G. Corelease of nitric oxide and prostaglandins mediates flow-dependent dilation of rat gracilis muscle arterioles. *Am. J. Physiol.* **267**, H326–H332 (1994).
19. Masuda, H. *et al.* Increase in endothelial cell density before artery enlargement in flow-loaded canine carotid artery. *Arteriosclerosis* **9**, 812–823 (1989).
20. Rudic, R.D. *et al.* Direct evidence for the importance of endothelium-derived nitric oxide in vascular remodeling. *J. Clin. Invest.* **101**, 731–736 (1998).
21. Resnick, N. *et al.* Fluid shear stress and the vascular endothelium: for better and for worse. *Prog. Biophys. Mol. Biol.* **81**, 177–199 (2003).
22. Okuda, M. *et al.* Shear stress stimulation of p130(cas) tyrosine phosphorylation requires calcium-dependent c-Src activation. *J. Biol. Chem.* **274**, 26803–26809 (1999).
23. Li, S. *et al.* Fluid shear stress activation of focal adhesion kinase. Linking to mitogen-activated protein kinases. *J. Biol. Chem.* **272**, 30455–30462 (1997).
24. Mulryan, K. *et al.* Reduced vas deferens contraction and male infertility in mice lacking P2X1 receptors. *Nature* **403**, 86–89 (2000).
25. Cockayne, D.A. *et al.* Urinary bladder hyporeflexia and reduced pain-related behaviour in *P2X3*-deficient mice. *Nature* **407**, 1011–1015 (2000).
26. Vlaskovska, M. *et al. P2X3* knock-out mice reveal a major sensory role for urothelially released ATP. *J. Neurosci.* **21**, 5670–5677 (2001).
27. Tsuda, M. *et al.* P2X4 receptors induced in spinal microglia gate tactile allodynia after nerve injury. *Nature* **424**, 778–783 (2003).
28. Garg, U.C. & Hassid, A. Nitric oxide-generating vasodilators and 8-bromo-cyclic guanosine monophosphate inhibit mitogenesis and proliferation of cultured rat vascular smooth muscle cells. *J. Clin. Invest.* **83**, 1774–1777 (1989).
29. Kuhlencordt, P.J. *et al.* Role of endothelial nitric oxide synthase in endothelial activation: insights from eNOS knockout endothelial cells. *Am. J. Physiol. Cell Physiol.* **286**, C1195–C1202 (2004).
30. Butz, G.M. & Davisson, R.L. Long-term telemetric measurement of cardiovascular parameters in awake mice: a physiological genomics tool. *Physiol. Genomics* **5**, 89–97 (2001).

nature medicine

Carminerin contributes to chondrocyte calcification during endochondral ossification

Takashi Yamada[1], Hirotaka Kawano[1], Yu Koshizuka[1], Toru Fukuda[2], Kimihiro Yoshimura[2], Satoru Kamekura[1], Taku Saito[1], Toshiyuki Ikeda[1], Yosuke Kawasaki[1], Yoshiaki Azuma[3], Shiro Ikegawa[4], Kazuto Hoshi[1], Ung-il Chung[1], Kozo Nakamura[1], Shigeaki Kato[2] & Hiroshi Kawaguchi[1]

Endochondral ossification is an essential process not only for physiological skeletal development and growth, but also for pathological disorders. We recently identified a novel cartilage-specific molecule, carminerin (also known as cystatin 10 and encoded by *Cst10*), which is upregulated in synchrony with cartilage maturation and stimulates the later differentiation of cultured chondrocytes[1]. Although carminerin-deficient (*Cst10*$^{-/-}$) mice developed and grew normally, they had a microscopic decrease in the calcification of hypertrophic chondrocytes at the growth plate. When we created experimental models of pathological endochondral ossification, we observed suppression of chondrocyte calcification during formation of osteoarthritic osteophytes, age-related ectopic ossification and healing of bone fractures in *Cst10*$^{-/-}$ mice. Cultured *Cst10*$^{-/-}$ chondrocytes showed a reduction in calcification with activation of an SRY site in the promoter of the gene encoding nucleotide pyrophosphatase phosphodiesterase 1 (NPP1, encoded by *Enpp1*). Functional NPP1 is required for carminerin deficiency to suppress the pathological endochondral ossifications listed above. Carminerin is the first cartilage-specific protein that contributes to chondrocyte calcification during endochondral ossification under physiological and pathological conditions through the transcriptional inhibition of NPP1.

We generated *Cst10*$^{-/-}$ mice by homologous recombination in mouse embryonic stem cells using a targeting vector to replace exon 1 with the phosphoglycerate kinase-neomycin (PGKneo) cassette (**Fig. 1a**). Inbreeding of heterozygous *Cst10*$^{+/-}$ mice yielded *Cst10*$^{-/-}$ mice, as determined by Southern blot analysis, at the expected mendelian ratio (**Fig. 1b**). Neither *Cst10* transcripts nor carminerin protein was detected in the rib cartilage of *Cst10*$^{-/-}$ mice, confirming disruption of the *Cst10* gene (**Fig. 1c,d**). *Cst10*$^{-/-}$ mice developed and grew similarly to wild-type (*Cst10*$^{+/+}$) and *Cst10*$^{+/-}$ littermates without abnormalities of major organs (**Fig. 1e,f**).

Radiological analyses of femurs and tibiae in 8-week-old mice showed that *Cst10*$^{-/-}$ mice experienced decreases in trabecular bone volume mainly at the metaphysis, but not in cortical bone at the diaphysis, as compared to the wild-type littermates (**Fig. 2a,b** and **Supplementary Fig. 1** online). Histological examination of the proximal tibias indicated a decrease in trabecular bone volume beneath the growth plate of *Cst10*$^{-/-}$ mice (**Fig. 2c**). Although expression of carminerin was localized mainly in the wild-type hypertrophic chondrocytes, the columnar architecture, expression of type X collagen (Col X) and the entire width of the growth plate were comparable between wild-type and *Cst10*$^{-/-}$ mice, indicating that hypertrophic differentiation of chondrocytes was not affected by the carminerin deficiency (**Fig. 2c,d**). The width of the calcified layer and the number of calcified chondrocytes, as determined by von Kossa staining, however, were reduced (**Fig. 2c,d**). Bone volume in the *Cst10*$^{-/-}$ primary spongiosa just beneath the growth plate was significantly reduced ($P < 0.01$), with normal numbers of tartrate-resistant acid phosphatase (TRAP)-positive chondroclasts or osteoclasts, whereas the secondary spongiosa was not affected (**Fig. 2c,d** and **Supplementary Fig. 1**). In vertebral bodies that undergo less longitudinal growth by the thinner growth plate than femurs and tibiae, the histomorphometric parameters were comparable between the two genotypes in the growth plate and the primary and secondary spongiosa (**Supplementary Fig. 1**). These findings indicate that the decrease in trabecular bone adjacent to the growth plate of *Cst10*$^{-/-}$ long bones under physiological conditions resulted primarily from impairment of the calcification of hypertrophic chondrocytes, but not from the abnormality of cartilage resorption by chondroclasts or bone formation by osteoblasts.

We then examined the involvement of carminerin in pathological endochondral ossification by using experimental models involving wild-type and *Cst10*$^{-/-}$ littermates. First, we investigated the role of carminerin in the pathogenesis of osteoarthritis by inducing instability in the mouse knee joint[2]. The joint cartilage destruction was similarly visible at the posterior of the tibias (**Fig. 3a**) in both genotypes. The

[1]Department of Sensory & Motor System Medicine, Faculty of Medicine, University of Tokyo, Hongo 7-3-1, Bunkyo, Tokyo 113-8655, Japan. [2]Institute of Molecular and Cellular Biosciences, University of Tokyo, Yayoi 1-1-1, Bunkyo, Tokyo 113-0032, Japan. [3]Teijin Institute for Biomedical Research, Asahigaoka 4-3-2, Hino, Tokyo 191-8512, Japan. [4]Institute of Physical and Chemical Research (RIKEN), Shirokanedai, Minato, Tokyo 106-8639, Japan. Correspondence should be addressed to H.K. (kawaguchi-ort@h.u-tokyo.ac.jp).

Received 1 January; accepted 7 April; published online 7 May 2006; doi:10.1038/nm1409

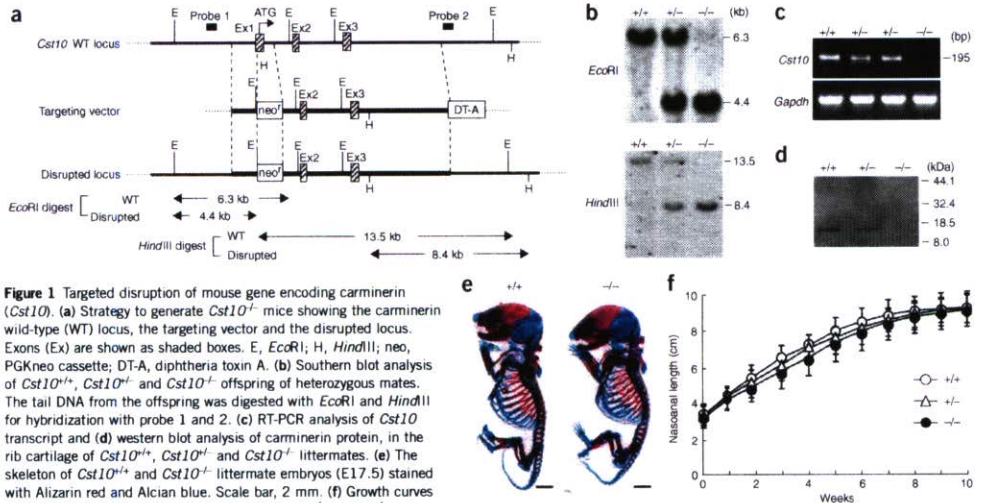

Figure 1 Targeted disruption of mouse gene encoding carminerin (*Cst10*). **(a)** Strategy to generate *Cst10*$^{-/-}$ mice showing the carminerin wild-type (WT) locus, the targeting vector and the disrupted locus. Exons (Ex) are shown as shaded boxes. E, *Eco*RI; H, *Hind*III; neo, PGKneo cassette; DT-A, diphtheria toxin A. **(b)** Southern blot analysis of *Cst10*$^{+/+}$, *Cst10*$^{+/-}$ and *Cst10*$^{-/-}$ offspring of heterozygous mates. The tail DNA from the offspring was digested with *Eco*RI and *Hind*III for hybridization with probe 1 and 2. **(c)** RT-PCR analysis of *Cst10* transcript and **(d)** western blot analysis of carminerin protein, in the rib cartilage of *Cst10*$^{+/+}$, *Cst10*$^{+/-}$ and *Cst10*$^{-/-}$ littermates. **(e)** The skeleton of *Cst10*$^{+/+}$ and *Cst10*$^{-/-}$ littermate embryos (E17.5) stained with Alizarin red and Alcian blue. Scale bar, 2 mm. **(f)** Growth curves determined by the nasoanal length of male *Cst10*$^{+/+}$, *Cst10*$^{+/-}$ and *Cst10*$^{-/-}$ mice. Data are expressed as mean ± s.e.m. for 15 mice per group. Females also showed similar skeletal development and growth in all genotypes.

carminerin expression was colocalized with Col X in the wild-type hypertrophic chondrocytes adjacent to the osteophyte (**Fig. 3b**). Although the hypertrophic differentiation of chondrocytes was not affected by the carminerin deficiency (**Fig. 3a**), osteophyte formation at the posterior of the tibias was significantly decreased (**Fig. 3a,c**). These findings confirmed by quantification by the Mankin grading score[3] and the osteophyte volume (**Fig. 3d**) indicate that carminerin produced in hypertrophic chondrocytes as a result of mechanical stress contributes to osteophyte formation through chondrocyte calcification, without affecting cartilage destruction or chondrocyte hypertrophy.

Similar findings were observed in ectopic ossification of the patellar ligament and the Achilles tendon with aging (**Supplementary Methods** online), which was significantly decreased by the carminerin deficiency ($P < 0.05$; **Supplementary Fig. 2** online). The colocalization of Col X and carminerin adjacent to the ectopic ossification indicates the involvement of carminerin-expressing hypertrophic chondrocytes in this disorder as well (**Supplementary Fig. 2**).

We further examined the involvement of carminerin in bone fracture healing at the midshaft of tibias[4,5]. *Cst10*$^{-/-}$ mice showed a bone gap upon X-ray 3 weeks after the fracture, with substantial formation of cartilaginous callus but impaired calcification, especially at the central area (**Fig. 4a**). Again, carminerin was expressed in the wild-type chondrocytes adjacent to the calcified callus. The time course of bone mineral content (BMC) showed that calcification in the central one-third portion, but not in the peripheral two-thirds portion, was significantly reduced during the endochondral ossification period (2–7 weeks after fracture) in the *Cst10*$^{-/-}$ callus, although bone union was eventually achieved from the *Cst10*$^{-/-}$ small callus through unaffected bone formation and remodeling thereafter (**Fig. 4b**). This model also indicates that the carminerin deficiency impaired endochondral ossification, but not intramembranous ossification or osteoblastic bone formation.

The effects of carminerin deficiency on endochondral ossification under the pathological conditions above were more obvious than those under physiological conditions, which showed only a microscopic change. The phenotype of the physiological *Cst10*$^{-/-}$ growth plate was milder than that seen in other disorders such as vitamin A deficiency, which causes not only impaired chondrocyte calcification but also insufficient resorption of unmineralized cartilage by chondroclasts, leading to a suppressed skeletal growth[6]. The difference may be caused by operation of compensatory mechanisms for endochondral ossification, including osteoblastic bone formation and remodeling unaffected by the carminerin deficiency, which are sufficient to compensate for the deficiency under physiological conditions, but not so under pathological conditions.

Carminerin was originally called cystatin 10 because its amino acid sequence contained similarity to the cystatin protein family; however, our examination has not detected legitimate cystatin activity, which inhibits cysteine proteinases (**Supplementary Table 1** and **Supplementary Methods** online). We therefore renamed this protein carminerin after 'cartilage mineralization'. To elucidate the actual mechanism of carminerin action on endochondral ossification, we compared *ex vivo* cultures of chondrocytes isolated from the growth plates of the wild-type and *Cst10*$^{-/-}$ tibias (**Supplementary Methods**). Although chondrocyte proliferation and differentiation were similar between the two genotypes, chondrocyte calcification was suppressed in the *Cst10*$^{-/-}$ culture (**Supplementary Fig. 3** online), indicating a cell-autonomous effect. In contrast, *ex vivo* cultures of primary osteoblasts obtained from wild-type and *Cst10*$^{-/-}$ calvariae confirmed that these cells do not express carminerin, so that there was no difference of bone formation by osteoblasts in this bone type (**Supplementary Fig. 3**).

As inorganic pyrophosphate (PPi) is known to be a crucial inhibitor of calcification[7], we compared the expression of a few molecules that

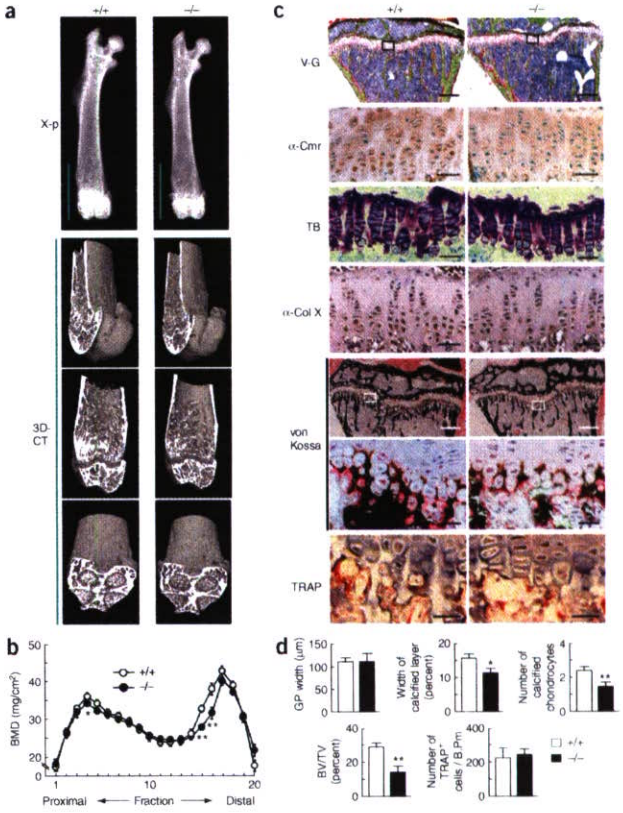

Figure 2 Radiological and histological findings of the long bones in wild-type (*Cst10*$^{+/+}$) and *Cst10*$^{-/-}$ littermates at 8 weeks of age under physiological conditions. **(a)** Plain X-ray of whole femurs, and three-dimensional computed tomography images of the distal part shown as green lines on the plain X-ray. **(b)** Bone mineral density (BMD) of the 20 equally divided fractions of femurs. **(c)** Histological findings of the proximal tibias. Villanueva-Goldner staining (V-G; scale bar, 200 μm). Inset boxes indicate the regions of the following three rows: immunostaining with an antibody to carminerin (α-Cmr; scale bar, 20 μm), toluidine blue staining (TB; scale bar, 20 μm), immunostaining with an antibody to Col X (α-Col X; scale bar, 20 μm). von Kossa staining (scale bars, 200 μm (top) and 20 μm (bottom)). Inset boxes indicate the regions of the bottom two rows. von Kossa staining and TRAP staining (scale bar, 20 μm). **(d)** Histomorphometric analyses of the growth plate and primary spongiosa just beneath it. The entire growth plate width (GP width) was measured on the TB sections, and the percent width of calcified layer to the entire growth plate and the number of calcified chondrocytes per column were measured on the von Kossa sections. Bone volume/tissue volume (BV/TV) and the number of TRAP^{+} cells in 100 mm of bone perimeter were measured in the primary spongiosa. Data are expressed as mean ± s.e.m. for 15 mice per group. $^{*}P < 0.05$, $^{**}P < 0.01$ compared to wild-type mice.

control the level of PPi in the cultured growth-plate chondrocytes, including: NPP1, which generates PPi from nucleoside triphosphates using nucleoside triphosphate pyrophosphohydrolase (NTPPPH) activity[8], tissue-nonspecific alkaline phosphatase (TNAP) which hydrolyzes PPi[9], and the multiple-pass transmembrane protein ANK, which mediates intracellular-to-extracellular channeling of PPi[10]. Among these proteins, the carminerin deficiency upregulated expression of only NPP1, and accordingly, increased NTPPPH activity (**Supplementary Fig. 3**). The reintroduction of carminerin into *Cst10*$^{-/-}$ chondrocytes (Ax-*Cmr*) restored the abnormalities in calcification, expression of NPP1 and NTPPPH activity to those similar to the wild-type culture (**Supplementary Fig. 3**). The promoter activity of an *Enpp1* promoter-luciferase construct (–964 *Enpp1* promoter-Luc) transfected into ATDC5 cells overexpressing carminerin (pCMV-*Cmr*/ATDC5) was lower than cells transfected with mock vector (pCMV/ATDC5; **Supplementary Fig. 3**). Deletion analysis of the *Enpp1* promoter region identified the core responsive element between the –360 and –324 regions, within which an SRY (sex-determining region Y) consensus sequence was predicted. Site-directed mutagenesis to eliminate the SRY site canceled the inhibition of *Enpp1* transcription by carminerin. Electrophoretic mobility shift assay confirmed specific binding of the SRY region by an oligonucleotide probe with nuclear extracts prepared from pCMV/ATDC5 and pCMV-*Cmr*/ATDC5 cells. Binding by the probe was weaker with the pCMV-*Cmr*/ATDC5 extracts than with the pCMV/ATDC5 extracts (**Supplementary Fig. 3**). As the binding was not detected using the synthetic carminerin protein instead of the nuclear extracts, carminerin itself was shown not to be the direct transcription factor for the SRY region. In contrast, nuclear extracts from the primary *Cst10*$^{-/-}$ growth plate chondrocytes showed stronger binding with the SRY site than those from the wild-type chondrocytes (**Supplementary Fig. 3**). Hence, the transcriptional inhibition of NPP1 expression by carminerin may result, at least partly, from the impaired binding of a transcription factor to the SRY site of the *Enpp1* promoter. Although Sox9, a potent regulator of chondrocyte differentiation[11,12], is the most probable transcription factor for this site, we did not observe a supershift of the DNA-protein complex when we added Sox9-specific antibody in the electrophoretic mobility shift assay (data not shown), indicating the involvement of other transcription factors in the regulation of the SRY site. In addition, in our efforts to identify the upstream regulator of NPP1, we did not find substantial regulation of expression or transcription of NPP1 by carminerin through the cytokines interleukin-1β (IL-1β), fibroblast growth factor-2 (FGF-2) or transforming growth factor-β (TGF-β), which previously have been reported to regulate NPP1 expression[13–15] (**Supplementary Fig. 4** online). Thus, further studies to elucidate a more detailed mechanism through which carminerin inhibits transcription of NPP1 will be necessary.

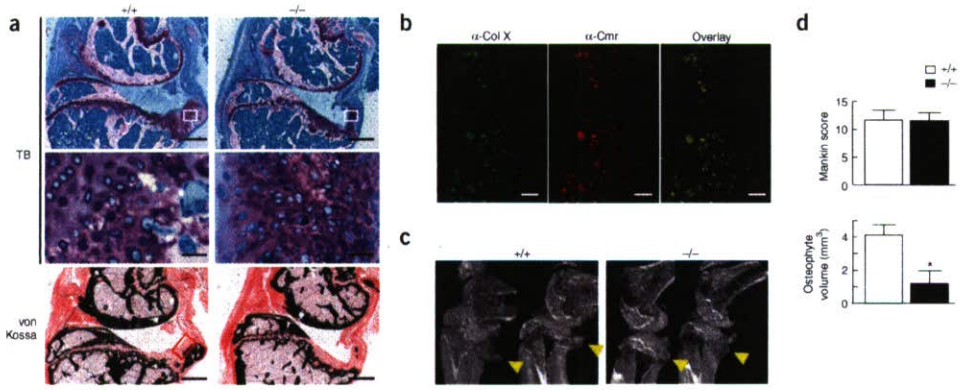

Figure 3 Histological and radiological findings of osteoarthritic joints in wild-type (*Cst10*$^{+/+}$) and *Cst10*$^{-/-}$ littermates. (**a**) Osteoarthritis was induced at the posterior tibias of the knee joint of 8-week-old mice by surgically imposing instability to the joint. Histological features; toluidine blue (TB; inset boxes in the top figures indicate regions shown in middle row; scale bars, 200 μm (top) and 20 μm (middle)) and von Kossa stainings (scale bar, 200 μm) of the sagittal sections of knee joints 10 weeks after surgery (left side of each photo is anterior side). (**b**) Immunostainings with an antibody to Col X (α-Col X, green), an antibody to carminerin (α-Cmr, red) and the overlay (yellow) analyzed by confocal microscopy in the region indicated in the inset of the image of von Kossa staining of wild-type knee in **a**. Scale bar, 20 μm. (**c**) Three-dimensional computed tomography images of the knee joints from the posterolateral projection. Arrowheads indicate osteophytes. (**d**) Quantification of the cartilage destruction and the osteophyte formation as determined by the Mankin grading score (top) and the osteophyte volume measured on the three-dimensional computed tomography images (bottom), respectively. Data are expressed as mean ± s.e.m. for ten mice per group. *$P < 0.01$ compared to wild-type mice.

Finally, we carried out *in vitro* fertilization and embryo transfer from *Cst10*$^{-/-}$ mice and the *Enpp1*$^{-/-}$ mice, which lack expression of functional NPP1 (ref. 16), and generated four genotypes of mice: *Cst10*$^{+/+}$*Enpp1*$^{+/+}$, *Cst10*$^{-/-}$*Enpp1*$^{+/+}$, *Cst10*$^{+/+}$*Enpp1*$^{-/-}$ and *Cst10*$^{-/-}$*Enpp1*$^{-/-}$. When we used the experimental models, there was no difference in formation of osteoarthritic osteophytes, age-related ectopic ossification or high phosphate–induced auricular ossification between the NPP1-deficient mice (*Cst10*$^{+/+}$*Enpp1*$^{-/-}$) and the double-deficient mice (*Cst10*$^{-/-}$*Enpp1*$^{-/-}$), confirming that functional NPP1 is essential for suppression of the pathological endochondral ossification by the carminerin deficiency *in vivo* (**Supplementary Fig. 5** online).

Our previous *in vitro* study showed that overexpression of carminerin in ATDC5 cells accelerated not only calcification but also

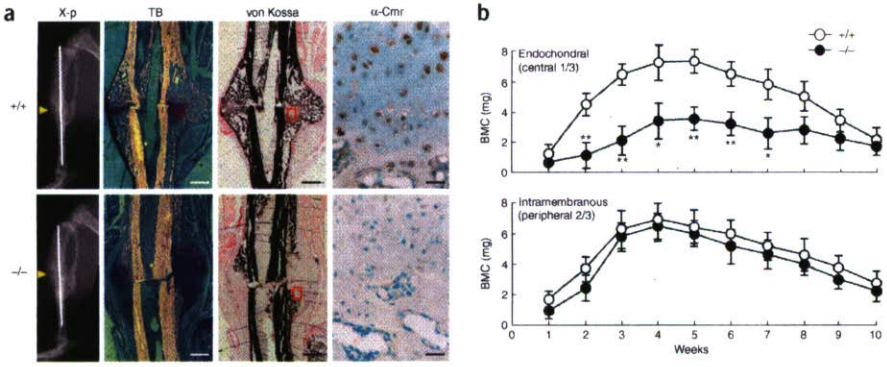

Figure 4 Radiological and histological findings of bone fracture healing in wild-type (*Cst10*$^{+/+}$) and *Cst10*$^{-/-}$ littermates. Fracture was produced by a transverse osteotomy that was stabilized with an intramedullary nail at the midshaft of tibias in 8-week-old mice. (**a**) Plain X-ray, toluidine blue (TB), von Kossa and a carminerin-specific antibody (α-Cmr) immunostainings 3 weeks after fracture. Insets in the image of von Kossa staining indicate regions of immunostaining. Scale bar, 20 μm for immunostaining, and 200 μm for the others. (**b**) Time course of bone mineral content (BMC) at the fracture callus for 10 weeks after fracture. BMC of the central one-third portion was measured as the endochondral ossification, and BMC of the peripheral two-thirds as the intramembranous ossification. Data are expressed as mean ± s.e.m. for six mice per time per group. *$P < 0.05$, **$P < 0.01$ compared to wild-type mice.

hypertrophic differentiation[1]. In contrast, the present *in vivo* and *in vitro* studies on deficiency of carminerin showed no abnormality in hypertrophic differentiation of chondrocytes. This discrepancy might owe to the involvement of insulin signaling by way of NPP1 regulation because in addition to the enzymatic function of synthesizing PPi, NPP1 is known to suppress the tyrosine kinase activity of the insulin receptor[17]. Considering that our previous ADTC5 cell culture was carried out in the presence of insulin (10 μg/ml), which was essential to induce hypertrophic differentiation[18], overexpression of carminerin might cause suppression of NPP1, which in turn increases sensitivity to insulin and enhances hypertrophic differentiation. The fact that the serum insulin levels in wild-type and *Cst10*$^{-/-}$ mice were similar (0.32 ± 0.08 and 0.35 ± 0.06 ng/ml, respectively; mean ± s.e.m. of five mice per genotype) and were much lower than the *in vitro* concentration, indicates that the regulation of chondrocyte calcification by endogenous carminerin *in vivo* was not mediated by insulin signaling.

Pi has been suggested to be rate limiting for calcification, which may explain why clinical disorders in homeostasis of Pi lead to, for example, rickets, osteomalacia[19] and ectopic calcification[20]. Considering that carminerin was isolated as a protein that was upregulated by a high-phosphate diet in association with calcification of mouse auricular cartilage, carminerin might partly mediate Pi-induced cartilage calcification. In fact, carminerin deficiency decreased calcification of auricular cartilage in wild-type mice on a high-phosphate diet (**Supplementary Fig. 5**). Carminerin may therefore be the first cartilage-specific protein that induces chondrocyte calcification during endochondral ossification under physiological and pathological conditions.

METHODS

Generation of *Cst10*$^{-/-}$ mice. We obtained a *Cst10* genomic clone by screening a bacterial artificial chromosome (BAC) library using a BAC PCR screening system (Genome Systems). We used a 120-kb fragment of a BAC clone containing all exons (1–3) of *Cst10* to construct the targeting vector. We constructed the targeting vector to replace exon 1, including the transcription initiation site, by the neomycin-resistance gene. We introduced the linearized targeting vector by electroporation into embryonic stem (ES) cells as previously described[21], and identified two independent targeted ES cell clones by Southern blot analysis, using 5′ (probe 1) and 3′ (probe 2) external probes. We generated chimeric males and crossed them with C57BL/6 females, and verified germline transmission by Southern blot analysis. All *Cst10*$^{-/-}$ mice used in this study had been backcrossed for ten generations into the C57BL/6 background. We used RT-PCR to determine the presence of the *Cst10* transcripts. We determined presence of carminerin protein by western blot analysis, as previously described, using a polyclonal antibody to the full-length carminerin protein, which was raised in rabbits using a synthetic peptide of carminerin[1].

Mice conditions. We fed mice a standard rodent diet (CE-2; CLEA Japan) or a high-phosphate diet containing 1.86% phosphorus. In each experiment, we compared littermate wild-type and *Cst10*$^{-/-}$ mice generated from the intercross between heterozygous mice. All experiments were performed on male mice, according to the protocol approved by the Animal Care and Use Committee of the University of Tokyo.

Skeletal preparations. We fixed whole skeletons of wild-type and *Cst10*$^{-/-}$ littermate embryos (E17.5) in 99.5% ethanol, transferred them into acetone and stained them as previously described[21]. We kept specimens in 20% glycerol-1% KOH until skeletons became clearly visible.

Radiological analyses. We took plain radiographs using a soft X-ray apparatus. We measured the bone mineral density (BMD) of the 20 equally divided fractions of the entire femur and bone mineral content (BMC) of the fracture callus with dual energy X-ray absorptiometry using a bone mineral analyzer. We carried out micro–computed tomography scanning using a composite X-ray analyzer, and reconstructed cross-sectional tomograms of 10 μm thickness at 12 × 12 pixels into a three-dimensional feature by the volume-rending method; we then measured the ossification volume using a computer. We performed peripheral quantitative computed tomography scans at the metaphysis of 0.2 mm below the proximal growth plate and at the midshaft of tibias.

Histological analyses. For Villanueva-Goldner, toluidine blue and von Kossa stainings, we fixed samples with 70% ethanol, embedded them in glycol methacrylate without decalcification and sectioned them into 3-μm slices. We carried out histomorphometric analyses in the growth plate, primary spongiosa just beneath it (0.3 mm in length) and secondary spongiosa (1.0 mm in length from 0.3 mm below the growth plate) of the proximal tibias and the fifth vertebra using an image analyzer. For double labeling to analyze the dynamic bone remodeling, we subcutaneously injected mice with 8 mg/kg body weight of calcein at 10 d and 3 d before killing. We stained TRAP^{+} cells at pH 5.0 in the presence of L(+)-tartaric acid using naphthol AS-MX phosphate in *N,N*-dimethyl formamide as the substrate. We performed histomorphometric measurements in eight optical fields, according to the American Society for Bone and Mineral Research nomenclature report[22], and calculated the averages per mouse. For H&E staining, we perfused mice with 4% buffered paraformaldehyde, decalcified bones with 4.13% EDTA, embedded them in paraffin, and cut them into 6 μm–thick sections. For immunohistochemical analyses, we treated sections as previously described[4], using polyclonal rabbit antibody to carminerin or Col X (Santa Cruz Biotechnology). For double staining, we treated sections with 1% BSA, incubated them with a mixture of carminerin-specific antibody and mouse monoclonal Col X–specific antibody and with Texas red-conjugated goat antibody to rabbit IgG. They were then reacted with biotin-conjugated antibodies to mouse IgG+IgA+IgM and FITC-streptoavidin. The localizations were observed by confocal laser scanning microscopy.

Osteoarthritis model. Eight-week-old mice underwent a microsurgery to produce instability in the knee joints as we reported previously[2]. Mice were killed 10 weeks after surgery, and cartilage destruction was quantified as the Mankin grading score[3] of the most severe change among multiple serial toluidine blue sections in each mouse. We measured osteophyte volume with three-dimensional computed tomography as described above.

Fracture model. We produced fracture at the midshaft of tibias of 8-week-old mice as we reported previously[4,5]. Several mice were killed each week for 10 weeks after the surgery. After the entire callus was longitudinally divided into three equal portions on a bone mineral analyzer image, we measured BMC at the central one-third portion as the endochondral ossification and that at the peripheral two-thirds as the intramembranous ossification. We performed histological analyses 3 weeks after fracture.

Statistical analysis. All data are expressed as mean ± s.e.m. Means of groups were compared by ANOVA and significance of differences was determined by *post hoc* testing using the Bonferroni method.

Note: Supplementary information is available on the Nature Medicine website.

ACKNOWLEDGMENTS

This study was supported by a Grant-in-aid for Scientific Research from the Japanese Ministry of Education, Culture, Sports, Science, and Technology (#14370454), and by the Investigation Committee on the Ossification of Spinal Ligaments, Japanese Ministry of Public Health and Welfare.

COMPETING INTERESTS STATEMENT

The authors declare that they have no competing financial interests.

Published online at http://www.nature.com/naturemedicine/
Reprints and permissions information is available online at http://npg.nature.com/reprintsandpermissions/

1. Koshizuka, Y. *et al.* Cystatin 10, a novel chondrocyte-specific protein, may promote the last steps of the chondrocyte differentiation pathway. *J. Biol. Chem.* **278**, 48259–48266 (2003).
2. Kamekura, S. *et al.* Osteoarthritis development in novel experimental mouse models induced by knee joint instability. *Osteoarthritis Cartilage* **13**, 632–641 (2005).

3. Mankin, H.J., Johnson, M.E. & Lippiello, L. Biochemical and metabolic abnormalities in articular cartilage from osteoarthritic human hips. III. Distribution and metabolism of amino sugar-containing macromolecules. *J. Bone Joint Surg. Am.* **63**, 131–139 (1981).
4. Shimoaka, T. *et al.* Impairment of bone healing by insulin receptor substrate-1 deficiency. *J. Biol. Chem.* **279**, 15314–15322 (2004).
5. Chikuda, H. *et al.* Cyclic GMP-dependent protein kinase II is a molecular switch from proliferation to hypertrophic differentiation of chondrocytes. *Genes Dev.* **18**, 2418–2429 (2004).
6. Wolbach, S.B. Vitamin-A deficiency and excess in relation to skeletal growth. *J. Bone Joint Surg.* **29**, 171–192 (1947).
7. Terkeltaub, R.A. Inorganic pyrophosphate generation and disposition in pathophysiology. *Am. J. Physiol. Cell Physiol.* **281**, C1–C11 (2001).
8. Bollen, M., Gijsbers, R., Ceulemans, H., Stalmans, W. & Stefan, C. Nucleotide pyrophosphatases/phosphodiesterases on the move. *Crit. Rev. Biochem. Mol. Biol.* **35**, 393–432 (2000).
9. Balcerzak, M. *et al.* The roles of annexins and alkaline phosphatase in mineralization process. *Acta Biochim. Pol.* **50**, 1019–1038 (2003).
10. Ryan, L.M. The ank gene story. *Arthritis Res.* **3**, 77–79 (2001).
11. de Crombrugghe, B., Lefebvre, V. & Nakashima, K. Regulatory mechanisms in the pathways of cartilage and bone formation. *Curr. Opin. Cell Biol.* **13**, 721–727 (2001).
12. Akiyama, H., Chaboissier, M.C., Martin, J.F., Schedl, A. & de Crombrugghe, B. The transcription factor Sox9 has essential roles in successive steps of the chondrocyte differentiation pathway and is required for expression of Sox5 and Sox6. *Genes Dev.* **16**, 2813–2828 (2002).
13. Lotz, M. *et al.* Interleukin 1 beta suppresses transforming growth factor-induced inorganic pyrophosphate (PPi) production and expression of the PPi-generating enzyme PC-1 in human chondrocytes. *Proc. Natl. Acad. Sci. USA* **92**, 10364–10368 (1995).
14. Solan, J.L., Deftos, L.J., Goding, J.W. & Terkeltaub, R.A. Expression of the nucleoside triphosphate pyrophosphohydrolase PC-1 is induced by basic fibroblast growth factor (bFGF) and modulated by activation of the protein kinase A and C pathways in osteoblast-like osteosarcoma cells. *J. Bone Miner. Res.* **11**, 183–192 (1996).
15. Oyajobi, B.O., Caswell, A.M. & Russell, R.G. Transforming growth factor beta increases ecto-nucleoside triphosphate pyrophosphatase activity of human bone-derived cells. *J. Bone Miner. Res.* **9**, 99–109 (1994).
16. Okawa, A. *et al.* Mutation in Npps in a mouse model of ossification of the posterior longitudinal ligament of the spine. *Nat. Genet.* **19**, 271–273 (1998).
17. Goldfine, I.D., Maddux, B.A., Youngren, J.F., Trischitta, V. & Frittitta, L. Role of PC-1 in the etiology of insulin resistance. *Ann. NY Acad. Sci.* **892**, 204–222 (1999).
18. Shukunami, C. *et al.* Chondrogenic differentiation of clonal mouse embryonic cell line ATDC5 *in vitro*: differentiation-dependent gene expression of parathyroid hormone (PTH)/PTH-related peptide receptor. *J. Cell Biol.* **133**, 457–468 (1996).
19. Laroche, M. Phosphate, the renal tubule, and the musculoskeletal system. *Joint Bone Spine* **68**, 211–215 (2001).
20. Jono, S. *et al.* Phosphate regulation of vascular smooth muscle cell calcification. *Circ. Res.* **87**, E10–E17 (2000).
21. Nakamichi, Y. *et al.* Chondromodulin I is a bone remodeling factor. *Mol. Cell. Biol.* **23**, 636–644 (2003).
22. Parfitt, A.M. *et al.* Bone histomorphometry: standardization of nomenclature, symbols, and units. Report of the ASBMR Histomorphometry Nomenclature Committee. *J. Bone Miner. Res.* **2**, 595–610 (1987).

Topical vitamin D3 and low-calcemic analogs induce thymic stromal lymphopoietin in mouse keratinocytes and trigger an atopic dermatitis

Mei Li*, Pierre Hener*, Zhikun Zhang*, Shigeaki Kato†, Daniel Metzger*, and Pierre Chambon*‡

*Institut de Génétique et de Biologie Moléculaire et Cellulaire and Institut Clinique de la Souris, BP10142, 67404 Illkirch Cedex, France; and †Institute of Molecular and Cellular Biosciences, University of Tokyo, 1-1-1 Yayoi, Bunkyo-ku, Tokyo 113-0032, Japan

Contributed by Pierre Chambon, June 5, 2006

We have demonstrated that cytokine thymic stromal lymphopoietin (TSLP), whose expression is rapidly induced upon keratinocyte-selective ablation of retinoid X receptors (RXRs) -α and -β in the mouse (RXRαβ$^{ep-/-}$ mice), plays a key role in initiating a skin and systemic atopic dermatitis-like phenotype. We show here that topical application of the physiologically active ligand [1α,25-(OH)$_2$D$_3$; calcitriol] of the vitamin D receptor, or of its low-calcemic analog MC903 (calcipotriol; Dovonex), induces TSLP expression in epidermal keratinocytes, which results in an atopic dermatitis-like syndrome mimicking that seen in RXRαβ$^{ep-/-}$ mutants and transgenic mice overexpressing TSLP in keratinocytes. Furthermore, topical application of retinoic acid receptor RARγ-selective agonist BMS961 also induces TSLP expression either on its own or synergistically with 1α,25-(OH)$_2$D$_3$. Our data demonstrate that RXR/vitamin D receptor and RXR/retinoic acid receptor-γ heterodimers and their ligands cell-autonomously control the expression of TSLP in epidermal keratinocytes of the mouse. We propose molecular mechanisms through which vitamin D3 and retinoic acid signalings could be involved in the pathogenesis of atopic diseases.

retinoic acid | vitamin D receptor | retinoid X receptor | retinoic acid receptor | skin

Nuclear receptors (NRs) belong to a superfamily of ligand-dependent transcriptional regulators (1, 2). Within this superfamily, retinoid X receptors (RXRs) -α, -β, and -γ play a key role through heterodimerization with some 15 NR partners, e.g., retinoic acid receptors (RARs), vitamin D receptor (VDR), peroxisome proliferator-activated receptors, and liver X receptors (1, 2). We reported (3) that selective ablation of RXRα and RXRβ in adult mouse epidermal keratinocytes (RXRαβ$^{ep-/-}$ mice) triggers a skin and systemic syndrome similar to human atopic dermatitis (AD), a chronic skin inflammatory disease with a strong genetic component that affects children (10–20%) and adults (1–3%) (4). These mice exhibit the major features of the human AD syndrome that include (*i*) skin eczematous-like lesions with xerosis and pruritus, associated with a skin inflammatory infiltrate mainly composed of CD4$^+$ T helper (Th) type 2 cells, dendritic cells, eosinophils, and mast cells and (*ii*) systemic abnormalities, including elevated serum IgE and IgG levels and blood and tissue eosinophilia.

We found that expression of the cytokine thymic stromal lymphopoietin (TSLP), known to be produced in epidermal keratinocytes of AD patients (5), is rapidly induced in keratinocytes of RXRαβ$^{ep-/-}$ mice. Furthermore, we showed that K14-TSLP transgenic mice overexpressing TSLP in keratinocytes exhibit an AD-like phenotype similar to that of RXRαβ$^{ep-/-}$ mice (3), demonstrating that TSLP can act as an initiating cytokine at the top of a chain of immunological events that lead to an AD-like phenotype, in keeping with other recent studies on mouse models of human allergic inflammatory diseases (asthma and AD) (6–9).

We suggested that up-regulation of keratinocytic TSLP expression upon RXRα and -β ablation could be due to the relief of a transcriptional repression mediated by RXR/NR heterodimers (3). This study was aimed at revealing the identity of the possible NR partner(s) of RXRα and RXRβ.

Results

Topical Application of 1α,25-(OH)$_2$D$_3$ or Its Low-Calcemic Analog MC903 Activates TSLP Expression in Epidermal Keratinocytes. Because RXR/NR heterodimers in which an agonistic ligand is not bound to the NR partner can act as transcriptional repressors (10), we examined whether TSLP expression could be induced by NR agonists. Four nanomoles of ligands were topically applied to whole ears of WT mice for 4 consecutive days (days 1–4), and TSLP RNA levels were determined on day 5. Application of 1α,25-(OH)$_2$D$_3$ (the physiologically active vitamin D3) led to a dramatic increase (>300-fold) in TSLP transcripts at day 5, whereas they were modestly but significantly increased (5-fold) upon application of a RARγ-selective agonist (BMS961) (11) (Fig. 1*a*). In contrast, agonists for RXRs (BMS649), proliferator-activated receptor (PPAR)α (fenofibrate), PPARβ (GW501516), PPARγ (rosiglitazone), and liver X-activated receptors (25-hydroxycholesterol) had no effect on TSLP expression (Fig. 1*a*).

Because, at this dose, 1α,25-(OH)$_2$D$_3$ application resulted in hypercalcemia and death of the mice, we applied its analog MC903 (calcipotriol; Dovonex) (12) that exhibits a low-calcemic activity and is used for psoriasis treatment (13). MC903 and ethanol (vehicle) were applied to WT mouse right and left ears, respectively. Two shaved areas (1 cm^2 each) of dorsal skin were also treated with MC903 or ethanol. One day after the first application (day 2), TSLP RNA levels were increased in right ears and further increased on days 3 and 4, whereas no increase occurred in left ears (Fig. 1*b Left*). Transcripts of *CYP24A1*, a 1α,25-(OH)$_2$D$_3$-inducible gene (14), were increased upon MC903 application, as expected (Fig. 1*b*, *Right*). TSLP RNA was also increased in MC903-treated dorsal skin (Fig. 1*c*), and serum TSLP levels were increased at days 2–4, whereas undetectable at day 0 (before treatment) (Fig. 1*d*). Increasing doses of MC903 (0.4, 1, or 4 nmol per ear) led to a dose-dependent increase of TSLP transcripts, which was similarly observed with other low-calcemic analogs of 1α,25-(OH)$_2$D$_3$, including EB1089 and KH1060 (12, 15) (data not shown).

To examine whether MC903-induced expression of TSLP was skin-restricted, various other organs were analyzed at day 5. No increase in TSLP transcripts was observed in these organs (Fig. 1*e*). Immunohistochemistry (IHC) did not reveal TSLP expression in epidermis or dermis of ethanol-treated ear and dorsal skin, whereas it was readily detected at day 4 upon MC903 treatment (Fig. 1*f*; ear skin, *Upper*; dorsal skin, *Lower*). Double IHC for TSLP and keratin 1 (K1), a suprabasal keratinocyte marker, showed that TSLP was

Conflict of interest statement: No conflicts declared.

Abbreviations: AD, atopic dermatitis; CT, control; IHC, immunohistochemistry; NR, nuclear receptor; RA, retinoic acid; RAG1, recombination activating gene 1; RAR, RA receptor; RXR, retinoid X receptor; Th, T helper; TLR, Toll-like receptor; TSLP, thymic stromal lymphopoietin; VDR, vitamin D receptor

‡To whom correspondence should be addressed. E-mail: chambon@igbmc.u-strasbg.fr.

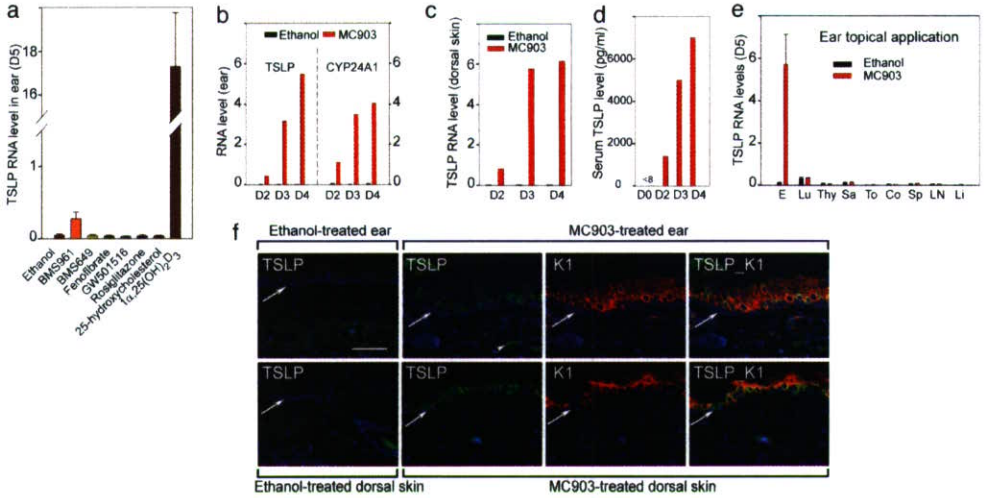

Fig. 1. Skin topical application of $1\alpha,25\text{-}(OH)_2D_3$ and MC903 activates TSLP expression in epidermal keratinocytes. (*a*) TSLP RNA at day 5 in ears topically treated with NR agonists (4 nmol). (*b–e*) Induction of TSLP expression is a rapid and local skin effect. TSLP and CYP24A1 RNA levels in an ethanol-treated left ear and MC903-treated right ear (*b*), TSLP RNA levels in ethanol-treated and MC903-treated dorsal skin at days 2, 3, and 4 (*c*), and increased serum TSLP levels at days 2, 3, and 4 (*d*), in contrast to undetectable level (<8 pg/ml) at day 0 (before treatment). Data are representative of three independent experiments. D, day. (*e*) TSLP RNA levels at day 5 in ear (E), lung (Lu), thymus (Thy), salivary gland (Sa), tongue (To), colon (Co), spleen (Sp), lymph node (LN), and liver (Li) of mice topically treated by ethanol or MC903 on ears. (*f*) IHC of TSLP (green) at day 4 in sections of ear (*Upper*) and dorsal skin (*Lower*) topically treated with ethanol or MC903. The same sections from MC903-treated skin were stained with keratin 1 antibody (K1, red), and overlaid images of TSLP and K1 staining are shown, as indicated. Blue corresponds to DAPI staining of nuclei. The white arrowhead points to autofluorescent erythrocytes, and white arrows point to the dermal/epidermal junction. (Scale bar, 50 μm.)

mainly located in these keratinocytes of both MC903-treated ear and dorsal skin, whereas it could also be detected at a lower level in basal keratinocytes (expressing keratin 14) (Fig. 1*f*, and data not shown).

Topical Application of MC903 Triggers an AD-Like Syndrome. Because TSLP expression appears to be critically involved in the initiation of AD-like dermatitis in the mouse (3, 8), we investigated whether a MC903 long-term treatment could induce an AD-like phenotype. MC903 (4 nmol) was applied daily for 16 days to ears of WT mice. No hypercalcemia or overall health impairment and weight loss was observed. Ethanol application did not cause any change in ear appearance, whereas reddening and swelling that worsened with time were observed from day 5 on MC903-treated ears (data not shown). At day 17, these ears were red, scaly, swollen, and crusted (Fig. 2, compare *a* and *b*), and frequent ear scratching (data not shown) suggested a pruritus. Histological analysis revealed epidermal hyperplasia and a heavy dermal cell infiltrate, in which numerous eosinophils were easily identified upon hematoxylin/eosin-staining (Fig. 2*d* and *Inset*). Their identity was confirmed with Luna's staining (data not shown). In contrast, no eosinophils were found in ethanol-treated ears (Fig. 2*c*). IHC with an anti-GR1 antibody (recognizing granulocytes and monocytes) revealed a large number of positive cells in dermis, of which eosinophils, but not neutrophils, were a major component (Fig. 2*f* and data not shown). Numerous T lymphocytes ($CD3^+$) were observed in MC903-treated dermis (Fig. 2*h*), whereas only a few resident T lymphocytes could be detected in ethanol-treated ears (Fig. 2*g*). Most of the infiltrated T cells were $CD4^+$ helper T cells (Fig. 2*j*), and only a few $CD8^+$ cytotoxic T cells were found (Fig. 2*l*). A large increase in $CD11c^+$ dermal dendritic cells was also observed in MC903-treated ears (Fig. 2 *m* and *n*), whereas mast cells were 4-fold increased in the dermis (Fig. 2 *o* and *p* and data not shown).

Because topical application of $1\alpha,25\text{-}(OH)_2D_3$ at a dose of 4 nmol per ear resulted in mouse death within 7 days, WT mice were thus treated every other day at a dose of 0.25 nmol per ear, to examine whether the treatment would result in a skin inflammation similar to that generated with MC903. At this dose, TSLP expression was significantly induced at day 18, and an inflammatory infiltrate comprising $CD4^+$ T lymphocytes, dendritic cells, eosinophils, and mast cells could also be observed (data not shown).

Taken together, these data indicated that the inflammatory cell infiltrate observed in skin of MC903- and $1\alpha,25\text{-}(OH)_2D_3$-treated ears had the characteristics of an AD-like skin inflammation (3). This finding was fully supported by analysis of cytokines expressed in MC903-treated ears. At day 16, TSLP transcripts were markedly increased (Fig. 2*q*), and Th2-type cytokine transcripts (IL-4, -5, -13, -31, -10, and -6) (3) were all significantly increased (Fig. 2*q*). Expression of the Th1-type cytokine IFN-γ was also enhanced, whereas that of TNF-β, another Th1-type cytokine, was unchanged. Importantly, this cytokine profile, which is essentially that of a Th2-type inflammation, was similar to those observed in skins of $RXR\alpha\beta^{ep-/-}$ and K14-TSLP transgenic mice (3), indicating that the increase of these cytokines was most probably due to enhanced TSLP production in keratinocytes.

Systemic abnormalities, including elevated serum IgE and IgG levels, associated with blood and tissue eosinophilia, have been observed in $RXR\alpha\beta^{ep-/-}$ and K14-TSLP mice, exhibiting similarities to those observed in AD patients (3). Serum IgE and IgG levels were increased in mice to which MC903 was topically applied for 16 days on ears (Fig. 2*r*). Moreover, at day 16, MC903-treated mice exhibited an increased number of eosinophils in ear-draining lymph nodes, liver, and spleen (Fig. 2*s* and data not shown). Differential blood cell counts also revealed a marked increase in eosinophils in MC903-treated mice (693 ± 220 cells per μl, versus 204 ± 134 cells per μl in ethanol-treated mice). Thus, MC903 topical application leads to a skin and systemic phenotype mimicking that of human AD.

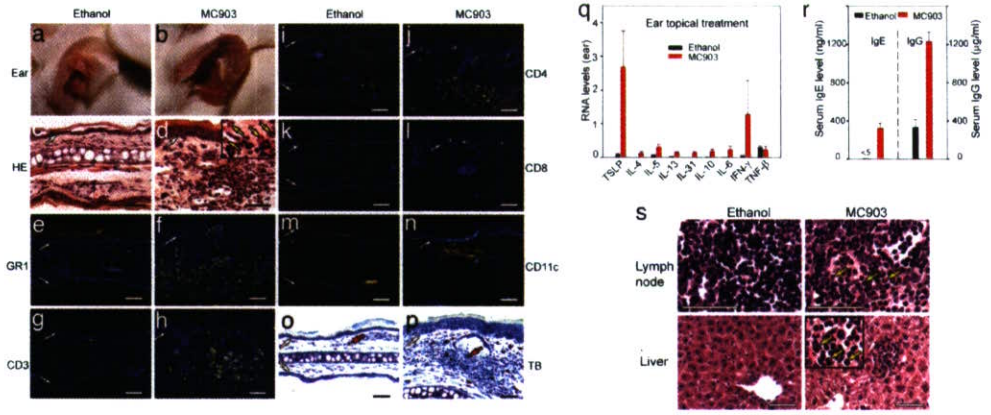

Fig. 2. Topical treatment with MC903 triggers an AD-like skin inflammation. (*a* and *b*) Appearance of ethanol- and MC903-treated ears at day 17. (*c* and *d*) Hematoxylin and eosin-stained ear sections of ethanol- and MC903-treated mice at day 17. Eosinophils displaying cytoplasmic red staining are indicated by yellow arrows in *d Inset*. (*e–n*) IHC performed on ear sections from ethanol- or MC903-treated mice at day 17, with antibodies against GR1 (*e* and *f*), CD3 (*g* and *h*), CD4 (*i* and *j*), CD8 (*k* and *l*), and CD11c (*m* and *n*). Yellow corresponds to staining of antibodies, whereas blue corresponds to DAPI staining of nuclei. (*o* and *p*) Toluidin blue (TB) staining of ear sections. Red arrows point to one of the mast cells with intense blue in the dermis. White arrows in c–p point to the dermal/epidermal junction. (*q*) Cytokine RNA levels in ethanol- and MC903-treated ears at day 17. (*r*) Serum IgE and IgG levels of ethanol- and MC903-treated mice at day 17. (*s*) Hematoxylin and eosin-stained sections of ear-draining lymph node and liver of ethanol- and MC903-treated mice at day 17. Yellow arrows point to three of many eosinophils (red cytoplasmic staining) in sections of lymph node and liver of MC903-treated mice. (Scale bars, 50 μm.)

Both Keratinocytic VDR and RXR Are Required for Induction of TSLP Expression and Generation of an AD-Like Skin Inflammation Upon MC903 Treatment. To investigate whether the MC903-induced TSLP expression and appearance of an AD-like skin inflammation were mediated through VDR, MC903 was topically applied on ears of "floxed" VDR control (CT) mice ($VDR^{1.2/1.2}$ mice in which both VDR alleles bear LoxP sites) and of their $VDR^{ep-/-}$ littermates [K14-$Cre^{(tg/0)}$/$VDR^{1.2/1.2}$ mice] in which the VDR alleles are selectively ablated in keratinocytes (ref. 16 and our unpublished data). At day 17 of MC903 treatment, an inflammation was obvious on ears of VDR CT mice, whereas $VDR^{ep-/-}$ ears did not show any sign of inflammation (Fig. 3 *a* and *b*). Accordingly, a massive dermal infiltrate of inflammatory cells, including eosinophils, $CD4^+$ Th cells, dendritic cells, and mast cells was detected in ear sections of MC903-treated VDR CT (Fig. 3*c* and data not shown) but not in those of $VDR^{ep-/-}$ mice (Fig. 3*d*). Similarly, no AD-like skin inflammation was developed upon topical MC903 treatment of $VDR^{-/-}$ (germ-line knockout) mice (17) (data not shown).

TSLP expression was strongly induced in MC903-treated skin of VDR CT mice (Fig. 3*e*, lanes 1 and 2) but not at all in MC903-treated skin of $VDR^{-/-}$ mice (lanes 5 and 6), whereas it was weakly increased in MC903-treated skin of $VDR^{ep-/-}$ mutants (lanes 3 and 4). This latter increase may reflect a faint response to MC903 in nonkeratinocytic skin cells. In any event, our data clearly demonstrated that induction of TSLP expression in keratinocytes upon MC903 application is a VDR-dependent cell-autonomous event.

To examine whether the effect of MC903 was transduced through RXR/VDR heterodimers, ears of $RXR\alpha\beta^{ep-/-}$ mice (3) as well as their control littermates ($RXR\alpha\beta$ CT) were topically treated with MC903 (Fig. 3*f*). As expected (3), selective $RXR\alpha\beta$ ablation in keratinocytes of adult mice led to increased TSLP expression (lanes 1 and 3). However, the further induction of TSLP by MC903 was severely reduced in $RXR\alpha\beta^{ep-/-}$ skin (lanes 2 and 4), indicating an essential function of keratinocytic RXRs in TSLP induction by VDR agonists, most probably reflecting the involvement of RXR/VDR heterodimers.

VDR and RARγ Agonistic Ligands Synergize to Induce Skin TSLP Expression. Although much less potent than that of a VDR agonist, application of a RARγ-selective agonist (BMS961) on mouse ear skin led to significant increase of TSLP transcripts (Fig. 1*a*), and topical application of retinoic acid (RA) resulted in a similar induction (data not shown). To examine whether VDR and RARγ agonists could synergize in up-regulating TSLP expression, WT mouse ears were topically treated for 3 days with ethanol, BMS961 (4 nmol), a limiting dose of $1\alpha,25\text{-}(OH)_2D_3$ (0.4 nmol), or a combination of the two ligands. Ear TSLP transcripts and serum TSLP were determined at day 4. A clear synergism was observed between the effects of BMS961 and $1\alpha,25\text{-}(OH)_2D_3$ (Fig. 4*a*), indicating a synergistic involvement of RAR- and VDR-mediated events in transcriptional activation of TSLP expression.

TSLP Production and Skin Inflammation Induced by MC903 Are T and B Lymphocyte-Independent. As a direct effect of $1\alpha,25\text{-}(OH)_2D_3$ on naïve $CD4^+$ T cells may enhance the development of Th2 cells (18), we investigated whether $CD4^+$ T cells are required for development and progression of the active vitamin D3-induced AD-like phenotype. Ethanol or MC903 was applied on ears of $RAG1^{-/-}$ mice, which are devoid of mature B and T lymphocytes (19). As observed in WT mice, keratinocytic TSLP expression at day 4 was induced in MC903-treated, but not in ethanol-treated, $RAG1^{-/-}$ mice (see Fig. 6 *a*, *b*, and *k*, which is published as supporting information on the PNAS web site). At day 16, MC903-treated $RAG1^{-/-}$ mice exhibited thickened and scaly red ears (Fig. 6*d*), associated with a dermal cell infiltrate and an epidermal hyperplasia (Fig. 6*f*),

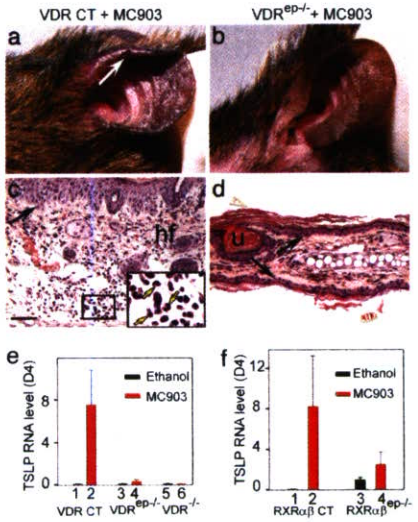

Fig. 3. Keratinocytic VDR and RXR are required for generation of an AD-like skin inflammation and induction of TSLP expression upon MC903 treatment. Appearance of MC903-treated ears of VDR CT (*a*) and VDR$^{ep-/-}$ mice (*b*) at day 17. White arrow in *a* points to lesioned skin. (*c* and *d*) Hematoxylin and eosin-stained ear sections. Yellow arrows in *c Inset* point to three of many eosinophils (red cytoplasmic staining) in MC903-treated CT skin. Black arrows point to dermal/epidermal junction. hf, hair follicle; u, utriculi (resulting from hair follicle degeneration in VDR$^{ep-/-}$ mice). (Scale bar, 50 μm.) (*e*) TSLP RNA levels at day 4 in ethanol- and MC903-treated ears of VDR CT (lanes 1 and 2), VDR$^{ep-/-}$ (lanes 3 and 4), and VDR$^{-/-}$ (lanes 5 and 6) mice. (*f*) TSLP RNA levels at day 4 in ethanol- and MC903-treated ears of RXRαβ CT (lanes 1 and 2) and RXRαβ$^{ep-/-}$ (lanes 3 and 4) mice.

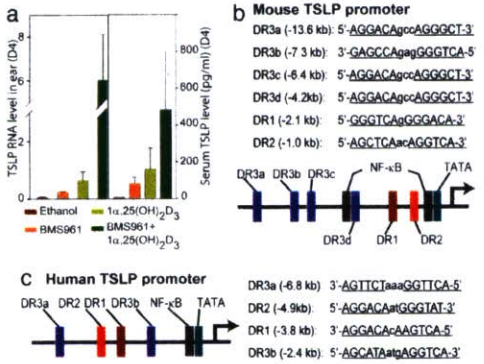

Fig. 4. Agonist-liganded VDR and RARγ synergistically induce TSLP expression. (*a*) Mouse ears were treated with ethanol, BMS961 (4 nmol), 1α,25-$(OH)_2D_3$ (0.4 nm), or BMS961 (4 nmol) plus 1α,25-$(OH)_2D_3$ (0.4 nmol), as indicated. TSLP RNA levels in the ears (*Left*) and serum TSLP levels (*Right*) were measured at day 4. (*b*) Putative VDREs (DR3) and RAREs (DR2 and DR1) upstream of the mouse TSLP promoter. (*c*) Putative VDREs (DR3) and RAREs (DR2 and DR1) upstream of the human TSLP promoter.

whereas ethanol-treated RAG1$^{-/-}$ ears had a normal appearance (Fig. 6 *c* and *e*). As expected, lymphocytes were absent in RAG1$^{-/-}$ skin sections (data not shown). However, we detected an increased number of infiltrated eosinophils (Fig. 6 *f* vs. *e*), mast cells (Fig. 6 *h* vs. *g*), and dermal dendritic cells (Fig. 6 *j* vs. *i*) in MC903-treated RAG1$^{-/-}$ skin. Thus, enhancement of TSLP expression and generation of a skin inflammation upon MC903-treatment do not require the presence of mature B and T lymphocytes.

Moreover, whereas transcripts of Th2-type cytokines IL-5, -13, and -31 were not increased in MC903-treated RAG1$^{-/-}$ skin (as compared with ethanol treatment), an increase in transcripts of other Th2-type cytokines IL-4, -6, and -10 was observed (Fig. 6*k*), indicating that these cytokines can be produced by nonlymphocytic cells upon topical MC903 treatment. A marginal increase of IFN-γ was also observed (Fig. 6*k*). Eosinophilia in blood and some tissues (e.g., ear-associated lymph nodes, liver, and spleen) was also observed in MC903-treated RAG1$^{-/-}$ mice (data not shown), whereas no immunoglobulins could be detected in sera (data not shown), indicating that increased levels of IgE or IgG were not indispensable for generating an AD-like syndrome.

Discussion

Selective ablation of both RXRα and -β in mouse skin keratinocytes results in a marked increase of TSLP expression that leads to the development of an AD-like phenotype (3). Because (*i*) putative NR response elements are present in mouse and human (20) TSLP promoters (see Fig. 4 *b* and *c*); (*ii*) TSLP repression did not require the AF-2 activation function of RXRs; and (*iii*) TSLP induction could not be triggered by an RXR agonist (Fig. 1*a*), we proposed (3) that this TSLP overexpression could reflect the relief of a transcriptional repression exerted by nonpermissive RXR/NR(s) heterodimers (21) in which the NR partner is unliganded. We demonstrate here that RXRα(β)/VDR heterodimers are such heterodimers, because topical treatment of mouse skin with 1α,25-$(OH)_2D_3$ or its low-calcemic analogs strongly induces TSLP expression in skin keratinocytes and triggers a skin and systemic AD-like syndrome mimicking that observed in RXRαβ$^{ep-/-}$ mutant and K14-TSLP transgenic mice (3). Moreover, the induction of TSLP by active vitamin D3 is a cell-autonomous event, because it is abolished upon keratinocyte-selective ablation of either VDR or RXRα and -β. We also show that, although less efficiently than RXRα(β)/VDR heterodimers, RXRα(β)/RARγ heterodimers liganded with RA or the RARγ-selective agonist BMS961, also mediate induction of TSLP expression but to a level too low to trigger, on its own, an overt AD-like phenotype. In keeping with these data, TSLP expression can be induced by 1α,25-$(OH)_2D_3$ and RA in a mouse epithelial tumor cell line (C1271, derived from a mammary carcinoma) (our unpublished data); TSLP was also shown to be induced by 1α,25-$(OH)_2D_3$ in a human epithelial tumor cell line (SCC25, derived from a tongue squamous cell carcinoma) (20). Furthermore, that agonists of VDR and RARγ could induce TSLP expression either on their own or synergistically indicates that the corresponding RXR heterodimers bind to distinct cognate response elements. In this respect, it is noteworthy that both mouse and human TSLP promoter regions contain putative response elements (Fig. 4 *b* and *c*) that may bind RXR/VDR heterodimers [vitamin D response element (VDRE):DR3] or RXR/RAR heterodimers [RA response element (RARE):DR2 and DR1] (22).

Based on this evidence, we propose a model accounting for the modulation of TSLP promoter activity by RXRα(β)/VDR and RXRα(β)/RARγ heterodimers (schematized in Fig. 5). The promoter region of mouse and human TLSP genes includes a TATA box element and proximal elements (e.g., NF-κB-binding sites) (the basal promoter) as well as putative VDREs and RAREs (Fig. 4 *b* and *c*). Because, under homeostatic conditions *in vivo*, there is no RA and very little, if any, active vitamin D3 (see below) in epidermal keratinocytes, the TSLP promoter basal activity is silenced by unliganded RXRα(β)/VDR and RXRα(β)/RARγ heterodimers associated with corepressors (10) (Fig. 5*a*). This repression can be efficiently exerted by either RXRα(β)/VDR or RXRα(β)/RARγ heterodimers, because it cannot be relieved by ablation of either VDR or RARγ (Fig. 3*e* and data not shown; Fig. 5 *b* and *c*). RXRα and -β ablation (Fig. 5*d*), which releases both heterodimers from their binding sites, abolishes this repression and allows basal promoter-bound transcription factors to stimulate TSLP transcription to a basal activity (see Fig. 3*f*, lane 3) that is sufficient to trigger the generation of an AD-like phenotype (3). Topical application of either active vitamin D3 or a low-calcemic analog (MC903) (Fig. 5*e*) generates RXR/VDR-coactivator complexes whose transcriptional activity (see Fig. 3*f*, lane 2) is efficient enough to not only relieve the repression exerted by RXR/RARγ corepressor complexes but also to further enhance the basal promoter activity. Interestingly, the RXR/RARγ coactivator complexes formed upon application of BMS961 are much less efficient (Fig. 5*f*), because they generate lower TSLP transcript levels (Fig. 1*a*) than those resulting from the basal promoter activity, as observed in keratinocytes ablated for RXRα and -β (see Fig. 3*f*, lane 3). However, upon cotreatment with BMS961 and a limiting dose of 1α,25-$(OH)_2D_3$ (Fig. 5*g*), liganded RXR/RARγ and RXR/VDR heterodimers can efficiently synergize to enhance the activity of TSLP basal promoter.

It should be stressed that, even though the present model accounts for all of our present observations, its refinement will require additional genetic (selective ablation of both VDR and RARγ in epidermal keratinocytes; mutation of the putative VDRE and RARE in the mouse) and biochemical (e.g., ChIP assays) studies to determine to which elements the RXR/VDR and RXR/RAR heterodimers bind, and whether VDR or RARγ preferentially heterodimerize with RXRα or RXRβ. In any event, the rapid and regulable induction of TSLP in mouse keratinocytes upon topical treatment with low-calcemic vitamin D3 analogs (e.g., MC903) provides a highly convenient AD preclinical model for exploring therapeutic avenues as well as a mouse model allowing characterization of various aspects of AD pathogenesis from its onset to the fully established disease phenotype. In this respect, we have found that epidermal thickening and dermal infiltration are observed in MC903-treated skin of both WT and RAG1$^{-/-}$ mice lacking mature T and B cells, showing that, even though 1α,25-$(OH)_2D_3$ could directly enhance the formation of Th2 cells from naïve CD4$^+$ T cells (18), these cells are actually not required for TSLP-induced development of an AD-like inflammation. Thus, the presence of eosinophils, mast cells, and dermal dendritic cells in MC903-treated RAG1$^{-/-}$ mice suggests that TSLP could act directly on these and other myeloid-derived cells to initiate an atopic inflammation, whereas the additional accumulation of CD4$^+$ Th2 cells in MC903-treated WT mice may correspond to a secondary effect of TSLP expression that serves for further progression of the AD-like phenotype. A similar conclusion was recently reached by Yoo *et al.* (8) using TCRβ$^{-/-}$ mice that lack T cells. As expected, no IgE could be detected in both MC903-treated and untreated RAG1$^{-/-}$ mice, indicating that IgE are dispensable for development of the AD-like phenotype, in keeping with the observation that, although elevated serum IgE is a frequently associated clinical feature in AD, ≈20% of AD patients have a normal serum IgE level (4).

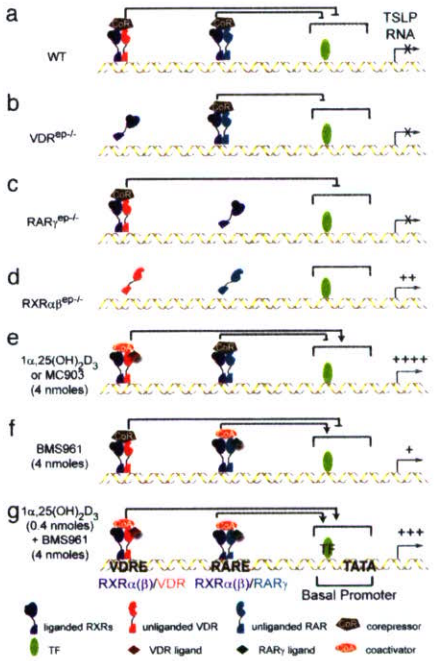

Fig. 5. Schematic model of RXRα(β)/VDR- and RXRα(β)/RAR-mediated regulation of TSLP expression in mouse keratinocytes (see *Discussion*). As concluded from our study (25), keratinocytic RXRs are shown bound to a non-RA-agonistic ligand.

Recent reports (5–9), including ours (3), have shown that TLSP represents a master switch of allergic inflammation and established in the mouse a direct link between TLSP expression in keratinocytes and airway epithelial cells and the pathogenesis of atopic dermatitis and asthma, respectively. However, how TLSP expression is triggered in these cells upon allergen exposure remains to be unveiled. Our previous (3) and present reports indicate that RXR heterodimerized with VDR and RARγ actively suppress TSLP expression, whereas active vitamin D3 and, to a lesser extent, RA can relieve this repression, thus raising the question of whether and how these ligands could be instrumental in triggering TSLP production *in vivo*. In this respect, a possible direct involvement of vitamin D signaling in atopy is supported by the observation that VDR-null mutant mice fail to develop symptoms of experimental asthma (23). Furthermore, vitamin A deficiency is known to diminish Th2-mediated responses, whereas high dietary vitamin A enhances them (24), which may reflect a role of RA-liganded RAR in TSLP induction.

Under homeostatic conditions *in vivo*, epidermal keratinocytes lack RA (11, 25). In keeping with a very low level of TSLP transcripts, others (refs. 14 and 26 and references therein) have shown that there is very little, if any, active vitamin D3 in these cells in which the enzyme 25(OH)D_3-1α-hydroxylase, required for synthesis of 1α,25-$(OH)_2D_3$ from 25(OH)D_3, is apparently not expressed. What could then be the origin of active vitamin D3 that induces TSLP expression in atopic dermatitis? Interestingly, it has been recently reported that, upon microbe-derived ligand activation of their Toll-like receptors (TLRs) that mediate the synthesis of antimicrobial peptides involved in the innate immune response, human, but not mouse, macrophages can produce 25(OH)D_3-1α-hydroxylase and synthesize 1α,25-$(OH)_2D_3$ (27, 28). We suggest that similar activation by allergen-derived ligands, of skin macrophage, dendritic cell, or, possibly, keratinocyte TLRs (29–31) may provide 1α,25-$(OH)_2D_3$ to keratinocytes in either a paracrine or autocrine manner. Thus, upon exposure of skin to an allergen, TSLP production might be triggered through a TLR-mediated production of active vitamin D3, raising the interesting possibility

that genetic or acquired defects of TLRs' function could be implicated in the pathogenesis of AD. Whether, upon allergen exposure, a TLR-mediated mechanism might also be involved in the production of RA is unknown.

That vitamin D could be instrumental to the pathogenesis of atopic diseases in humans is supported by an association between vitamin D supplementation in infancy and an increased risk of atopy later in life (32, 33). Our present study indicates that this association could be related to an increase of TSLP production in epithelial cells upon exposure to allergens during the perinatal period, which may ultimately result in an increase of allergen-specific Th2 memory cells which could be instrumental to triggering allergic reactions later in life. Interestingly, genetic investigations have also indicated that vitamin D signaling could be implicated in the pathogenesis of atopic diseases, as shown by association of VDR genetic variants with childhood and adult asthma, and atopic response (34, 35). These observations suggest that genetic predisposition to atopic disorders may implicate alteration of other components of vitamin D (and possibly vitamin A) signaling, which will ultimately result in TSLP overproduction. Dysregulation of vitamin D signaling may therefore be a key contributor to both genetic and environmental factors that underlie atopic diseases.

The therapeutic use of vitamins D and A has been considered for AD patients (36–39). Our present data indicate that, on the contrary, administration of these vitamins may exacerbate AD and, very likely, asthma by promoting expression of TSLP in skin and lungs. On the other hand, topical administration of vitamins D and/or A antagonists to AD patients may be beneficial, because it could enhance the repression exerted by RXR/VDR and RXR/RARγ heterodimers (40) on TSLP expression. It has also been recently suggested that low-calcemic VDR agonists (e.g., MC903) could be used to boost the innate immune response (through enhanced antimicrobial peptide production), for instance, to protect against infections and to accelerate wound healing, notably in the case of chronic ulcerated skin wounds (28, 39, 41, 42). Our results indicate that such therapy may not be beneficial to patients prone to atopy. Finally, our study also provides insight into the molecular mechanism that could underlie the use of low-calcemic vitamin D analogs in the treatment of psoriasis (13), a Th1 cell-driven skin disease. Interestingly, the most-common side effect of this treatment is a skin irritation (red, dry, and itchy skin) (43) exhibiting similarities with AD lesions. What our data, therefore, suggest is that a Th1 to Th2 skewing of Th cell differentiation triggered by induction of TSLP expression in keratinocytes may contribute to the therapeutic effect of topical MC903 on psoriatic lesions.

Methods

Experimental Animals and Skin Topical Application. $VDR^{-/-}$ (17), $RXR\alpha\beta^{ep-/-}$ (tamoxifen-treated K14-Cre-$ER^{T2(tg/0)}$/$RXR\alpha^{1.2/1.2}$/$RXR\beta^{1.2/1.2}$) (3), and $RAG1^{-/-}$ mice (The Jackson Laboratory) were as described. $VDR^{ep-/-}$ (K14-$Cre^{(tg/0)}$/$VDR^{1.2/1.2}$) mice were obtained by crossing K14-$Cre^{(tg/0)}$ transgenic mice (16) with floxed $VDR^{1.2/1.2}$ mice (our unpublished data). 1α,25-$(OH)_2D_3$ (Biomol), MC903 (12), and BMS961 (11) were dissolved in ethanol and topically applied on ears or shaved dorsal skin (1 cm^2) of either 6- to 8-week-old female CD1 WT mice or mice with indicated genotypes.

Other Methods. Histopathology, IHC, RNA analysis, serum cytokine and Ig determination, hematology assays, and statistic analysis are described in *Supporting Materials and Methods*, which is published as supporting information on the PNAS web site.

We thank the staff of the mouse, histopathology, hematology, and transgenic facilities and the Secretariat of the Institut de Génétique et de Biologie Moléculaire et Cellulaire (IGBMC) and Institut Clinique de la Souris for their kind help; Drs. N. Rochel-Guiberteau (IGBMC) and D. Moras (IGBMC) for vitamin D3 analogs; Bristol Meyer Squibb for BMS961; Dr. S. Chan (IGBMC) for $RAG1^{-/-}$ mice and helpful discussion; and Dr. F. Geissmann for a critical reading of the manuscript. This work was supported by funds from the Centre National de la Recherche Scientifique, the Institut National de la Santé et de la Recherche Médicale, the Collège de France, the Ministère de la Recherche, and European Community Project EUMORPHIA PLRT-CT-2001-00930.

1. Laudet, V. & Gronemeyer, H. (2002) *The Nuclear Receptor: Factsbook* (Academic, San Diego).
2. Mangelsdorf, D. J., Thummel, C., Beato, M., Herrlich, P., Schutz, G., Umesono, K., Blumberg, B., Kastner, P., Mark, M., Chambon, P., *et al.* (1995) *Cell* **83,** 835–839.
3. Li, M., Messaddeq, N., Teletin, M., Pasquali, J. L., Metzger, D. & Chambon, P. (2005) *Proc. Natl. Acad. Sci. USA* **102,** 14795–14800.
4. Leung, D. Y., Boguniewicz, M., Howell, M. D., Nomura, I. & Hamid, Q. A. (2004) *J. Clin. Invest.* **113,** 651–657.
5. Soumelis, V., Reche, P. A., Kanzler, H., Yuan, W., Edward, G., Homey, B., Gilliet, M., Ho, S., Antonenko, S., Lauerma, A., *et al.* (2002) *Nat. Immunol.* **3,** 673–680.
6. Liu, Y. J. (2006) *J. Exp. Med.* **203,** 269–273.
7. Zhou, B., Comeau, M. R., De Smedt, T., Liggitt, H. D., Dahl, M. E., Lewis, D. B., Gyarmati, D., Aye, T., Campbell, D. J. & Ziegler, S. F. (2005) *Nat. Immunol.* **6,** 1047–1053.
8. Yoo, J., Omori, M., Gyarmati, D., Zhou, B., Aye, T., Brewer, A., Comeau, M. R., Campbell, D. J. & Ziegler, S. F. (2005) *J. Exp. Med.* **202,** 541–549.
9. Al-Shami, A., Spolski, R., Kelly, J., Keane-Myers, A. & Leonard, W. J. (2005) *J. Exp. Med.* **202,** 829–839.
10. Perissi, V. & Rosenfeld, M. G. (2005) *Nat. Rev. Mol. Cell Biol.* **6,** 542–554.
11. Chapellier, B., Mark, M., Messaddeq, N., Calleja, C., Warot, X., Brocard, J., Gerard, C., Li, M., Metzger, D., Ghyselinck, N. B., *et al.* (2002) *EMBO J.* **21,** 3402–3413.
12. Carlberg, C. (2003) *J. Cell. Biochem.* **88,** 274–281.
13. Kragballe, K. & Iversen, L. (1993) *Dermatol. Clin.* **11,** 137–141.
14. Jones, G., Strugnell, S. A. & DeLuca, H. F. (1998) *Physiol. Rev.* **78,** 1193–1231.
15. Carlberg, C., Mathiasen, I. S., Saurat, J. H. & Binderup, L. (1994) *J. Steroid Biochem. Mol. Biol.* **51,** 137–142.
16. Li, M., Chiba, H., Warot, X., Messaddeq, N., Gerard, C., Chambon, P. & Metzger, D. (2001) *Development (Cambridge, U.K.)* **128,** 675–688.
17. Yoshizawa, T., Handa, Y., Uematsu, Y., Takeda, S., Sekine, K., Yoshihara, Y., Kawakami, T., Arioka, K., Sato, H., Uchiyama, Y., *et al.* (1997) *Nat. Genet.* **16,** 391–396.
18. Boonstra, A., Barrat, F. J., Crain, C., Heath, V. L., Savelkoul, H. F. & O'Garra, A. (2001) *J. Immunol.* **167,** 4974–4980.
19. Mombaerts, P., Iacomini, J., Johnson, R. S., Herrup, K., Tonegawa, S. & Papaioannou, V. E. (1992) *Cell* **68,** 869–877.
20. Wang, T. T., Tavera-Mendoza, L. E., Laperriere, D., Libby, E., MacLeod, N. B., Nagai, Y., Bourdeau, V., Konstorum, A., Lallemant, B., Zhang, R., *et al.* (2005) *Mol. Endocrinol.* **19,** 2685–2695.
21. Chambon, P. (2005) *Mol. Endocrinol.* **19,** 1418–1428.
22. Leid, M., Kastner, P. & Chambon, P. (1992) *Trends Biochem. Sci.* **17,** 427–433.
23. Wittke, A., Weaver, V., Mahon, B. D., August, A. & Cantorna, M. T. (2004) *J. Immunol.* **173,** 3432–3436.
24. Stephensen, C. B. (2001) *Annu. Rev. Nutr.* **21,** 167–192.
25. Calleja, C., Messaddeq, N., Chapellier, B., Yang, H., Krezel, W., Li, M., Metzger, D., Mascrez, B., Ohta, K., Kagechika, H., *et al.* (2006) *Genes Dev.* **20,** 1525–1538.
26. Vanhooke, J. L., Prahl, J. M., Kimmel-Jehan, C., Mendelsohn, M., Danielson, E. W., Healy, K. D. & DeLuca, H. F. (2006) *Proc. Natl. Acad. Sci. USA* **103,** 75–80.
27. Kupper, T. S. & Fuhlbrigge, R. C. (2004) *Nat. Rev. Immunol.* **4,** 211–222.
28. Liu, P. T., Stenger, S., Li, H., Wenzel, L., Tan, B. H., Krutzik, S. R., Ochoa, M. T., Schauber, J., Wu, K., Meinken, C., *et al.* (2006) *Science* **311,** 1770–1773.
29. Fritsche, J., Mondal, K., Ehrnsperger, A., Andreesen, R. & Kreutz, M. (2003) *Blood* **102,** 3314–3316.
30. Takeda, K., Kaisho, T. & Akira, S. (2003) *Annu. Rev. Immunol.* **21,** 335–376.
31. Chu, A. C. & Morris, J. F. (2005) in *Skin Immune System*, ed. Bos, J. D. (CRC, Boca Raton, FL), pp. 77–99.
32. Wjst, M. & Dold, S. (1999) *Allergy* **54,** 757–759.
33. Hypponen, E., Sovio, U., Wjst, M., Patel, S., Pekkanen, J., Hartikainen, A. L. & Jarvelinb, M. R. (2004) *Ann. N.Y. Acad. Sci.* **1037,** 84–95.
34. Poon, A. H., Laprise, C., Lemire, M., Montpetit, A., Sinnett, D., Schurr, E. & Hudson, T. J. (2004) *Am. J. Respir. Crit. Care Med.* **170,** 967–973.
35. Raby, B. A., Lazarus, R., Silverman, E. K., Lake, S., Lange, C., Wjst, M. & Weiss, S. T. (2004) *Am. J. Respir. Crit. Care Med.* **170,** 1057–1065.
36. Worm, M. (2002) *Curr. Opin. Investig. Drugs* **3,** 1596–1603.
37. Lehmann, B., Querings, K. & Reichrath, J. (2004) *Exp. Dermatol.* **13,** Suppl 4, 11–15.
38. Zasloff, M. (2005) *J. Invest. Dermatol.* 125, xvi-xvii.
39. Zasloff, M. (2006) *Nat. Med.* **12,** 388–390.
40. Germain, P., Iyer, J., Zechel, C. & Gronemeyer, H. (2002) *Nature* **415,** 187–192.
41. Gombart, A. F., Borregaard, N. & Koeffler, H. P. (2005) *Faseb J.* **19,** 1067–1077.
42. Wang, T. T., Nestel, F. P., Bourdeau, V., Nagai, Y., Wang, Q., Liao, J., Tavera-Mendoza, L., Lin, R., Hanrahan, J. H., Mader, S., *et al.* (2004) *J. Immunol.* **173,** 2909–2912.
43. Gottlieb, A. B. (2005) *J. Am. Acad. Dermatol.* **53,** S3–S16.

MOLECULAR AND CELLULAR BIOLOGY, Nov. 2006, p. 7966–7976 Vol. 26, No. 21
0270-7306/06/$08.00+0 doi:10.1128/MCB.00713-06

Turning Off Estrogen Receptor β-Mediated Transcription Requires Estrogen-Dependent Receptor Proteolysis[▽]

Yukiyo Tateishi,[1]† Raku Sonoo,[2]† Yu-ichi Sekiya,[1] Nanae Sunahara,[1] Miwako Kawano,[1] Mitsutoshi Wayama,[1] Ryuichi Hirota,[2] Yoh-ichi Kawabe,[1] Akiko Murayama,[1] Shigeaki Kato,[3] Keiji Kimura,[1] and Junn Yanagisawa[1,2]*

Graduate School of Life and Environmental Sciences, University of Tsukuba, Tsukuba Science City, Ibaraki 305-8572, Japan[1]; Ankhs Incorporated, Tsukuba Industrial Liaison and Cooperative Research Center, University of Tsukuba, Tsukuba Science City, Ibaraki 305-8577, Japan[2]; and Institute of Molecular and Cellular Biosciences, University of Tokyo, Bunkyo-ku, Tokyo 113-0032, Japan[3]

Received 25 April 2006/Returned for modification 12 June 2006/Accepted 17 August 2006

Recent studies have shed light on the ligand-dependent transactivation mechanisms of nuclear receptors (NRs). When the ligand dose is reduced, the transcriptional activity of NRs should be downregulated. Here we show that a ubiquitin-proteasome pathway plays a key role in turning off transcription mediated by estrogen receptor β (ERβ). ERβ shows estrogen-dependent proteolysis, and its degradation is regulated by two regions in the receptor. The N-terminal 37-amino acid-region is necessary for the recruitment of the ubiquitin ligase, i.e., the carboxyl terminus of HSC70-interacting protein (CHIP), to degrade ERβ. In contrast, the C-terminal F domain protects ligand-unbound ERβ from proteolysis to abrogate proteasome association. Suppression of CHIP by interfering RNA inhibited this switching off of receptor-mediated transcription when the ligand dose was reduced. Our results suggest that after ligand withdrawal, the active form of the NR is selectively eliminated via ligand-dependent proteolysis to downregulate receptor-mediated transcription.

Estrogen is a growth factor that stimulates cell growth and differentiation in diverse tissues. Dramatic changes in the levels of estrogen in the blood occur during the normal human menstrual cycle. During the first 7 to 10 days, the level of estrogen is low. In the middle of the cycle (days 11 to 15), it rises and then falls abruptly. The effects of estrogen are mediated through the estrogen receptors (ERs), ERα and ERβ, which function as ligand-induced transcription factors and belong to the nuclear receptor (NR) superfamily (2, 5, 12, 20, 31, 33, 41, 49). When the estrogen level is high, estrogen binds to ERs to activate the transcription of target genes. This induces the ligand-binding domain (LBD) to undergo a characteristic conformational change, whereupon the receptor dimerizes, binds to DNA, and subsequently stimulates gene expression (10). ERα is stimulated by two distinct activation regions, activation function 1 (AF-1) and AF-2, which are located in the LBD and exert ligand-dependent transcriptional activity. Crystal structure analysis of ERs and other NRs has revealed the presence of 12 conserved helices in their LBDs (46). The LBD forms a structure described as a sandwich of 12 α-helices (helices 1 to 12) with a central hydrophobic ligand-binding pocket. Helix 12, the most C-terminal of these helices, has been identified as the critical core (AD core) of the AF-2 function of the receptor and plays an important role in coactivator binding to the ligand-bound receptor (6, 19, 24, 25, 33, 35, 39, 43, 45, 55, 56).

When the level of estrogen is decreased, receptor-mediated transcription should be downregulated. Because the response to estrogen is tightly controlled, the downregulation of ER-mediated transcription should also be tightly regulated. Although such regulation of the NRs has generated intense interest, the molecular mechanisms regulating these processes are not understood (38). To switch off transcription, there are at least two possible mechanisms. The first involves the dissociation of ligands from the hormone-binding pocket of the receptor. However, the dissociation rate of the ligand from its receptor is very low, because the receptor locks the hormone within its activation pocket and covers it with coactivators (16). Another possible mechanism is the rapid degradation of active receptors. Several nuclear receptors, such as the ER and those for progesterone, glucocorticoid, thyroid hormone receptor, retinoid X, and retinoic acid, are ubiquitinated and degraded in the course of their nuclear activities (8, 11, 13, 26, 29, 32, 36, 47, 51, 57). These degradation steps might be involved in turning off NR-mediated transcription.

Evidence now suggests that proteasome-dependent degradation of receptors is necessary for the activation of these receptors (38). Moreover, this requires NR-mediated transcriptional activity, implying that the degradation and the transactivation of NRs are mutually independent processes. In the ubiquitin-proteasome pathway, proteins destined for degradation are conjugated by polyubiquitin chains, in which one ubiquitin molecule is conjugated by another through one of its seven lysine residues, typically K48. These polyubiquitin chains are then recognized by the regulatory complex of the 26S proteasome.

Here we show that there is a ubiquitin-proteasome pathway for ERβ that is not coupled to transactivation. To investigate this, we purified the ubiquitin ligase complex for ERβ and

* Corresponding author. Mailing address: Graduate School of Life and Environmental Sciences, University of Tsukuba, Tsukuba Science City, Ibaraki 305-8572, Japan. Phone: 81-29-853-6632. Fax: 81-29-853-4605. E-mail: junny@agbi.tsukuba.ac.jp.
† These authors contributed equally to this work.
▽ Published ahead of print on 28 August 2006.

identified a protein complex containing the carboxyl terminus of heat shock cognate 70 (HSC70)-interacting protein (CHIP) (1). CHIP binds directly to the N-terminal 37-amino-acid region of ERβ and ubiquitinates it to induce ERβ degradation. In contrast, the C-terminal F domain inhibits the binding of proteasome to the receptor and protects it from proteolysis in the absence of estrogen. Suppression of CHIP by interfering RNA (RNAi) inhibited the switching off of receptor-mediated transcription that occurs when the ligand dose is reduced. Our results suggest that ligand-dependent degradation selectively and rapidly eliminates the active form of a nuclear receptor to downregulate receptor-mediated transcription after ligand withdrawal.

MATERIALS AND METHODS

Expression vectors. The ERα/β and CHIP expression plasmids and their deletion mutants have been described previously (48). ERE-TATA-Luc and ERE-TATA-LucCP were constructed by inserting three consensus estrogen response elements into a luciferase reporter plasmid encoding a TATA box, pGL3-Basic or phRG(R2.2)-Basic. pGL3-Basic, phRG(R2.2)-Basic, and pGL3-Control vectors were purchased from Promega (Madison, WI).

Antibodies. Anti-FLAG-M2 mouse monoclonal antibody (Sigma, St. Louis, MO), anti-hemagglutinin (HA) mouse monoclonal antibody (Roche), anti-human ERα antibody (Chemicon, Temecula, CA), anti-human ERβ antibody (PPMX), and anti-glyceraldehyde-3-phosphate-dehydrogenase mouse monoclonal antibody (American Research Products, Inc.) were used at appropriate dilutions, according to the manufacturers' instructions. A rabbit polyclonal antibody directed against CHIP was provided by T. Chiba (Tokyo Metropolitan Institute of Medical Science).

Cell culture and transfection. MDA-MB231 breast cancer cells and human embryonic kidney 293 cells were routinely maintained in Dulbecco's modified Eagle's medium (DMEM) supplemented with 10% fetal bovine serum (FBS). Twenty-four hours before transfection, the medium was changed to phenol red-free DMEM containing 4% charcoal-stripped FBS. Transfection was performed using PerFectin transfection reagent (Gene Therapy Systems) or TransFast transfection reagent (Promega) according to the manufacturers' protocols. The cells were treated with or without MG132 (10^{-6} M) and estrogen (10^{-8} M). Twenty-four hours after the addition of estrogen, the cells were harvested and analyzed by Western blotting using the appropriate antibodies.

Coimmunoprecipitation and Western blotting. The 293 cells were transfected with the appropriate plasmids and lysed in TNE buffer (10 mM Tris-HCl [pH 7.8], 0.5% Nonidet P-40 [NP-40], 0.15 M NaCl, 1 mM EDTA, 1 μM phenylmethylsulfonyl fluoride [PMSF], 1 μg/ml aprotinin). Extracted proteins were immunoprecipitated with antibody-coated protein A/G-Sepharose (Amersham) or anti-FLAG M2 agarose (Sigma). The bound proteins were separated by sodium dodecyl sulfate-polyacrylamide gel electrophoresis (SDS-PAGE), transferred onto polyvinylidene difluoride membranes (Millipore), and detected with the appropriate antibodies and secondary antibodies conjugated with horseradish peroxidase. Specific proteins were detected using an enhanced chemiluminescence Western blot detection system (Amersham).

Luciferase assay. For luciferase assays, ERE-TATA-Luc plasmids were cotransfected with expression vector encoding ERβ or its mutants. As a reference plasmid with which to normalize transfection efficiency, the pRSVβGAL vector or the pRL-CMV vector was cotransfected in all experiments. Twenty-four hours after transfection, the culture medium was replaced with fresh medium containing 0.2% FBS, either estrogen (10^{-8} M) or ethanol vehicle was added, and the cells were incubated for an additional 24 h. Cell extracts were prepared, and luciferase assays were performed following the manufacturer's protocol (Promega). β-Galactosidase activity was measured to control for the efficiency of each transfection. Individual transfections, each consisting of triplicate wells, were repeated at least three times.

Protein purification. Glutathione *S*-transferase (GST) protein or an immobilized 37-amino-acid region that we designated the "domain required for degradation" (DRD) fused to GST (GST-DRD) was preincubated for 1 h at 4°C in GST-binding buffer (20 mM Tris-HCl [pH 7.9], 180 mM KCl, 0.2 mM EDTA, 0.5 mM PMSF, and 1 mM dithiothreitol) containing bovine serum albumin (BSA; 1 mg/ml). Bead-immobilized proteins were then incubated at 4°C for 6 to 10 h with 293 cell extracts. After the beads had been washed three times with GST buffer (GST-binding buffer with 0.1% NP-40), they were washed again with GST buffer containing 0.2% *N*-lauroyl sarcosine. Proteins bound to the DRD were eluted with 15 mM reduced glutathione in elution buffer (50 mM Tris-HCl [pH 8.3], 150 mM KCl, 0.5 mM EDTA, 0.5 mM PMSF, 5 mM NaF, 0.08% NP-40, 0.5 mg/ml BSA, and 10% glycerol). Recombinant CHIP was expressed in *Escherichia coli* and purified using Ni-agarose.

Immunofluorescence. The 293 cells were grown on poly-L-lysine-coated 12-well culture dishes and transfected with plasmids. Twenty-four hours after transfection, the cells were fixed with 4% paraformaldehyde in phosphate-buffered saline (PBS) for 10 min and permeabilized with Triton buffer (50 mM Tris-HCl [pH 7.5], 0.5% Triton X-100, 150 mM NaCl, 2 mM EDTA) for 15 min. The cells in each well were blocked with PBS containing 1% BSA and 0.5% goat serum for 3 h at 37°C. The cells were incubated with the appropriate antibody in PBS containing 1% BSA for 2 h at 37°C. After the cells had been washed with PBS, they were incubated with Alexa-Fluor-488-conjugated goat anti-rat immunoglobulin G or Alexa-Fluor-594-conjugated goat anti-mouse immunoglobulin G (Molecular Probes) for 1 h at 37°C and washed with PBS. The samples were mounted with Vectashield mounting medium (Vector Laboratories) and analyzed using a Keyence Biozero BZ-8000.

Pulse-chasing. The 293 cells were transfected with ERβ, and 48 h after transfection the cells were labeled for 30 min at 37°C with [^{35}S]methionine (50 μCi/ml) in methionine-free DMEM. The cells were then washed twice and incubated in DMEM containing 0.2% FBS for the indicated periods (chase). At each time point, cell lysates were immunoprecipitated with anti-ERβ antibody. The immunoprecipitates were resolved by SDS-PAGE and visualized by autoradiography. A phosphorimager was used to quantify the metabolically labeled ERβ present at each time point.

RNAi. The 293gp cells were transfected with pSINsi-hU6 vector (Takara) containing the target sequence of CHIP or LacZ (control) and with vesicular stomatitis virus-encoded envelope protein G to generate the small interfering RNA (siRNA) retroviral supernatant. MDA-MB-231 cells were transfected with retroviral supernatant in the presence of Polybrene (8 μg/ml). Twenty-four hours after transfection, the viral supernatant was replaced with fresh DMEM containing 10% FBS. The transfected cells were selected with G418 (1 mg/ml). The target sequences were 5′-GCACGACAAGTACATGGCGGA-3′ for CHIP and 5′-GCTACACAAATCAGCGATT-3′ for LacZ.

RESULTS

An N-terminal 37-amino-acid region is essential for ERβ degradation. The level of ERβ protein was reduced by the addition of estrogen to the MDA-MB-231 breast cancer cell line. This degradation was inhibited by the proteasome inhibitors MG132 (Fig. 1A) and lactacystin (data not shown). In a ubiquitination assay, ERβ was ubiquitinated in both the presence and the absence of estrogen (Fig. 1B). Thus, ERβ is degraded via ubiquitin-proteasome pathways. Preliminary biochemical study showed that a single K48-linked polyubiquitin chain is sufficient to target a substrate to the 26S proteasome. Therefore, we investigated the ubiquitin linage of the chains using a ubiquitin mutant lacking specific lysines, Ub(K48R). HA-tagged ubiquitin (HA-Ub) or Ub(K48R) was transfected into 293 cells, and the level of ERβ protein and the ubiquitination status were determined by Western blotting using an anti-FLAG-M2 or an anti-HA antibody. Expression of Ub(K48R) reduced the degradation (Fig. 1C) and the ubiquitination status (Fig. 1D) of ERβ, suggesting that the polyubiquitin chains of ERβ are linked via K48. These results indicate that whereas ERβ is polyubiquitinated via K48 in ubiquitin in both the presence and the absence of estrogen, the proteolysis is estrogen dependent. Our observations imply that ubiquitination in itself is not the only way to regulate ERβ.

To investigate the molecular mechanism by which ERβ is degraded, DNA sequences encoding truncated forms of ERα or ERβ were transfected into 293 cells, and the protein levels were examined by Western blot analysis. ERα(Δ181), which does not contain the A/B domain, still underwent

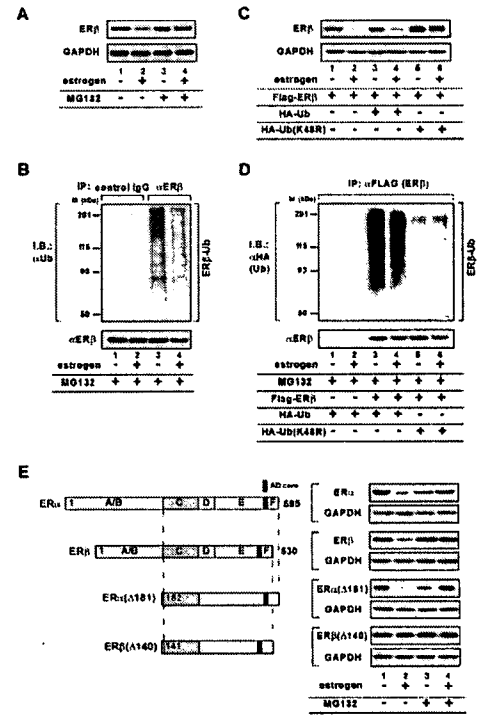

FIG. 1. ERβ is degraded through ubiquitin-proteasome pathways. (A) ERβ is degraded in an estrogen-dependent manner. ERβ-transfected MDA-MB-231 cells were cultured in the presence or the absence of estrogen (10^{-8} M) and the proteasome inhibitor MG132 (10^{-6} M). ERβ level was analyzed by use of Western blots probed with the indicated antibody. (B) ERβ is degraded via ubiquitin-proteasome pathways. ERβ-transfected MDA-MB-231 cells were cultured in the presence or the absence of estrogen (10^{-8} M) and MG132 (10^{-6} M). ERβ was immunoprecipitated (IP) using anti-ERβ antibody. Upper panel: the ubiquitination status of ERβ was analyzed by Western blotting (IB) and probed with an anti-ubiquitin antibody. Lower panel: immunoprecipitated ERβ was detected by Western blotting and probed with an anti-ERβ antibody. IgG, immunoglobulin G; M, molecular mass. (C) The estrogen-dependent degradation of ERβ is inhibited by mutated ubiquitin Ub(K48R). FLAG-tagged ERβ and DNA encoding HA-Ub (1,000 ng) or HA-Ub(K48R) (1,000 ng) were transfected into 293 cells in the presence or the absence of estrogen (10^{-8} M). ERβ was detected by use of Western blots probed with anti-FLAG-M2 antibody. (D) The polyubiquitin chain of ERβ is linked via K48. FLAG-tagged ERβ and DNA encoding HA-Ub (1,000 ng) or HA-Ub(K48R) (1,000 ng) were transfected into 293 cells in the presence or the absence of estrogen (10^{-8} M) and MG132 (10^{-6} M). FLAG-tagged ERβ was immunoprecipitated with anti-FLAG-M2 antibody. Upper panel: the ubiquitination status of ERβ was analyzed by use of Western blots probed with anti-HA antibody. Lower panel: immunoprecipitated ERβ was detected by use of Western blots probed with anti-FLAG antibody. (E) The A/B domain is necessary for the estrogen-dependent degradation of ERβ. DNA (500 ng) encoding the indicated FLAG-tagged ER deletion mutants was transfected into 293 cells. These cells were cultured in the presence or the absence of estrogen (10^{-8} M) and MG132 (10^{-6} M). To evaluate the protein levels of the ER mutants, Western blot analysis was performed using anti-FLAG-M2 antibody.

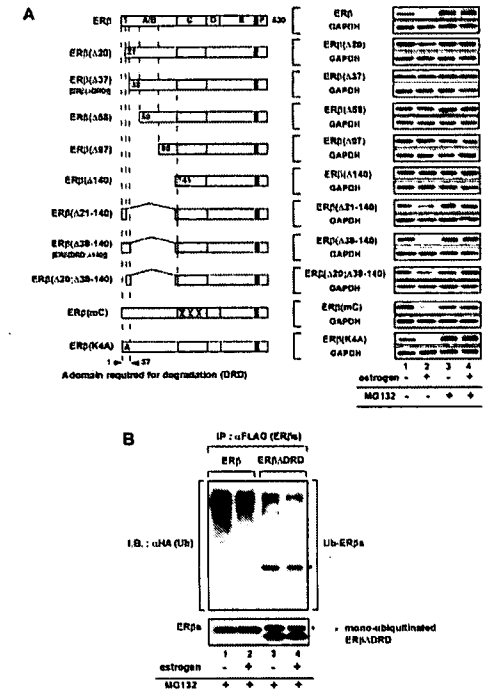

FIG. 2. DRD-mediated degradation is involved in the downregulation of ERβ-mediated transcription. (A) The N-terminal 37-amino-acid region is essential for estrogen-mediated ERβ degradation. DNA sequences (500 ng) encoding the indicated FLAG-tagged ERβ deletion mutants were transfected into 293 cells. These cells were cultured in the presence or the absence of estrogen (10^{-8} M) and MG132 (10^{-6} M). To evaluate the protein levels of the ERβ mutants, Western blot analysis was performed using an anti-FLAG-M2 antibody. (B) DRD-regulated ubiquitination of ERβ. DNA (500 ng) encoding the indicated FLAG-tagged ERβ mutants and DNA (1,000 ng) encoding HA-tagged ubiquitin were transfected into 293 cells in the presence or the absence of estrogen (10^{-8} M). Upper panel: FLAG-tagged ERβ mutants were immunoprecipitated (IP) with anti-FLAG-M2 antibody. The ubiquitination status of ERβ was analyzed by use of Western blots probed with anti-HA antibody. Lower panel: immunoprecipitated ERβ mutants were detected by use of Western blots probed with an anti-FLAG-M2 antibody. I.B., Western blotting.

ligand-dependent degradation (Fig. 1E). In contrast, truncation of the A/B domain of ERβ, forming ERβ(Δ140), produced no ligand-dependent degradation, suggesting that the A/B domain of ERβ is necessary for its ligand-dependent degradation (Fig. 1E).

We then investigated the region responsible for the degradation of ERβ. The levels of truncated ERβ protein in the presence and the absence of estrogen were examined by Western blotting. As shown in Fig. 2A, ERβ(Δ20), in which the 20 N-terminal amino acids are deleted, was elevated in the pres-

ence of estrogen compared with wild-type ERβ. ERβ(Δ37) exhibited almost no degradation, indicating that the N-terminal 37 amino acids are essential for the ligand-dependent degradation of ERβ (Fig. 2A). To assess whether this region is sufficient for the ligand-dependent degradation of ERβ, it was fused to ERβ(Δ140), which does not contain the A/B domain and shows little ligand-dependent degradation. In contrast to that of ERβ(Δ140), the level of ERβ(Δ38-140) protein, in which the 37-amino-acid region is fused to ERβ(Δ140), was reduced in an estrogen-dependent manner (Fig. 2A). This reduction was abrogated by the addition of MG132, indicating that ERβ(Δ38-140) is degraded by proteasomal pathways. Interestingly, the degradation of ERβ(mC), which has three amino acid substitutions in the DNA-binding domain (C domain) and has almost no ability to bind DNA (30), was similar to that of wild-type ERβ (Fig. 2A), indicating that binding to the DNA element is not necessary for ligand-dependent receptor degradation. Similar results were obtained when other cell lines, such as MCF-7 or MDA-MB-231, were used (data not shown). From these observations, we concluded that the N-terminal 37-amino-acid region of ERβ is involved in its ligand-dependent degradation and designated this region the DRD. We next determined the ubiquitination status of the truncated forms of ERβ. The DRD deletion accumulated a monoubiquitinated form and showed a reduced level of the polyubiquitinated form (Fig. 2B), suggesting that the DRD is required for the polyubiquitination of ERβ.

Purification and identification of an E3 ubiquitin ligase that specifically binds to the DRD of ERβ. To investigate why the DRD induces ubiquitination, we examined two possibilities. First, the DRD may contain a lysine residue that is ubiquitinated by a ubiquitin ligase specific for ERβ. Second, there may be a ubiquitin ligase that specifically recognizes and binds to the DRD to ubiquitinate ERβ.

To test the first possibility, we introduced an amino acid substitution at the lysine residue in the DRD. ERβ(K4A), in which the lysine residue in the DRD is replaced by alanine, showed ligand-dependent degradation similar to that of the wild type (Fig. 2A), implying that the lysine residue in the DRD is not a target for ubiquitination. Therefore, we investigated the other possibility.

We generated a GST-fused 37-amino-acid region (GST-DRD) with which to purify proteins that specifically bind to the DRD. Whole-cell extracts prepared from 293 cells were incubated with either GST-DRD or GST. The bound proteins were precipitated with glutathione beads and separated using SDS-PAGE (Fig. 3A). Mass fingerprinting methods revealed that the proteins that specifically bound to the DRD were the carboxyl terminus of CHIP, HSP70, and HSP90 (Fig. 3A).

CHIP has E3 ubiquitin ligase activity mediated by its carboxyl-terminal U-box domain and has the ability to bind to chaperones HSP/HSC70 via its tetratricopeptide repeat (TPR) domain (7, 48). A pull-down assay showed that recombinant CHIP bound to the GST-DRD (Fig. 3B). A coimmunoprecipitation assay demonstrated specific binding of CHIP and HSP70 to ERβ in both the absence and the presence of estrogen (Fig. 3C). ERβΔDRD showed no ability to bind CHIP (Fig. 3D). Therefore, we tested whether CHIP enhances ERβ ubiquitination. When ERβ was coexpressed with CHIP, smeary bands of ubiquitin-conjugated ERβ products were observed

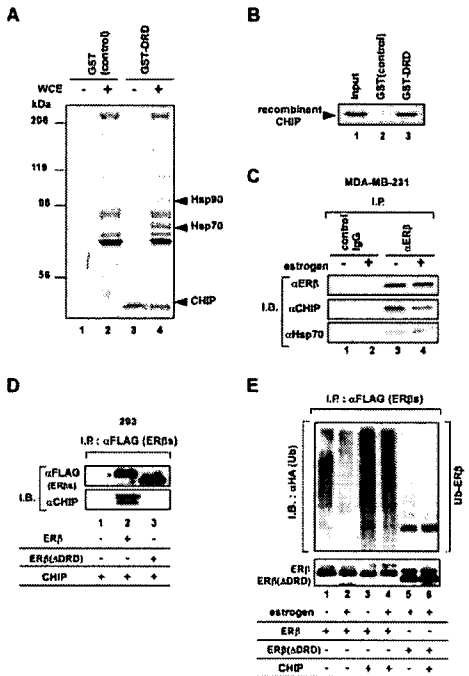

FIG. 3. The DRD associates with a protein complex containing the carboxyl terminus of HSC70-interacting protein (CHIP) and HSC/HSP70. (A) Purification and identification of DRD-interacting proteins. Whole-cell extracts (WCE) prepared from 293 cells were incubated with GST-DRD or with GST as the control. Bound proteins were precipitated with GST-conjugated beads, eluted with glutathione, and subjected to SDS-PAGE followed by silver staining. The fractions eluted from GST and GST-DRD are shown. Proteins eluted from the DRD peptide were examined by mass spectrometry. (B) CHIP binds the DRD. Recombinant CHIP was incubated with GST-DRD or GST. The bound proteins were precipitated with glutathione beads. CHIP bound to GST-DRD was separated by SDS-PAGE. (C) Interaction between ERβ and CHIP in vivo. ERβ-transfected MDA-MB-231 cells were lysed and immunoprecipitated (I.P.) with anti-ERβ antibody in the presence or the absence of estrogen (10^{-8} M). The precipitates were Western blotted (I.B.) and probed with antibodies directed against CHIP and HSP70. IgG, immunoglobulin G. (D) DRD is necessary for the interaction between ERβ and CHIP. ERβ or ERβΔDRD was transfected into 293 cells. These cells were lysed and immunoprecipitated with anti-FLAG-M2 antibody. The precipitates were Western blotted and probed with antibodies directed against CHIP and HSP70. (E) CHIP induces the ubiquitination of ERβ. DNA (500 ng) encoding FLAG-tagged ERβ and DNA (1,000 ng) encoding HA-tagged ubiquitin were transfected into 293 cells with or without DNA (50 ng) encoding CHIP in the presence or the absence of estrogen (10^{-8} M). FLAG-tagged ERβ or ERβ(ΔDRD) was immunoprecipitated using anti-FLAG-M2 antibody. The ubiquitination status of ERβ was analyzed by use of Western blots probed with anti-HA antibody.

(Fig. 3E). In contrast, CHIP expression had no effect on the ubiquitination status of ERβ(ΔDRD). Thus, CHIP appears to mediate the ubiquitination of ERβ.

CHIP participates in the degradation of ERβ. ERβ is known to localize predominantly in the nucleus. Although a large proportion of the CHIP protein was localized in the cytoplasm, a small amount was observed in the nucleus by immunostaining (Fig. 4A) and Western blot analysis (Fig. 4B, left panel). To test whether CHIP-mediated ubiquitination induces the degradation of ERβ, DNA encoding ERβ was transfected into 293 cells with or without DNA encoding CHIP. Western blot analysis revealed that the steady-state level of ERβ decreased in both the nucleus and the cytoplasm when CHIP was produced (Fig. 4B, left panel). ERβ in MDA-MB-231 cells also decreased with the production of CHIP (Fig. 4B, right panel). We further determined CHIP's function by producing MDA-MB-231 cells in which endogenous CHIP expression was suppressed by the introduction of a siRNA complementary to sequences present in the CHIP mRNA. The introduction of the siRNA vector into MDA-MB-231 cells suppressed the expression of CHIP mRNA (data not shown) and protein (Fig. 4C, left panel) and the accumulation of ERβ protein (Fig. 4C, right panel). In contrast, a control vector failed to alter the CHIP or ERβ protein levels (Fig. 4C, right panel). Thus, CHIP appears to be involved in estrogen-dependent ERβ degradation. To confirm this, pulse-chase experiments were performed. In the presence of estrogen, the half-life of ERβ exceeded 8 h, but it had a half-life of about 4 h when CHIP was expressed (Fig. 4D).

To confirm that the DRD is necessary for CHIP-dependent ERβ degradation, DNA sequences encoding truncated forms of ERβ were transfected into 293 cells with or without DNA encoding CHIP. CHIP expression enhanced the degradation of ERβ, ERβ(mC), ERβ(DRD;Δ140), and ERβ(AF-1), all of which contain the DRD, but did not enhance the degradation of ERβ(ΔDRD) or ERβ(Δ140), neither of which contains the DRD (Fig. 5A). To test the specificity of this effect, we created constructs in which the TPR and U-box domains of CHIP were deleted (ΔTPR and ΔU-box, respectively). CHIP binds to HSP/HSC70 via its TPR motif and displays E3 ubiquitin ligase activity mediated by its U-box domain. Although the expression of these truncated proteins was similar to that of full-length CHIP (data not shown), deletion of either of these domains abolished the effects of CHIP on ERβ (Fig. 5B). Such a requirement for a TPR motif indicates that CHIP may have to interact with HSP/HSC70 to promote ERβ degradation. The functional requirement for the U-box confirms that CHIP regulates ERβ ubiquitination.

In a previous report, we showed that CHIP binds ERα in the absence of estrogen (48). Since ERα and ERβ heterodimerize readily in the presence of each other, we examined the effect of cointroducing ERα on CHIP-dependent degradation of ERβ. As shown in Fig. 5C, the degradation of ERβ was not affected by coexpression of ERα.

The F domain regulates ERβ degradation negatively. Our results showed that whereas CHIP binds and ubiquitinates ERβ in both the presence and the absence of estrogen, the degradation of ERβ is estrogen dependent. To investigate this discrepancy, DNA sequences encoding truncated forms of ERs were transfected into 293 cells and the protein levels were

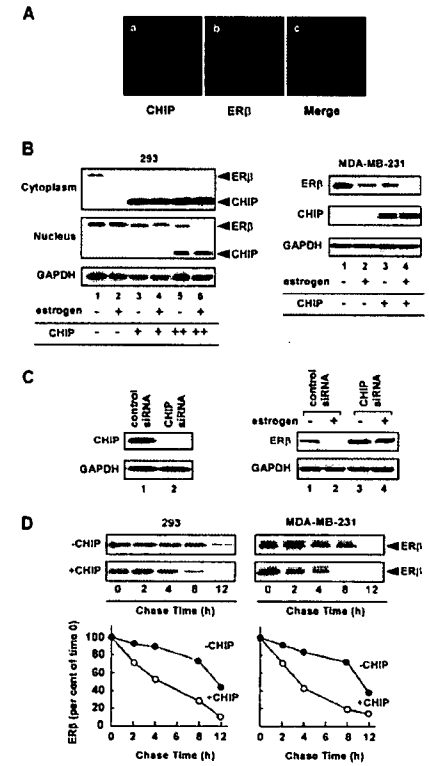

FIG. 4. CHIP enhances the degradation of ERβ. (A) CHIP protein was observed in both the cytoplasm and the nucleus. The 293 cells were transiently transfected with plasmids encoding HA-tagged CHIP and FLAG-tagged ERβ. Mounted cells were examined by immunofluorescence microscopy as described in Materials and Methods. (a) The distribution of CHIP in the cell is shown. (b) The distribution of ERβ is shown. (c) Merged images of panels a and b. (B) CHIP expression reduced the steady-state level of ERβ. DNA (50 ng) encoding HA-tagged CHIP was cotransfected into 293 or MDA-MB-231 cells with DNA (500 ng) encoding FLAG-tagged ERβ in the absence or the presence of estrogen (10^{-8} M). The level of ERβ protein was examined by use of Western blots probed with anti-FLAG (293) or anti-ERβ (MDA-MB-231) antibody. (C) ERβ accumulated after the siRNA-mediated suppression of endogenous CHIP. Plasmids encoding a siRNA specific for CHIP or the control vector were introduced into MDA-MB-231 cells. These cells were selected with G418. Levels of CHIP and ERβ proteins were assessed by immunoblotting the whole-cell lysates with specific antibodies, as indicated. (D) CHIP facilitates the degradation of ERβ. 293 or MDA-MB-231 cells were transfected with DNA (50 ng) encoding CHIP or with DNA (500 ng) encoding FLAG-tagged ERβ in the presence of estrogen (10^{-8} M). Cells were pulse-labeled with [^{35}S]methionine and then chased for the indicated times in medium containing unlabeled methionine. ^{35}S-labeled ERβ in the immunoprecipitate was quantified by phosphorimaging, and the levels in control cells (closed circles) and CHIP-expressing cells (open circles) were plotted relative to the amount present at time zero.

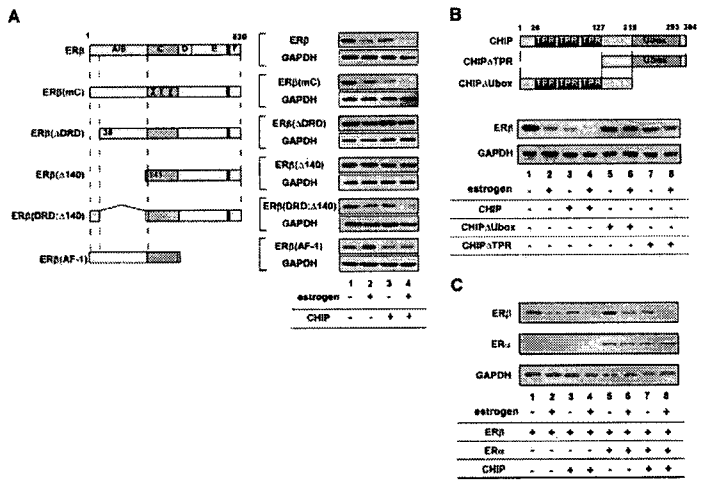

FIG. 5. CHIP regulates DRD-mediated ubiquitination and degradation. (A) The DRD is necessary for CHIP-dependent ERβ degradation. DNA (500 ng) encoding the indicated FLAG-tagged ERβ mutants was transfected into 293 cells, with or without DNA encoding CHIP. These cells were cultured in the presence or the absence of estrogen (10^{-8} M). To evaluate the levels of ERβ mutant proteins, Western blot analysis was performed using anti-FLAG-M2 antibody. (B) Both the TPR and U-box domain of CHIP are necessary for ERβ degradation. DNA (50 ng) encoding CHIP, CHIPΔTPR, or CHIPΔUbox was transfected into 293 cells with or without DNA (500 ng) encoding FLAG-tagged ERβ. Levels of ERβ protein were examined by use of Western blots probed with anti-FLAG-M2 antibody. (C) The CHIP-dependent ERβ degradation is not affected by ERα. DNA (500 ng) encoding FLAG-tagged ERβ was transfected into 293 cells with or without DNA (500 ng) encoding FLAG-tagged ERα and DNA (50 ng) encoding CHIP. Levels of ERβ and ERα protein were examined by use of Western blots probed with anti-FLAG-M2 antibody.

examined. The AD core domain is necessary for estrogen-dependent degradation of ERα (29, 48). Consistent with this observation, ERα(ΔAD) was stabilized by ligand binding and thus accumulated in response to estrogen (Fig. 6A). Interestingly, the deletion of the AD core of ERβ resulted in a dramatic reduction in ERβ in the absence of estrogen (Fig. 6A). This observation raises the possibility that the C-terminal region of ERβ is necessary for the stabilization of ERβ. To test this possibility, DNA sequences encoding deletion mutants of the C terminus of ERβ were transfected into 293 cells and levels of expressed protein were determined by Western blot analysis. When the F domain was deleted [ERβ(ΔF)], a dramatic reduction in ERβ protein was observed in the absence of estrogen (Fig. 6B). This reduction in ERβ was inhibited by MG132, indicating that the F domain suppresses the proteasome-dependent degradation of ERβ. The degradation of ERβ(ΔF) required the DRD, because ERβ(ΔDRD;ΔF) was not degraded in the absence of estrogen. In contrast, the degradation of ERβ(Δ140;ΔF) was enhanced by fusion with the DRD [ERβ(DRD;Δ140;ΔF)] in both the presence and the absence of estrogen (Fig. 6B). These results suggest that the F domain suppresses the DRD-dependent degradation of ERβ in the absence of estrogen.

In contrast to what was seen for ERβ, the deletion of the F domain in ERα did not affect its degradation. To study this, we generated a chimeric ERβ, ERβ (αF), in which the F domain was substituted with an ERα F domain. However, there is almost no homology between the ERα F and ERβ F domains, and the F domain of ERα was able to protect ERβ from proteolysis in the absence of estrogen (Fig. 6B).

Next, we determined the ubiquitination statuses of ERβ and ERβ(ΔF). That of ERβ(ΔF) was similar to that of full-length ERβ (Fig. 7A), indicating that the F domain does not regulate the ubiquitination step of ERβ. Thus, the F domain may inhibit the accession of 26S proteasome to ERβ structurally. Therefore, we evaluated the binding between ERβ and proteasomes. FLAG-tagged ERβ or ERβ(ΔF) was transfected into 293 cells with SUG-1, which is one of the components of regulatory subunit of 26S proteasome. A coimmunoprecipitation experiment revealed that deletion of the F domain enhanced association between ERβ and SUG-1 (Fig. 7B). In addition, SUG-1 efficiently reduced ERβ(ΔF) rather than ERβ (Fig. 7C). Thus, in the absence of estrogen, the F domain appears to abrogate the binding of the 26S proteasome to ERβ to protect the receptor from proteolysis.

Receptor degradation is involved in the downregulation of transcription of the gene for ERβ after ligand withdrawal. Recent evidence indicates that receptor degradation is coupled to transactivation and that the transcriptional activity of the gene for ERα is abrogated by the addition of MG132. The transcriptional activity of ERβ was also reduced by MG132 (Fig. 8A). Thus, it is likely that receptor degradation is necessary for the ligand-dependent transactivation of the ERβ gene. To investigate the association between CHIP-mediated receptor degradation and transactivation, we evaluated the transcriptional activities of ERβ deletion mutants by use of a transient reporter assay. As shown in Fig. 8B, ERβ(ΔDRD) exhibited a transcriptional activity higher than that of full-length ERβ. However, ERβ(Δ140) still showed transcriptional activity. When the DRD was fused to ERβ(Δ140) to form ERβ(DRD;Δ140), its transcriptional activity was reduced (Fig. 8B). Similarly, ERβ(Δ140; ΔF) exhibited higher transcriptional activity than ERβ(ΔF), but fusion of DRD decreased its transcriptional activity (Fig. 8B). In agreement with these results, CHIP expression downregulated the transcriptional activity of the ERβ gene (Fig. 8C). In contrast, CHIP siRNA enhanced transcriptional activity (Fig. 8C). The transcriptional activity of ERβ(ΔDRD) was not affected by expression of CHIP (Fig. 8C). Overall, our results indicate that CHIP-mediated degradation is not necessary for receptor-mediated transactivation. In addition, CHIP is able to ubiquitinate and to degrade ERβ(mC) (Fig. 5A), indicating that binding to the DNA element is not necessary for CHIP-mediated receptor degradation. These results show that large amounts of liganded ERβ protein are selectively and rapidly degraded independently of receptor-mediated transcription by CHIP.

To investigate the biological significance of this "wastefulness," we hypothesized that CHIP-mediated degradation selectively and rapidly degrades the active form of ERβ to shut off ERβ-mediated transcription when the estrogen dose is reduced. To test this hypothesis, we measured the transcriptional activities of constructs encoding ERβ and ERβ(ΔDRD) after estrogen withdrawal. DNA sequences encoding either ERβ or ERβ(ΔDRD) were transfected into 293 cells together with a plasmid in which the PEST sequence was fused to the luciferase gene (ERE-TATA-LucCP), and the luciferase activity was measured at various time points after estrogen withdrawal. As shown in Fig. 9A, the transcriptional activity of the ERβ sequence was reduced much faster than that of ERβ(ΔDRD). Using MDA-MB-231 cells that stably express either control siRNA or CHIP siRNA, we tested whether CHIP is involved in the downregulation of ERβ-mediated transcription after reduction of the ligand dose. Plasmids containing the PEST-fused luciferase gene were transfected into MDA-MB-231 cells expressing either control siRNA or CHIP siRNA. ERβ gene-mediated transcription was downregulated faster in the MDA-

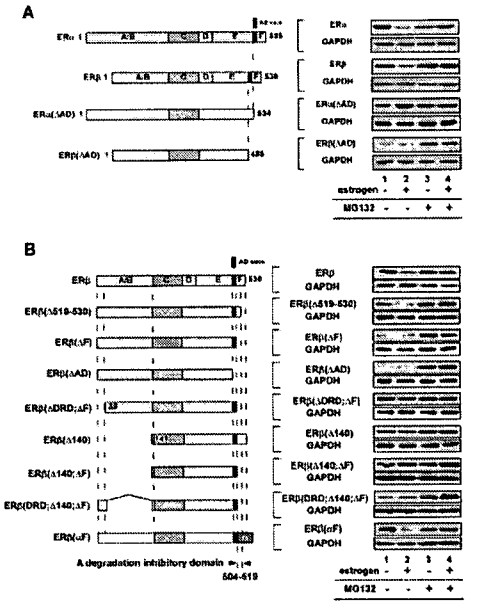

FIG. 6. The F domain suppresses DRD-mediated proteolysis of ERβ. (A) AD core deletion in ERβ increased the degradation of ligand-unbound receptor. DNA sequences (500 ng) encoding the indicated FLAG-tagged ER deletion mutants were transfected into 293 cells. These cells were cultured in the presence or the absence of estrogen (10^{-8} M) and MG132 (10^{-6} M). To evaluate the protein levels of the ER mutants, Western blot analysis was performed using anti-FLAG-M2 antibody. (B) F domain protects ERβ from DRD-mediated degradation. DNA sequences (500 ng) encoding the indicated FLAG-tagged ERβ deletion mutants were transfected into 293 cells cultured in the presence or the absence of estrogen (10^{-8} M) and MG132 (10^{-6} M). To evaluate the protein levels of the ERβ mutants, Western blot analysis was performed using anti-FLAG-M2 antibody.

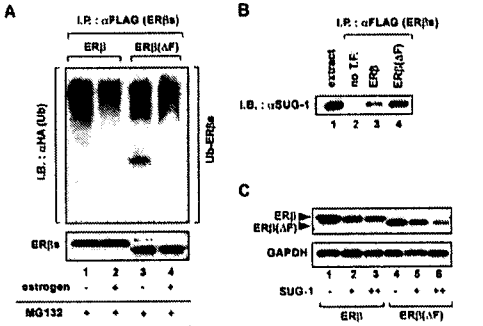

FIG. 7. F domain abrogates the association of proteasomes with ERβ. (A) Deletion of the F domain does not alter the ubiquitination status of ERβ. DNA sequences (500 ng) encoding the indicated FLAG-tagged ERβ mutants and DNA (1,000 ng) encoding HA-tagged ubiquitin were transfected into 293 cells in the presence or the absence of estrogen (10^{-8} M). Upper panel: FLAG-tagged ERβ mutants were immunoprecipitated (I.P.) with anti-FLAG-M2 antibody. The ubiquitination status of ERβ was analyzed by use of Western blots probed with anti-HA antibody. I.B., Western blotting. Lower panel: immunoprecipitated ERβ mutants were detected by use of Western blots probed with anti-FLAG antibody. (B) The F domain abrogates the association of SUG-1 with ERβ. DNA sequences (500 ng) encoding either ERβ or ERβ(ΔF) were transfected into 293 cells. FLAG-tagged ERβ or ERβ mutants were immunoprecipitated with anti-FLAG-M2 antibody. The precipitates were Western blotted and probed with an antibody against SUG-1. T.F., transfection. (C) The F domain protects ERβ from SUG-1-dependent degradation. DNA sequences (100 ng) encoding SUG-1 were cotransfected into 293 cells with or without DNA sequences (500 ng) encoding FLAG-tagged ERβ or ERβ(ΔF). The levels of ERβ or ERβ(ΔF) protein were examined by Western blotting and probed with anti-FLAG antibody.

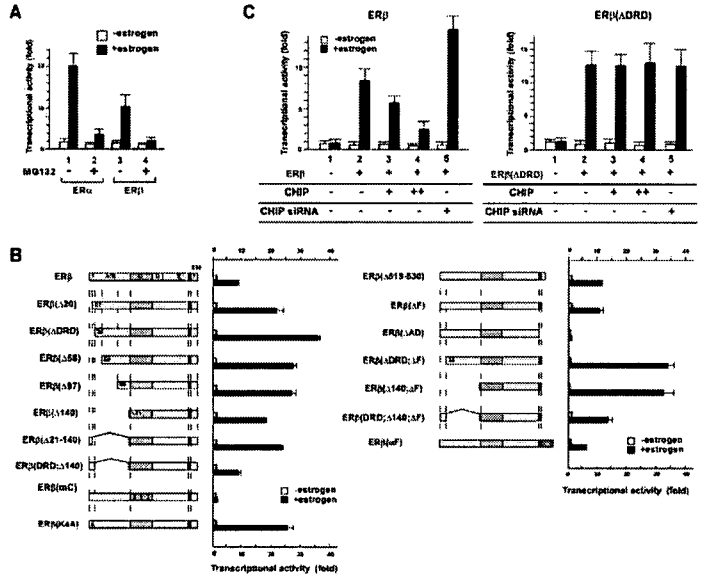

FIG. 8. CHIP decreases transcriptional activity of ERβ by degradation. (A) Proteasome-dependent degradation is necessary for the transactivation of ERs. DNA sequences (0.05 ng) encoding the ERβ or ERα were cotransfected into 293 cells with ERE-TATA-Luc (50 ng) and pRSVβGAL (50 ng) in the presence or absence of MG132 (10^{-6} M), and the cell extracts were used in a luciferase assay. (B) DRD-mediated degradation is not coupled to ligand-dependent receptor transactivation. DNA sequences (0.05 ng) encoding the indicated ERβ mutants were cotransfected into 293 cells with ERE-TATA-Luc (50 ng) and pRSVβGAL (50 ng), and the cell extracts were used in a luciferase assay. (C) CHIP production reduced the transcriptional activity of ERβ. ERE-TATA-Luc (50 ng), pRSVβGAL (50 ng), and DNA sequences (0.05 ng) encoding either ERβ or ERβ(ΔDRD) were cotransfected into 293 cells with or without DNA encoding CHIP and CHIP RNAi, and the cell extracts were used in a luciferase assay.

MB-231 cells expressing control siRNA than in the cells expressing CHIP siRNA (Fig. 9A).

The serum estrogen concentration varies from 1.5×10^{-10} M to 1.8×10^{-9} M during the menstrual cycle. Therefore, we investigated the dose response of the CHIP-dependent degradation of ERβ. As shown in Fig. 9B, CHIP-dependent ERβ degradation was changed in the levels of estrogen in the blood during the menstrual cycle.

Overall, these results suggest that CHIP-mediated degradation selectively and rapidly eliminates the active form of the NR to downregulate receptor-mediated transcription after ligand withdrawal.

DISCUSSION

In this study, we have shown that ERβ is ubiquitinated and degraded in an estrogen-dependent manner. We identified two regions within ERβ that are essential for the regulation of ERβ ubiquitination and degradation. The N-terminal 37-amino-acid region, the DRD, is necessary for the polyubiquitination of ERβ. Thus, ERβ seems to be constitutively exposed to attack by ubiquitin ligases because it contains the DRD. The C-terminal F domain abrogates DRD-dependent ERβ degradation, and the ubiquitination status of ERβ(ΔF) was similar to that of full-length ERβ. In addition, coimmunoprecipitation experiments revealed that the F domain inhibits the binding of unliganded ERβ to the regulatory subunit of 26S proteasome. Thus, the F domain may regulate not ubiquitination itself but the step involving proteasomal degradation. When estrogen binds to ERβ, the conformation of the C-terminal region, including the F domain, is changed, and the protective effect of the F domain is abolished to induce degradation. Some members of the NR superfamily have an F domain, but its function is unknown. Our observations provide the first evidence that the F domain of ERβ is involved in the regulation of its proteasome-dependent degradation.

The activation of NRs appears to be coupled to their degradation by the ubiquitin-proteasome pathway (3, 4, 8). Furthermore, several components of the ubiquitin-proteasome pathway, including SUG1/TRIP1 (17, 27, 32), RSP5/RPF1 (23), E6-AP (37), and UBC9 (42), have been identified as NR-interacting proteins. TBL1/TBLR1, which are components of the NR corepressor complex, also mediate corepressor/coactivator exchange by the ligand-dependent recruitment of the ubiquitin-19S proteasome complex (40). Thus, the ubiquitin-proteasome pathway appears to play an important role in regulating NR levels and restricting the duration and magnitude of receptor activity in response to ligands. Furthermore, proteasome-dependent degradation of the steroid receptor requires transcriptional activity, suggesting that receptor degradation and receptor transactivation are mutually interdependent.

Several recent studies have focused on the involvement of the ubiquitin-proteasome pathway in the estrogen-dependent transactivation of ERα (14, 29, 36, 44, 48, 50). Moreover, ERα and its coactivators cycle onto and off of estrogen-responsive promoters in ligand-dependent manners (35, 44, 45). In this process, ERα is reportedly ubiquitinated after each round of transcription, facilitating its release from the promoter, which may be essential for subsequent ERα-mediated transcription. We have shown that there is a degradation pathway for ERβ that is not coupled to transcription. Using ERβ(ΔDRD), we also have shown that transcription-uncoupled receptor degradation is necessary to abolish transcription via the proteolysis of the liganded receptor when the ligand dose is reduced. ERβ(ΔDRD) still exhibited slight ligand-dependent degradation, indicating that there may be other degradation pathways for ERβ. These pathways could be coupled to the transactivation of ERβ.

To investigate the ubiquitin-proteasome pathway for ERβ, we purified the ubiquitin ligase complex that specifically binds to the DRD and identified a protein complex containing CHIP. CHIP was first reported to induce the ubiquitination of GR bound to HSP90 for proteasomal degradation (7). Recent observations have indicated that CHIP targets a number of HSP70/90-associated proteins for ubiquitination and degradation (15, 18, 21, 22, 28, 34, 48, 52–54). We (48) and others (9) have previously shown that CHIP binds unliganded ERα as a protein complex containing HSP90, HSC70, HSP70, HSP40, BAG-1, and BAG-2, all of which possess or assist chaperone functions, and a DnaJ-like protein, KIAA0678. CHIP preferentially induces the hydrolysis of abnormal or mutant forms of ERα, acting as an E3 ubiquitin ligase capable of distinguishing the nonnative states from the native states of the receptor in vivo.

Our results obtained from the analysis of ERβ suggest that CHIP is involved both in the "quality control" of receptor proteins and in switching off receptor-mediated transcription (Fig. 10). The response of endocrine target tissues to hormones is tightly regulated and is dependent upon circulating levels of available hormonal ligands. When the dose of circulating ligand is reduced, receptor-mediated transcription should be downregulated. The dissociation rate of estrogen

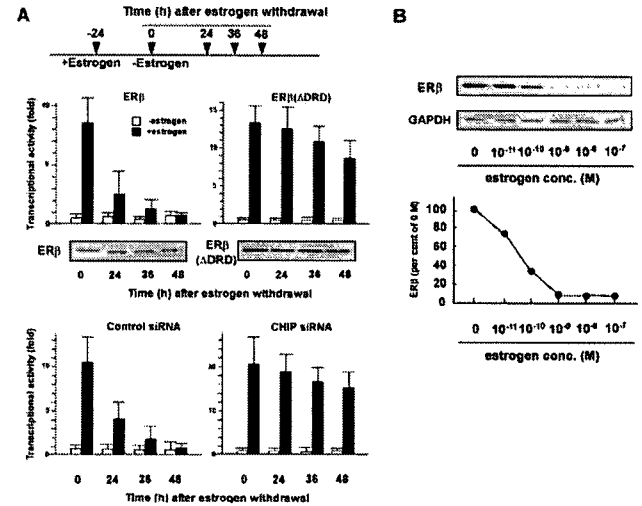

FIG. 9. CHIP switches off ERβ-mediated transcription after the estrogen dose is reduced. (A) Downregulation of CHIP inhibits the turning off of ERβ-mediated transcription after estrogen withdrawal. Upper panel: DRD-mediated degradation is involved in the downregulation of ERβ-mediated transcription after estrogen withdrawal. The 293 cells were transfected with expression plasmids encoding FLAG-tagged ERβ or ERβ(ΔDRD), together with ERE-TATA-LucCP (50 ng) and pRSVβGAL (50 ng). Twenty-four hours after transfection, the cells were treated with estrogen (10^{-8} M) for an additional 24 h, after which the estrogen was withdrawn (time 0). These cells were harvested for luciferase assays and Western blotting at the indicated time points after estrogen withdrawal. Lower panel: CHIP is involved in the downregulation of ERβ-mediated transcription when the ligand dose is reduced. Plasmids encoding a siRNA specific for CHIP or control vector were introduced into MDA-MB-231 cells. These cells were selected with G418. FLAG-tagged ERβ (100 ng), ERE-TATA-LucCP (400 ng), and pGL3-Control (10 ng) were transfected into these cell lines. Twenty-four hours after transfection, the cells were treated with estrogen (10^{-8} M) for an additional 24 h, after which the estrogen was withdrawn (time 0). These cells were harvested for luciferase assays and Western blotting at the times indicated after estrogen withdrawal. (B) Dose-response curve of the estrogen-induced CHIP-dependent degradation of the ERβ. DNA (500 ng) encoding the FLAG-tagged ERβ was transfected into 293 cells, with or without DNA encoding CHIP. These cells were cultured in the presence of the indicated concentration (conc.) of estrogen (from 10^{-11} M to 10^{-7} M). Levels of ERβ protein were examined by use of Western blots probed with anti-FLAG-M2 antibody.

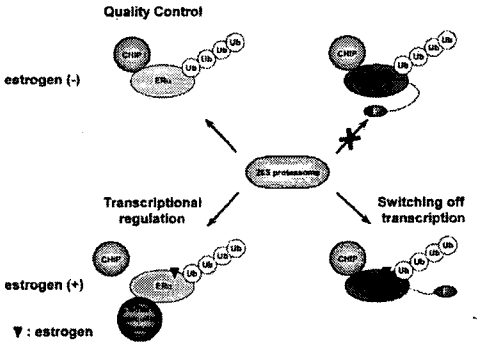

FIG. 10. Schematic representation of the degradation pathways of ERα and ERβ. ERα binds CHIP in the absence of estrogen. When the estrogen binds ERα, CHIP dissociates. ERβ binds CHIP in both the absence and the presence of estrogen. In the absence of estrogen, the degradation of ubiquitinated ERβ is inhibited by the F domain. When the estrogen binds ERβ, the conformation of the F domain is changed to recruit 26S proteasome.

from its receptor is very low because a coactivator complex contacts the protein surface above the ligand pocket (16). Thus, it is difficult to cause rapid downregulation by ligand dissociation from its receptor. Our results provide the first evidence that receptor degradation is involved in the cessation of transcription when the ligand dose is reduced. Several nuclear receptors are reported to exhibit agonist-dependent degradation. Therefore, it is possible that other forms of receptor-mediated transcription are downregulated by the same mechanism as ERβ when the agonist dose is reduced.

ERβ is subject to proteasome-mediated degradation in the presence of estrogen, which subsequently limits transcriptional output of ERβ regardless of whether estrogen is removed or persistently available. As shown in Fig. 8C, CHIP downregulates the ERβ-mediated transactivation in the presence of estrogen. Thus, the CHIP-dependent degradation is involved both in the downregulation of ERβ activity and in switching off ERβ-mediated transcription.

REFERENCES

1. **Ballinger, C. A., P. Connell, Y. Wu, Z. Hu, L. J. Thompson, L. Y. Yin, and C. Patterson.** 1999. Identification of CHIP, a novel tetratricopeptide repeat-containing protein that interacts with heat shock proteins and negatively regulates chaperone functions. Mol. Cell. Biol. **19**:4535–4545.
2. **Beato, M., P. Herrlich, and G. Schutz.** 1995. Steroid hormone receptors: many actors in search of a plot. Cell **83**:851–857.
3. **Blanquart, C., O. Barbier, J. C. Fruchart, B. Staels, and C. Glineur.** 2002. Peroxisome proliferator-activated receptor alpha (PPARalpha) turnover by the ubiquitin-proteasome system controls the ligand-induced expression level of its target genes. J. Biol. Chem. **277**:37254–37259.
4. **Boudjelal, M., Z. Wang, J. J. Voorhees, and G. J. Fisher.** 2000. Ubiquitin/proteasome pathway regulates levels of retinoic acid receptor gamma and retinoid X receptor alpha in human keratinocytes. Cancer Res. **60**:2247–2252.
5. **Chambon, P.** 1996. A decade of molecular biology of retinoic acid receptors. FASEB J. **10**:940–954.
6. **Cheskis, B. J., N. J. McKenna, C. W. Wong, J. Wong, B. Komm, C. R. Lyttle, and B. W. O'Malley.** 2003. Hierarchical affinities and a bipartite interaction model for estrogen receptor isoforms and full-length steroid receptor coactivator (SRC/p160) family members. J. Biol. Chem. **278**:13271–13277.
7. **Connell, P., C. A. Ballinger, J. Jiang, Y. Wu, L. J. Thompson, J. Hohfeld, and C. Patterson.** 2001. The co-chaperone CHIP regulates protein triage decisions mediated by heat-shock proteins. Nat. Cell Biol. **3**:93–96.
8. **Dace, A., L. Zhao, K. S. Park, T. Furuno, N. Takamura, M. Nakanishi, B. L. West, J. A. Hanover, and S. Cheng.** 2000. Hormone binding induces rapid proteasome-mediated degradation of thyroid hormone receptors. Proc. Natl. Acad. Sci. USA **97**:8985–8990.
9. **Dai, Q., S. B. Qian, H. H. Li, H. McDonough, C. Borchers, D. Huang, S. Takayama, J. M. Younger, H. Y. Ren, D. M. Cyr, and C. Patterson.** 2005. Regulation of the cytoplasmic quality control protein degradation pathway by BAG2. J. Biol. Chem. **280**:38673–38681.
10. **DeMayo, F. J., B. Zhao, N. Takamoto, and S. Y. Tsai.** 2002. Mechanisms of action of estrogen and progesterone. Ann. N. Y. Acad. Sci. **955**:48–59, 86–88, 396–406.
11. **Dennis, A. P., R. U. Haq, and Z. Nawaz.** 2001. Importance of the regulation of nuclear receptor degradation. Front. Biosci. **6**:D954–D959.
12. **Deroo, B. J., and K. S. Korach.** 2006. Estrogen receptors and human disease. J. Clin. Investig. **116**:561–570.
13. **Deroo, B. J., C. Rentsch, S. Sampath, J. Young, D. B. DeFranco, and T. K. Archer.** 2002. Proteasomal inhibition enhances glucocorticoid receptor transactivation and alters its subnuclear trafficking. Mol. Cell. Biol. **22**:4113–4123.
14. **Fan, M., A. Park, and K. P. Nephew.** 2005. CHIP (carboxyl terminus of Hsc70-interacting protein) promotes basal and geldanamycin-induced degradation of estrogen receptor-alpha. Mol. Endocrinol. **19**:2901–2914.
15. **Galigniana, M. D., J. M. Harrell, P. R. Housley, C. Patterson, S. K. Fisher, and W. B. Pratt.** 2004. Retrograde transport of the glucocorticoid receptor in neurites requires dynamic assembly of complexes with the protein chaperone hsp90 and is linked to the CHIP component of the machinery for proteasomal degradation. Brain Res. Mol. Brain Res. **123**:27–36.
16. **Gee, A. C., K. E. Carlson, P. G. Martini, B. S. Katzenellenbogen, and J. A. Katzenellenbogen.** 1999. Coactivator peptides have a differential stabilizing effect on the binding of estrogens and antiestrogens with the estrogen receptor. Mol. Endocrinol. **13**:1912–1923.
17. **Gianni, M., A. Bauer, E. Garattini, P. Chambon, and C. Rochette-Egly.** 2002. Phosphorylation by p38MAPK and recruitment of SUG-1 are required for RA-induced RAR gamma degradation and transactivation. EMBO J. **21**: 3760–3769.
18. **He, B., S. Bai, A. T. Hnat, R. I. Kalman, J. T. Minges, C. Patterson, and E. M. Wilson.** 2004. An androgen receptor NH2-terminal conserved motif interacts with the COOH terminus of the Hsp70-interacting protein (CHIP). J. Biol. Chem. **279**:30643–30653.
19. **Heery, D. M., E. Kalkhoven, S. Hoare, and M. G. Parker.** 1997. A signature motif in transcriptional co-activators mediates binding to nuclear receptors. Nature **387**:733–736.
20. **Hewitt, S. C., and K. S. Korach.** 2002. Estrogen receptors: structure, mechanisms and function. Rev. Endocr. Metab. Disord. **3**:193–200.
21. **Hohfeld, J., D. M. Cyr, and C. Patterson.** 2001. From the cradle to the grave: molecular chaperones that may choose between folding and degradation. EMBO Rep. **2**:885–890.
22. **Imai, Y., M. Soda, S. Hatakeyama, T. Akagi, T. Hashikawa, K. I. Nakayama, and R. Takahashi.** 2002. CHIP is associated with Parkin, a gene responsible for familial Parkinson's disease, and enhances its ubiquitin ligase activity. Mol. Cell **10**:55–67.
23. **Imhof, M. O., and D. P. McDonnell.** 1996. Yeast RSP5 and its human homolog hRPF1 potentiate hormone-dependent activation of transcription by human progesterone and glucocorticoid receptors. Mol. Cell. Biol. **16**: 2594–2605.
24. **Ito, M., C. X. Yuan, H. J. Okano, R. B. Darnell, and R. G. Roeder.** 2000. Involvement of the TRAP220 component of the TRAP/SMCC coactivator complex in embryonic development and thyroid hormone action. Mol. Cell **5**:683–693.
25. **Kamei, Y., L. Xu, T. Heinzel, J. Torchia, R. Kurokawa, B. Gloss, S. C. Lin, R. A. Heyman, D. W. Rose, C. K. Glass, and M. G. Rosenfeld.** 1996. A CBP integrator complex mediates transcriptional activation and AP-1 inhibition by nuclear receptors. Cell **85**:403–414.
26. **Lange, C. A., T. Shen, and K. B. Horwitz.** 2000. Phosphorylation of human progesterone receptors at serine-294 by mitogen-activated protein kinase signals their degradation by the 26S proteasome. Proc. Natl. Acad. Sci. USA **97**:1032–1037.
27. **Lee, J. W., F. Ryan, J. C. Swaffield, S. A. Johnston, and D. D. Moore.** 1995. Interaction of thyroid-hormone receptor with a conserved transcriptional mediator. Nature **374**:91–94.
28. **Li, L., H. Xin, X. Xu, M. Huang, X. Zhang, Y. Chen, S. Zhang, X. Y. Fu, and Z. Chang.** 2004. CHIP mediates degradation of Smad proteins and potentially regulates Smad-induced transcription. Mol. Cell. Biol. **24**:856–864.
29. **Lonard, D. M., Z. Nawaz, C. L. Smith, and B. W. O'Malley.** 2000. The 26S proteasome is required for estrogen receptor-alpha and coactivator turnover and for efficient estrogen receptor-alpha transactivation. Mol. Cell **5**:939–948.
30. **Mader, S., V. Kumar, H. de Verneuil, and P. Chambon.** 1989. Three amino acids of the oestrogen receptor are essential to its ability to distinguish an oestrogen from a glucocorticoid-responsive element. Nature **338**:271–274.

31. **Mangelsdorf, D. J., C. Thummel, M. Beato, P. Herrlich, G. Schutz, K. Umesono, B. Blumberg, P. Kastner, M. Mark, P. Chambon, et al.** 1995. The nuclear receptor superfamily: the second decade. Cell **83**:835–839.
32. **Masuyama, H., and P. N. MacDonald.** 1998. Proteasome-mediated degradation of the vitamin D receptor (VDR) and a putative role for SUG1 interaction with the AF-2 domain of VDR. J. Cell. Biochem. **71**:429–440.
33. **McKenna, N. J., and B. W. O'Malley.** 2002. Combinatorial control of gene expression by nuclear receptors and coregulators. Cell **108**:465–474.
34. **Meacham, G. C., C. Patterson, W. Zhang, J. M. Younger, and D. M. Cyr.** 2001. The Hsc70 co-chaperone CHIP targets immature CFTR for proteasomal degradation. Nat. Cell Biol. **3**:100–105.
35. **Metivier, R., G. Penot, M. R. Hubner, G. Reid, H. Brand, M. Kos, and F. Gannon.** 2003. Estrogen receptor-alpha directs ordered, cyclical, and combinatorial recruitment of cofactors on a natural target promoter. Cell **115**: 751–763.
36. **Nawaz, Z., D. M. Lonard, A. P. Dennis, C. L. Smith, and B. W. O'Malley.** 1999. Proteasome-dependent degradation of the human estrogen receptor. Proc. Natl. Acad. Sci. USA **96**:1858–1862.
37. **Nawaz, Z., D. M. Lonard, C. L. Smith, E. Lev-Lehman, S. Y. Tsai, M. J. Tsai, and B. W. O'Malley.** 1999. The Angelman syndrome-associated protein, E6-AP, is a coactivator for the nuclear hormone receptor superfamily. Mol. Cell. Biol. **19**:1182–1189.
38. **Nawaz, Z., and B. W. O'Malley.** 2004. Urban renewal in the nucleus: is protein turnover by proteasomes absolutely required for nuclear receptor-regulated transcription? Mol. Endocrinol. **18**:493–499.
39. **Onate, S. A., S. Y. Tsai, M. J. Tsai, and B. W. O'Malley.** 1995. Sequence and characterization of a coactivator for the steroid hormone receptor superfamily. Science **270**:1354–1357.
40. **Perissi, V., A. Aggarwal, C. K. Glass, D. W. Rose, and M. G. Rosenfeld.** 2004. A corepressor/coactivator exchange complex required for transcriptional activation by nuclear receptors and other regulated transcription factors. Cell **116**:511–526.
41. **Pettersson, K., and J. A. Gustafsson.** 2001. Role of estrogen receptor beta in estrogen action. Annu. Rev. Physiol. **63**:165–192.
42. **Poukka, H., P. Aarnisalo, U. Karvonen, J. J. Palvimo, and O. A. Janne.** 1999. Ubc9 interacts with the androgen receptor and activates receptor-dependent transcription. J. Biol. Chem. **274**:19441–19446.
43. **Rachez, C., B. D. Lemon, Z. Suldan, V. Bromleigh, M. Gamble, A. M. Naar, H. Erdjument-Bromage, P. Tempst, and L. P. Freedman.** 1999. Ligand-dependent transcription activation by nuclear receptors requires the DRIP complex. Nature **398**:824–828.
44. **Reid, G., M. R. Hubner, R. Metivier, H. Brand, S. Denger, D. Manu, J. Beaudouin, J. Ellenberg, and F. Gannon.** 2003. Cyclic, proteasome-mediated turnover of unliganded and liganded ERalpha on responsive promoters is an integral feature of estrogen signaling. Mol. Cell **11**:695–707.
45. **Shang, Y., X. Hu, J. DiRenzo, M. A. Lazar, and M. Brown.** 2000. Cofactor dynamics and sufficiency in estrogen receptor-regulated transcription. Cell **103**:843–852.
46. **Shiau, A. K., D. Barstad, P. M. Loria, L. Cheng, P. J. Kushner, D. A. Agard, and G. L. Greene.** 1998. The structural basis of estrogen receptor/coactivator recognition and the antagonism of this interaction by tamoxifen. Cell **95**: 927–937.
47. **Tanaka, T., M. L. Rodriguez de la Concepcion, and L. M. De Luca.** 2001. Involvement of all-trans-retinoic acid in the breakdown of retinoic acid receptors alpha and gamma through proteasomes in MCF-7 human breast cancer cells. Biochem. Pharmacol. **61**:1347–1355.
48. **Tateishi, Y., Y. Kawabe, T. Chiba, S. Murata, K. Ichikawa, A. Murayama, K. Tanaka, T. Baba, S. Kato, and J. Yanagisawa.** 2004. Ligand-dependent switching of ubiquitin-proteasome pathways for estrogen receptor. EMBO J. **23**:4813–4823.
49. **Tontonoz, P., and D. J. Mangelsdorf.** 2003. Liver X receptor signaling pathways in cardiovascular disease. Mol. Endocrinol. **17**:985–993.
50. **Valley, C. C., R. Metivier, N. M. Solodin, A. M. Fowler, M. T. Mushek, L. Hill, and E. T. Alarid.** 2005. Differential regulation of estrogen-inducible proteolysis and transcription by the estrogen receptor alpha N terminus. Mol. Cell. Biol. **25**:5417–5428.
51. **Wallace, A. D., and J. A. Cidlowski.** 2001. Proteasome-mediated glucocorticoid receptor degradation restricts transcriptional signaling by glucocorticoids. J. Biol. Chem. **276**:42714–42721.
52. **Wang, X., and D. B. DeFranco.** 2005. Alternative effects of the ubiquitin-proteasome pathway on glucocorticoid receptor down-regulation and transactivation are mediated by CHIP, an E3 ligase. Mol. Endocrinol. **19**:1474–1482.
53. **Wickner, S., M. R. Maurizi, and S. Gottesman.** 1999. Posttranslational quality control: folding, refolding, and degrading proteins. Science **286**: 1888–1893.
54. **Xin, H., X. Xu, L. Li, H. Ning, Y. Rong, Y. Shang, Y. Wang, X. Y. Fu, and Z. Chang.** 2005. CHIP controls the sensitivity of transforming growth factor-beta signaling by modulating the basal level of Smad3 through ubiquitin-mediated degradation. J. Biol. Chem. **280**:20842–20850.
55. **Yanagisawa, J., H. Kitagawa, M. Yanagida, O. Wada, S. Ogawa, M. Nakagomi, H. Oishi, Y. Yamamoto, H. Nagasawa, S. B. McMahon, M. D. Cole, L. Tora, N. Takahashi, and S. Kato.** 2002. Nuclear receptor function requires a TFTC-type histone acetyl transferase complex. Mol. Cell **9**:553–562.
56. **Yanagisawa, J., Y. Yanagi, Y. Masuhiro, M. Suzawa, M. Watanabe, K. Kashiwagi, T. Toriyabe, M. Kawabata, K. Miyazono, and S. Kato.** 1999. Convergence of transforming growth factor-beta and vitamin D signaling pathways on SMAD transcriptional coactivators. Science **283**:1317–1321.
57. **Zhu, J., M. Gianni, E. Kopf, N. Honore, M. Chelbi-Alix, M. Koken, F. Quignon, C. Rochette-Egly, and H. de The.** 1999. Retinoic acid induces proteasome-dependent degradation of retinoic acid receptor alpha (RARalpha) and oncogenic RARalpha fusion proteins. Proc. Natl. Acad. Sci. USA **96**: 14807–14812.

Identification and characterization of noncalcemic, tissue-selective, nonsecosteroidal vitamin D receptor modulators

Yanfei Ma,[1] Berket Khalifa,[1] Ying K. Yee,[1] Jianfen Lu,[1] Ai Memezawa,[2] Rajesh S. Savkur,[1] Yoko Yamamoto,[2] Subba R. Chintalacharuvu,[1] Kazuyoshi Yamaoka,[2] Keith R. Stayrook,[1] Kelli S. Bramlett,[1] Qing Q. Zeng,[1] Srinivasan Chandrasekhar,[1] Xiao-Peng Yu,[1] Jared H. Linebarger,[1] Stephen J. Iturria,[1] Thomas P. Burris,[1] Shigeaki Kato,[2] William W. Chin,[1] and Sunil Nagpal[1]

[1]Lilly Research Laboratories, Eli Lilly and Company, Lilly Corporate Center, Indianapolis, Indiana, USA.
[2]Institute of Molecular and Cellular Biosciences, The University of Tokyo, Tokyo, Japan.

Vitamin D receptor (VDR) ligands are therapeutic agents for the treatment of psoriasis, osteoporosis, and secondary hyperparathyroidism. VDR ligands also show immense potential as therapeutic agents for autoimmune diseases and cancers of skin, prostate, colon, and breast as well as leukemia. However, the major side effect of VDR ligands that limits their expanded use and clinical development is hypercalcemia that develops as a result of the action of these compounds mainly on intestine. In order to discover VDR ligands with less hypercalcemia liability, we sought to identify tissue-selective VDR modulators (VDRMs) that act as agonists in some cell types and lack activity in others. Here, we describe LY2108491 and LY2109866 as nonsecosteroidal VDRMs that function as potent agonists in keratinocytes, osteoblasts, and peripheral blood mononuclear cells but show poor activity in intestinal cells. Finally, these nonsecosteroidal VDRMs were less calcemic in vivo, and LY2108491 exhibited more than 270-fold improved therapeutic index over the naturally occurring VDR ligand 1,25-dihydroxyvitamin D_3 [1,25-$(OH)_2D_3$] in an in vivo preclinical surrogate model of psoriasis.

Introduction

The biologically active form of vitamin D, 1,25-dihydroxyvitamin D_3 [calcitriol, 1,25-$(OH)_2D_3$], plays an important role in cell differentiation, proliferation, and immunomodulation and mineral homeostasis. 1,25-$(OH)_2D_3$ and its synthetic analogs exert these effects by binding to the vitamin D receptor (VDR) that belongs to the steroid/thyroid hormone nuclear receptor superfamily (1). VDR, a ligand-dependent transcription factor, functions as a heterodimer with another nuclear receptor, namely, retinoid X receptor (RXR). Upon ligand binding, VDR undergoes a conformational change that promotes RXR-VDR heterodimerization (2, 3). Liganded RXR-VDR heterodimer translocates to the nucleus, binds to the vitamin D response elements (VDREs) present in the promoter regions of responsive genes, and recruits chromatin-modifying enzymatic activities through interaction with coactivators and VDR-interacting protein (DRIP) complex, which ultimately leads to the initiation of transcription (4). Pleiotropic actions of VDR ligands on various cells types have prompted the testing of their therapeutic activities in several human diseases as well as in various animal models of these diseases. These efforts have resulted in the development of VDR ligands for the treatment of psoriasis, osteoporosis, and secondary hyperparathyroidism (5, 6). 1,25-$(OH)_2D_3$ and its synthetic analogs have also shown efficacy in various in vitro and in vivo models of autoimmune diseases (arthritis, multiple sclerosis, and inflammatory bowel disease) and cancers of head and neck, prostate, colon, and breast as well as leukemia (6–9). However, the major hurdle facing the translation of basic and applied research to therapeutic ligands is hypercalcemia associated with currently available VDR ligands. Although calcitriol and calcipotriol (a synthetic VDR ligand) have been approved as topical agents for the treatment of mild to moderate psoriasis, their use (especially oral) has at least in some cases been associated with an increased incidence of hypercalcemia/hypercalciuria (10–14), and they exhibit poor efficacy when compared with biologics (15). In the clinic, the therapeutic efficacy of calcitriol and calcipotriol is increased by their use in combination with topical steroids (16, 17). Therefore, there is an unmet clinical need for the identification of a new generation of VDR ligands that exhibit an improved therapeutic index (TI).

1,25-$(OH)_2D_3$ is a secosteroidal compound (Figure 1A), and most of the VDR ligands that have been described to date, including calcipotriol, have a secosteroidal backbone (18). Administration of VDR ligands results in hypercalcemia by increasing calcium absorption from the intestine. Consistent with this view, VDR-null mice display marked hypocalcemia (19). 1,25-$(OH)_2D_3$ action on duodenal enterocytes induces calcium transport protein 1 (CaT1) expression, which channels calcium from the intestinal lumen into the cell (20). VDR ligands also induce the expression of an EF-hand–containing carrier protein, calbindin 9k, that ferries the bound calcium from the apical to the basolateral membrane (20). Therefore, a tissue-selective/cell-context–dependent VDR ligand that is transcriptionally less active in intestinal cells but a potent agonist in other cell types (e.g., keratinocytes and lymphocytes) may exhibit reduced hypercalcemia liability. Such a tissue-selective VDR modulator (VDRM) may exhibit a better TI, which is required for the treatment of dermatological indications, including psoriasis, actinic keratosis, and squamous cell carcinoma of the skin. Since nonsteroidal structures have provided tissue-selective estrogen receptor modulators (SERMs) that are agonist in bone and antagonist or transcriptionally inactive in breast and uterine cells (21, 22), we synthesized nonsecosteroidal analogs of vitamin D and show here the identification and characterization of LY2108491 and LY2109866, the nonsecosteroidal VDRMs. We demonstrate that LY2108491 and LY2109866 function as potent and efficacious agonists in keratinocytes, human PBMCs, and osteoblasts but exhibit attenuated transcriptional activity in intestinal cells. This cell context–dependent activity translated in vivo into reduced hypercalcemic liability of these compounds. We also demonstrate that in a surrogate in vivo preclinical model of psoriasis, LY2108491 and LY2109866 show significantly improved therapeutic indices relative to 1,25-$(OH)_2D_3$.

Nonstandard abbreviations used: AIB, amplified in breast cancer; CaT1, calcium transport protein 1; EC_{50}, concentration of compound required to induce 50% of maximum activity; KerTr, transformed keratinocyte; LBD, ligand-binding domain; MOG_{35-55}, myelin oligodendrocyte glycoprotein; OCN, osteocalcin; 1,25-$(OH)_2D_3$, 1,25-dihydroxyvitamin D_3; PGC-1α, peroxisome proliferative activated receptor γ, coactivator 1α; PHA, phytohemagglutinin; RXR, retinoid X receptor; SRC, steroid receptor coactivator; TI, therapeutic index; TIF, transcription intermediary factor; TMED, threshold minimum effective dose; TPA, 12-O-tetradecanoyl phorbol-13-acetate; TR, thyroid hormone receptor; VDR, vitamin D receptor; VDRE, vitamin D response element; VDRM, VDR modulator.

Conflict of interest: The authors have declared that no conflict of interest exists.
Citation for this article: *J. Clin. Invest.* **116**:892–904 (2006). doi:10.1172/JCI25901.

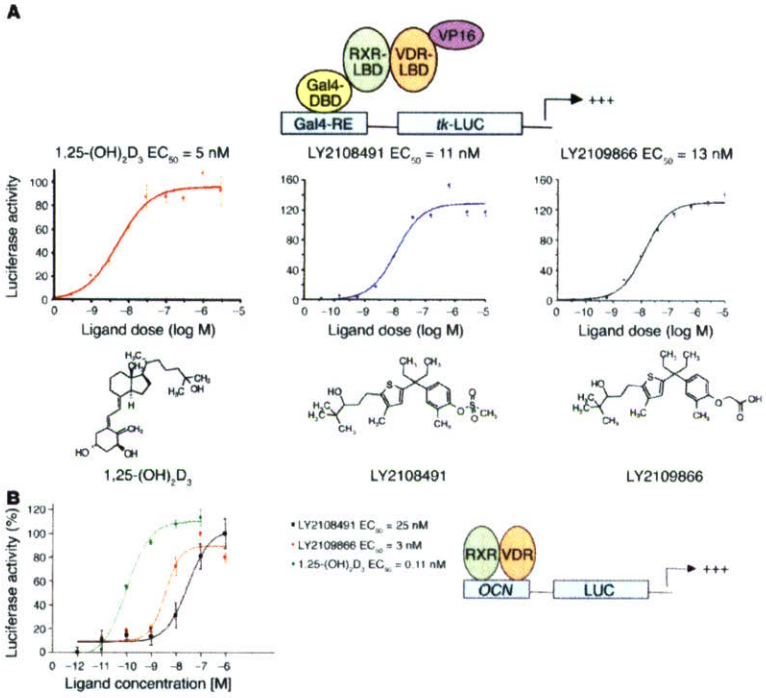

Figure 1
LY2108491 and LY2109866 are nonsecosteroidal VDR ligands. (**A**) Nonsecosteroidal compounds are potent agonists in a VDR-based ligand-sensing assay. SaOS-2 cells were cotransfected with expression vectors encoding Gal4-RXRα-LBD and VP16-VDR-LBD along with a Gal4-responsive luciferase reporter. After transfection, cells were treated with vehicle or various concentrations of 1,25-$(OH)_2D_3$, LY2108491, or LY2109866, and the reporter activity was expressed as light units ± SEM. A schematic of the ligand-sensing assay and the chemical structures of 1,25-$(OH)_2D_3$, LY2108491, and LY2109866 are also presented. *tk*-LUC, thymidine kinase–LUC. (**B**) Nonsecosteroidal VDR ligands induce VDRE-dependent expression of the rat osteocalcin promoter in osteoblasts. ROS17/2.8 cells stably transfected with rat osteocalcin reporter (OCN-LUC) were treated with various concentrations of 1,25-$(OH)_2D_3$, LY2108491, or LY2109866. Results are shown in percentage of the luciferase activity obtained by treating the cells with 1 μM 1,25-$(OH)_2D_3$. All the transfections were performed in triplicate.

Results

Identification of a nonsecosteroidal VDR agonist. One of the fundamental properties of 1,25-$(OH)_2D_3$ and its synthetic analogs is that they induce heterodimerization of VDR with RXR, resulting in the formation of an RXR-VDR heterodimer, the functional unit of vitamin D action (2, 3). RXR-VDR heterodimerization was used in a ligand-sensing assay since VDR ligands and not RXR ligands drive heterodimerization between RXR and VDR (3). Therefore,